João Luís Ruivo Carvalho Paulo

A Multimodal HMI Approach for Interaction, User Modeling and Automatic Gait Analysis on a Robotic Walker

Tese de Doutoramento em Engenharia Electrotécnica e de Computadores, ramo de especialização em Automação e Robótica, orientada pelo Prof. Dr. Paulo José Monteiro Peixoto e apresentada ao Departamento de Engenharia Electrotécnica e de Computadores da Faculdade de Ciências e Tecnologia da Universidade de Coimbra.

Junho 2018

· U C ·

UNIVERSIDADE DE COIMBRA

A Multimodal HMI Approach for Interaction, User Modeling and Automatic Gait Analysis on a Robotic Walker

João Luís Ruivo Carvalho Paulo

Tese de Doutoramento em Engenharia Electrotécnica e de Computadores, ramo de especialização em Automação e Robótica, orientada pelo Prof. Dr. Paulo José Monteiro Peixoto e apresentada ao Departamento de Engenharia Electrotécnica e de Computadores da Faculdade de Ciências e Tecnologia da Universidade de Coimbra.

December 2017

To my loving family and friends

Acknowledgements

This work is the outcome of research carried out at the Institute of Systems and Robotics (ISR) of the University of Coimbra during the last five years. When I started in late 2012, the research on “robotic walker” was a new experience to me, and an unexplored research area in ISR. To get here today, I received many direct and indirect contributions that helped me to overcome the challenges of this magnificent research area.

Undoubtedly, my first thanks go to my supervisor, Prof. Paulo Peixoto. Prof. Paulo Peixoto supervised me during my Ph.D. I owe him a lot of my training as a student and researcher. During this Ph.D work, Prof. Peixoto’s supervision was outstanding, by his methodological contributions, fruitful discussions, continuous motivation, friendship, and for offering me all the necessary means to carry out this work. He gave me also the freedom to follow my own directions.

Another indispensable acknowledgement goes to Prof. Urbano Nunes, I want to thank him for also providing crucial supervision. Supervision that resulted from fruitful discussions, from his continued support, friendship, enthusiastic and outstanding way to motivate me, and from introducing me important research concepts.

During my P.hD work, several people participated in the experiments. I’m deeply grateful to all of them. Their time, patience and contributions were crucial to validate the developed work during the Ph.D.

I owe a lot to ISR to have provided excellent conditions and resources that allowed me to accomplish my Ph.D work. I appreciate the availability of all its members, staff, researchers and administration.

I acknowledge a fellowship, from Fundação para a Ciência e a Tecnologia (FCT) under Grant SFRH/BD/88672/2012. This work has been in part supported by FCT, under the project RECI/EEI-AUT/0181/2012.

I am also very grateful to my friends and colleagues from ISR, Luís Garrote, Cristiano Premebida, Alireza Asvadi, Daniel Almeida, André Lopes, João Perdiz, Tiago Matias and Jérôme Mendes with whom I had some fruitful discussions. To all my friends, in particular, André Campos, João Tavares, João Fernandes, Nelson Figueira and Nuno Fernandes thanks for

their concern and motivation.

Finally, I would like to express my gratitude to my parents, my mother Maria, my father João, and my close family, in particular my cousin Filipe, for their concern and constant encouragement and support.

Abstract

This thesis proposes contributions in the domain of assistive robotics, focusing on user-centered methodologies towards intuitive and safe interaction with a robotic walker through novel modeling and analysis techniques. Robotic walkers are assistive robotic devices that offer mobility assistance to frail or elderly users, also providing a significant potential for lower limb rehabilitation.

The goal of this thesis is to consider a holistic user-centered approach, in which the user is the focal point of the device operation. This involves the design of a Human-machine interface (HMI) that accurately estimates the user's state and intention to guarantee his safety, as well as, the safer navigation of the device. Having awareness of the user's state can leverage other applications, like the use of the device as a rehabilitation aid by providing gait analysis and therapy assessment. To cope with this goal, a robotic walker framework was developed, the ISR-AIWALKER, an instrumented robotic platform designed to conduct research on rehabilitation and assistive robotics. Using this framework, the proposed contributions of this work are: (i) an intuitive and safe HMI, boasting a novel robot-assisted navigation module for safe mobility assistance, (ii) novel short-range modeling techniques of the user's lower limbs based on a multimodal sensor setup, and (iii) novel onboard gait analysis methods that learn the user's gait pattern, aiming to help identify pathologies and assess therapy's progression as a potential diagnostic tool for rehabilitation purposes.

Following a user-centered paradigm, a novel vison-based HMI that introduces a hand gripping pattern analysis through machine learning (ML) is proposed, to ensure the user is adequately gripping the walker's handles. Still focusing on the user, a navigation method using utility theory and a rapidly exploring random tree technique is proposed to find the safest path according to the user's intent. Taking into account the rehabilitation potential of walkers, this thesis contributes with the proposal of an onboard lower body motion capture and modeling system based on a multimodal sensor setup, used to classify the user's gait pattern. This is an important contribution of this thesis and was achieved using computer vision techniques and ML algorithms. The gait analysis is performed with two distinct approaches: a supervised approach for the discrimination of different gait patterns, and a novel unsupervised approach to track the evolution of a single user's gait pattern over time. This could contribute to the

assessment of the rehabilitation process of each individual user, allowing finer therapy session planning.

The proposed methodologies were evaluated by a group of volunteers that interacted with the ISR-AIWALKER, in a set of experiments designed to validate them. These experiments revealed promising results, that encourage further testing of the methods in a clinical environment, with patients exhibiting predominant gait disorders.

Resumo

Esta tese propõe contribuições no domínio da robótica assistiva, focando-se em metodologias centradas no utilizador para uma interacção intuitiva e segura com andarilhos robóticos, através de novas técnicas de modelação e análise. Os andarilhos robóticos são dispositivos robóticos assistivos que oferecem assistência de mobilidade a utilizadores debilitados ou idosos, além de proporcionar um potencial significativo para a reabilitação dos membros inferiores.

O objetivo desta tese é considerar uma abordagem holística centrada no utilizador, na qual o mesmo é o ponto central da operação do dispositivo. Para isso é necessário o design de uma interface homem-máquina que estime com precisão o estado e a intenção do utilizador de forma a garantir a sua segurança, bem como a navegação mais segura do dispositivo. Conhecer o estado do utilizador pode facilitar o desenvolvimento de outras aplicações, como o uso do dispositivo como ajuda para fins de reabilitação, fornecendo análise de marcha e avaliação terapêutica. Para alcançar esse objetivo, foi desenvolvido um andarilho robótico, o ISR-AIWALKER, uma plataforma robótica instrumentada projectada para realizar pesquisas sobre reabilitação e robótica assistiva. Com base nesta estrutura, as contribuições propostas deste trabalho são: (i) uma interface homem-máquina intuitiva e segura, integrando um inovador módulo de navegação para assistência de mobilidade segura, (ii) novas técnicas de modelação de curto alcance dos membros inferiores do utilizador com base numa estrutura de sensores multimodal, e (iii) novos métodos de análise de marcha a bordo, que aprendem o padrão de marcha do utilizador, visando ajudar a identificar patologias e avaliar a progressão da terapia, servindo como uma ferramenta de diagnóstico potencial para fins de reabilitação.

Seguindo um paradigma centrado no utilizador, propõe-se uma nova interface homem-máquina baseada em visão que introduz uma análise dos padrões de pega através da aprendizagem máquina, para garantir que o utilizador agarra adequadamente as pegas do andarilho. Ainda focado no utilizador, é proposto um método de navegação baseado em teoria de utilidade e em rapidly exploring random trees (RRT) para encontrar o caminho mais seguro de acordo com a intenção do utilizador. Tendo em conta o potencial de reabilitação dos andarilhos, esta tese contribui com a proposta de um sistema de captura e modelação do

movimento dos membros inferiores, a bordo do andarilho, com base numa estrutura multimodal de sensores, usada para classificar o padrão de marcha do utilizador. Este é um importante contributo desta tese e foi alcançado usando técnicas de visão computacional e algoritmos de aprendizagem máquina. A análise da marcha é realizada com duas abordagens distintas: uma abordagem supervisionada para a discriminação de diferentes padrões de marcha e uma nova abordagem não supervisionada para seguir a evolução do padrão de marcha de um utilizador individualmente ao longo do seu processo reabilitativo. Esta última, poderá contribuir para a avaliação do processo de reabilitação de cada utilizador, permitindo um planeamento mais refinado das sessões de terapia.

As metodologias propostas foram avaliadas por um grupo de voluntários que interagiram com o ISR-AIWALKER, através de um conjunto de testes projetados para validá-los. Esses testes revelaram resultados promissores, que incentivam testes adicionais dos métodos num ambiente clínico, com pacientes que apresentam distúrbios de marcha variados.

Table of Contents

List of Figures

List of Tables

List of Acronyms

AANN	Autoassociative Neural Network Encoder
DTW	Dynamic Time Warping
HMI	Human-Machine Interface
HRI	Human-Robot Interaction
HRS	Human-Robot System
IR	Infra Red
LED	Light Emitting Diode
LRF	Laser Range Finder
OC-SVM	One-Class Support Vector Machine
RGB-D	Red Green Blue - Depth
RRT	Rapidly Exploring Random Tree
SVM	Support Vector Machine
WHO	World Health Organization
wKDE	Weighted Kernel-Density Estimation
wLS	Weighted Least-Squares

Chapter 1

Introduction

"Science is not only a disciple of reason but, also, one of romance and passion."

Stephen Hawking, in "PARADE Magazine"

1.1 Motivation

Disability is an unavoidable condition of the human existence. Almost everyone will be temporarily or permanently impaired at some point in life, and those who live up to old age will face increasing challenges in functioning [1]. Limitations related to mobility can influence negatively the participation of the individuals in nearly all activities of daily living [2], [3]. Quality of life and perception of life's satisfaction have also been shown to be affected [4].

Disability is rapidly becoming a topic of relevance. The average life expectancy had a significant increase in recent decades, opposed by the decrease of fertility rates. This naturally leads to a significant aging of the population in developed countries. A strong indicator of this fact is the evolution in the old-age dependency ratio, which is projected to reach 54% in the year 2050. Instead of four persons within working age for each elderly person, the ratio will move to only two persons [5]. According to Census 2011, 19% of the Portuguese population was older than 65 years, and this value is expected to increase in the near future. According to Census 2001 [6], 6.2% of the Portuguese population suffers from one or more types of disabilities. Around 1.5% of the Portuguese population suffers from motor disabilities. Moreover, according to the Observatory of Inequalities [7], based on data provided by Eurostat, unemployment and inactivity rates are much higher among those who are disabled. This tendency brings an inevitable demand for more healthcare assistance to provide adequate conditions for a good quality of life. This implies the need for more caregiving personnel and more specialized devices, which will translate into an increase in healthcare costs.

The evidence that there is a concern with the increase of disability is the efforts already made by several world organizations. The World Health Organization (WHO) released a report discussing the importance of promoting healthcare rehabilitation services accessible to everyone [8]. Furthermore, the world report on disability [1] makes several recommendations to assist stakeholders in overcoming the barriers that people with disabilities experience. One recommendation is related to emphasize and support research on disability, to improve living standards of people with disabilities and to overcome barriers that prevent their further participation in society. To tackle this reality new technological approaches have been emerging. Such is the case of assistive robotics that intend to provide means to offer people,

requiring special needs, higher degrees of independence and less necessity for dedicated caregivers. By relieving the need for dedicated personnel, in the long run, costs with healthcare will be reduced. Robotic mobility devices, in particular, can offer increased mobility levels for people with motor disabilities and can also ultimately contribute to improve their social inclusion.

Assistive robotics will play a fundamental role in the near future. These systems will be integrated in a wide range of devices, from intelligent transportation systems, entertaining robots, and rehabilitation or mobility assistive robots. Most of these systems are designed to improve the performance or assist human users in different tasks. In the mobility devices domain, it is included conventional aids such as canes, walkers, and wheelchairs. From all these devices, the walker is the one that offers the best weight support, while promoting at the same time the rehabilitation of the lower limbs. It is typically prescribed for patients undergoing rehabilitation, like post-stroke or spinal cord injury patients, because it allows to stimulate mobility for people with lower limb residual strength. Since these devices are "Human-centered", the assistance provided to the user has to take into account the user's state. This involves Human-machine interfaces (HMI) that accurately estimate the user's intention and guarantee safety, as well as, safe navigation. Leveraging the rehabilitation capabilities of the device, gait analysis and therapy assessment can be implemented taking advantage of intelligent systems.

1.2 Challenges in Robotic-Assisted Mobility

Robot-assisted mobility is the assistance provided by a robotic agent to impaired individuals (frail or elderly users) in their daily-life activities that involve movement. These robotic agents can offer different levels of assistance, ranging from small force impulses to aid in the user's motion, such is the case of exoskeletons, to a full-body transportation assistance, in the case of wheelchairs. In this thesis, the focus is on the robotic walker, which lies between both of them. This platform offers assistance to individuals that suffer from some form of gait disorder, but that are still capable of a certain level of mobility.

In this context of robotic walkers, several challenges intrinsically related to the user interaction topology can be identified. One of the most pressing challenges is the accurate estimation of the user's intention and its translation to the platform's motion, accounting for the

user's condition/state. The user's issued commands to the walker, through a HMI, have to be consistent with the user's intention. At the same time, the motion of the platform has to take into account the user's motions and adequate the platform's motion, to avoid potential hazardous situations. For instance, the issued command may be a forward motion, but if the user's posture does not conform with the command, a potentially hazardous situation can arise, which may lead to a fall.

Another challenge, that is intimately related to the previous one, is the user's condition monitoring. This involves the development of systems and methods to model the user's posture and motion. Here, the challenge involves finding sensors capable of capturing the user's body, with an added complexity due to the user's body distance to the walker's frame, which is typically small. To tackle this challenge, a multimodal approach is conventionally most suited.

Focusing on the rehabilitation scenario using walkers, there is a challenge still briefly researched in the literature, which is onboard gait analysis. Following the previous challenge, from a user's model, systems to provide automatic assessment of a user's gait pattern are possible to develop. Techniques for pattern recognition can be employed to classify gait into different pathological classes, or techniques to track and identify evolution over time of the user's gait profile can be developed. This challenge represents a new paradigm of gait analysis using robotic walkers.

Another challenge which is transversal to the previous ones, but that directly influences all aspects of the development of robotic walkers is safety. Safety is a key issue when dealing with robots cooperating with humans. In this context, safety involves not just the knowledge of the user's condition, but as well the environment's condition. This is crucial for a safe navigation. Users suffering from gait disorders may as well be afflicted by visual impairments, as in the case of the elderly. In these cases, safety has to be accounted for, to ensure that users do not inadvertently get themselves into potentially hazardous situations. Instead of detecting falls, here, the focus is given to fall prevention. Hence, safety is considered in this thesis to be the avoidance of potentially dangerous scenarios. Preventing falls is a line of intervention that is far more important than detecting them, which the latter has been a common approach in the literature.

1.3 Main Goals and Contributions

The main goal of this thesis is to propose user-centered methodologies, in a robotic walker context, for safe and intuitive human-machine interaction and onboard user monitoring through body motion modeling for gait analysis and rehabilitation applications. The interaction between user and walker has to be as intuitive as possible, and unavoidably safe. Interacting with a walker is a task demanding full-body stimulation. The user suffering from a gait impairment, usually, presents reduced lower limbs strength, being heavily supported in the upper limbs. Motion commands are issued by the upper limbs exerting a force on the walker's frame. The proposed HMI considers both adequateness of the issued commands, for an accurate user's intention estimation, and the safety of the user's support on the walker, to ensure the user is firmly gripping the handles. Besides, addressing user's intention on a command level, an added layer of security is proposed through a safe navigation system, which avoids hazardous situations, always keeping the user in control. The rehabilitation potential of the walker is explored through the use of a multimodal sensor setup to model the user's body motion, for gait analysis applications. The use of computer vision techniques allows the construction of a 3D model of the user's body, and the use of machine learning approaches allows to assess the user's gait pattern. The following main contributions can be identified in this thesis (references to related published papers are also provided and listed in Annex 1):

- **Novel vision-based intuitive and safe HMI** ([A4][A6][A7][A8]): An HMI that breaks the force-based paradigm is proposed. The HMI replaces the use of a force sensor, with the use of a vision-based one. This allowed the use of a single sensor to deal with both issuing commands and addressing the integration of safety measures. Through the use of the sensor's hand tracking features, a machine learning approach is proposed to ensure that the reach-to-grasp gesture of the user corresponds to a safe gripping pattern. This guarantees that inadequate gripping schemes that could result in an accident due to incorrect body weight support can be avoided. The approach is based on a support vector machine (SVM) that classifies each reach-to-grasp pattern as adequate or not, according to a user-independent model previously trained.

- **Innovative walker direct control approach based on utility theory** ([A5]): This contribution is a collaborative work within the lab, being the main authorship of the method's proposal from Luís Garrote. Although the user is constantly defining the instantaneous navigational goal, the walker's control module maintains the most

adequate trajectory avoiding collisions and favoring a minimal distance to obstacles, resulting in an increased free space for surrounding people to also navigate the environment (social behavior). The user can navigate freely through the environment and if a potentially hazardous situation is detected, the system corrects the trajectory to avoid it, keeping the current goal of the user in focus. This is possible due to the use of environment perception techniques and path planning. The environment is perceived by a Microsoft's Kinect One and the main technique for path planning is based on a rapidly exploring random tree (RRT) based algorithm, which explores the traversable environment finding safe and viable paths.

- **Onboard short-range vision-based motion-capturing setup** ([A2][A4][A6]): To cope with the challenges presented by the short distance between the user and the walker, a novel motion-capturing system was proposed. A multimodal sensor approach mounted on board the device was used to capture the lower body motion while the user ambulates. Each sensor captures specific parts of the user's lower limbs. Due to the constraints of each region of interest (short distance and narrow field of view), different technologies of sensors are employed.

- **Novel 3D body motion modeling techniques** ([A2][A3][A4][A6]): Two techniques are proposed to model the user's lower body, taking into account the considered multimodal sensor setup. Both approaches combine techniques such as background subtraction, weighted kernel-density estimation (wKDE), weighted least-squares (wLS), and circular Hough transform, to segment body parts, as well as, techniques like 3D ellipsoid fitting to generate the 3D model. These techniques take advantage of stereo and RGB-D (Red Green Blue – Depth) data outputted from the multimodal sensor setup.

- **Innovative onboard gait analysis** ([A1][A2][A3][A4][A6]): Gait analysis methods based on machine learning are proposed. The goal is to characterize gait patterns using features extracted from the user's lower body model. The use of supervised machine learning techniques is proposed to extract features and classify the gait pattern of the user according to distinct pathological gait pattern classes. Furthermore, an unsupervised machine learning method was also proposed to identify changes in the gait pattern over time. The method is based on a combination of autoassociative neural network encoders (AANN) or autoencoders, and a one-class support vector machine (OC-SVM). This method analyzes the gait pattern through its unitary element, the gait cycle, using both a

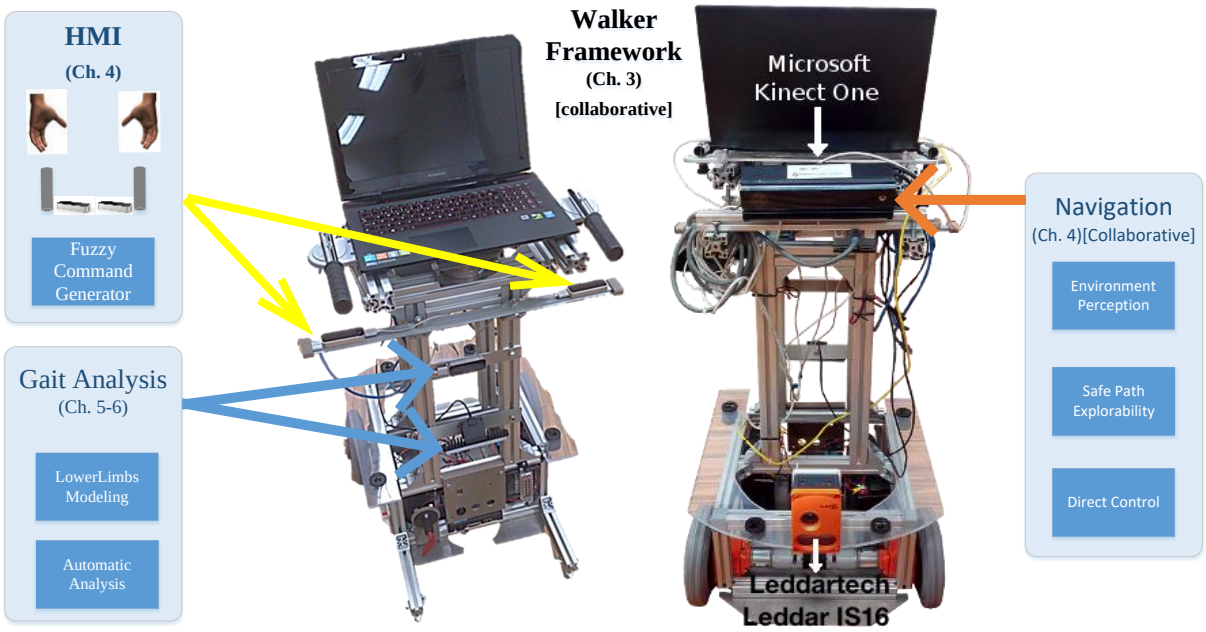

Figure 1.1. Thesis map with reference to chapters including original contributions and collaborative contributions (navigation system).

kinematic and a spatiotemporal feature extraction approach.

1.4 Thesis Outline

Figure 1.1 shows the thesis map, where chapters comprising the main contributions are highlighted. The remainder of this thesis is organized as follows.

Chapter 2. In this chapter, a comprehensive description of key concepts that guided the development of the robotic walker and its systems is provided. The state of the art of the two main topics explored in this thesis are also analyzed. For the first topic an overview of the developed HMIs for robotic walkers is presented. The other topic is the field of gait analysis, in particular, an overview of the works that have been conducted in the robotic walkers' context is provided.

Chapter 3. This chapter presents the robotic walker framework built to enable the development of the proposed methods presented in this thesis. It presents the mechanical structure of the walker, as well as, the multimodal sensor setup designed to implement both the HMI and the onboard gait analysis system.

Chapter 4. Here, the proposed mobility assistance solution is described. This involves both the HMI and the navigation system. Both systems compose the mobility assistance

module that simultaneously ensures user's intention estimation and safety.

Chapter 5. This chapter, which introduces the second main topic of this thesis, describes the two approaches developed to build a 3D model of the user's lower body. Two complementary safety systems to ensure an adequate walker handling based on the user's posture are also proposed. The systems directly influence the walker's behavior generated by the motion controller.

Chapter 6. This chapter presents the machine learning methods proposed to achieve both a supervised gait assessment, and the novelty detection strategy proposed to provide gait pattern shift detection over time. A brief summary of the related work of the unsupervised learning approaches used for gait analysis is also provided to contextualize the contribution of this thesis' chapter.

Chapter 7. Experimental results related to each developed module are presented in this chapter. Experiments were performed using the robotic walker framework presented in Chapter 3.

Chapter 8. This chapter draws the conclusions and proposes future work.

Chapter 2

State of the Art on Robotic Walkers

2.1 Introductory Concepts

2.1.1 Assistive Robotics

Assistive robotics has largely been referring to robots that assist people with motor disabilities through physical interaction. This definition is nevertheless outdated because currently assistive robots are used in a much broader scope, including assistance through non-contact interaction, such as those that interact with convalescent patients in a hospital or with senior citizens in nursing homes [9]. An assistive robot is a Human-Robot System (HRS) that follows a semi-autonomous control scheme, where both human and machine agents are able to influence the control of the system. Research in the fields of assistive robotics includes robotic wheelchairs [10]–[13], minimally invasive surgery [14], surveillance, search and rescue [15], [16], intelligent mobility assistants [17]–[20], companion and rehabilitation robots [21]–[25], manipulator arms for motor impaired humans [26], [27], or educational robots [23]. The robotic walker is part of this domain of robotics. It offers users with reduced mobility a means for locomotion. Walkers belong to the mobility devices category.

2.1.2 User's Intention

Intention recognition is an important task for human-agent interactions since it can make the robot respond adequately to the human's intention. Developmental psychology and cognitive neuroscience studies suggest humans have an inherent tendency to infer other people's intentions from their actions. This provides an intrinsic ability to understand other people's minds and plays a fundamental role in establishing coherent communication amongst people [28]. Inspired by this, different researchers have been working on detecting user's intention for improved human-machine interaction in general, [29]–[32]. Knowing a user's true intention opens up the possibility to: (i) understand his/her activity at the earliest (before the activity is even completed); (ii) constrain the space of possible future actions and provide context [4]; and (iii) correctly understand his/her action, for example, in the event of a motor neuron disorder where actions might not reflect true user's intention [33]. Consequently, detecting user's intention has, in recent years, gained significant attention in human-robot

interaction (HRI) research. Endowing robots with the ability to understand humans' intentions opens up the possibility to create robots that can successfully interact with people in a social setting as humans would do. By observing user's intention, a robot can potentially consider implicit commands and user's desires that are not explicitly stated. In this thesis, the reference to user's intention is assumed to be related to the navigational intention of a user when operating a mobility assistance device. In this context, the robot has to understand the user's intention through the user's motions and assist the human with an adequate motion. This concept of user's intention guided the design and development of the walker's HMI.

2.1.3 Human Gait

To develop an efficient and usable gait analysis system, first, it is essential to understand human gait, specifically its phases and the relevant body part components involved in the process.

In the medical and rehabilitation fields, the heel strike is used to divide the gait cycles [34]. Each heel strike on the ground separates the left and right strides. In [34] a study was performed to assess the relevant parameters needed to be monitored in order to fully characterize a gait cycle. Both a spatiotemporal and a joint excursion analysis of the patients' legs were performed. The conclusion was that the best parameters that should be considered for the analysis of the gait cycle (from heel strike to heel strike) are gait speed, step length and frequency (spatiotemporal parameters) and parameters related to the hip, knee and ankle joints (kinematic parameters). These considerations guided the development of the gait analysis system proposed in this thesis.

Since the target population of walkers is individuals suffering from gait impairments, gait analysis for evaluation of such impaired gait persons needs to be compared with data from healthy people. Walkers are intended to operate either in a domestic scenario, as in the case of elderly people, or in a clinical scenario, as in the cases of surgery recovery or rehabilitation therapies, due to injuries and degenerative diseases. The studies presented in [35][36] provide reference data for spatiotemporal and joint angle parameters. These studies reference data from 233 healthy subjects at different gait speeds. Another study [37] provides data for gait parameters obtained in a walker-assisted scenario with disabled subjects. This work is very helpful to provide an insight on how gait parameters are influenced in such cases. These studies concluded that between normal and assisted-gait, the most relevant difference is a shorter step length in the latter case and that the overall spatiotemporal parameters all suffer a reduction. Furthermore, in healthy individuals, no differences were observed between left and right stride,

which means that a healthy gait does not present an asymmetrical pattern.

Gait analysis, however, does not just relate to lower limbs tracking. In fact, the upper body is also relevant. The analysis of the trunk's movements and posture as well as the shoulders alignment, provide relevant information when facing free ambulation. In the scope ofthis thesis, upper body monitoring was not tackled, due to the fact that the user is supporting his body weight on the walker's handles. However, The author considers that upper body motion can potentially be of relevance, even in this case, and as such that analysis for the future work is proposed.

2.2 User's Intention on Robotic Walkers

One of the main goals of this thesis focuses on determining the user's intention specifically for walker platforms. However, in this section works that address the user's intention estimation considering other mobility aids will also be referred, for a better understanding of the panorama of HMIs currently available for mobility devices.

The research around the user's intention estimation for the wheelchair framework is the most mature. A lot of works arise from this particular framework, but the majority are not suitable for the walker framework. Most of the research focuses on the user's intention estimation based on the use of joysticks or hand movement, as well as, more unorthodox ones like tongue or chin control. The control of a wheelchair using a joystick is the most conventional interface, already commercialized with every electric wheelchair. Some researchers implemented new techniques to improve the joystick paradigm. A good example is presented in [38], where a force feedback is applied to the joystick providing the user with an assistive interface that varies the force required to move the joystick in different directions according to the distance to obstacles detected by 16 sensors.

The hand control interface is a newer approach. The hand posture and motion is captured by the use of wearable sensors, like accelerometers and gyroscopes, and then different gestures are classified. The user's intention is determined by each gesture to control the wheelchair. In [39] the hand gestures are obtained through the use of a three-dimensional accelerometer. The sampled data are segmented and trained using a Hidden Markov Model. Gestures recognized are applied to the wheelchair control.

These previously mentioned HMIs are suitable in the context of wheelchairs, however, in

a robotic walker scenario, they do not apply. The user needs both hands to support his body weight, and as such, HMIs which involve hand gestures or joystick control are not suitable.

There is another approach using a Brain-Computer Interface. This interface does not require the user to move any physical part of his body. Instead, it requires the user to wear a helmet with several electrodes. The user focuses on a specific stimulus to perform an action. So far, the outputs are discrete in time and list-based decisions, for example, left or right, or a short list of destinations. For the walker scenario, this HMI would, in fact, allow the user to use his upper-limbs solely for support. However, the problem with this approach is that the user is moving around which induces a lot more noise into the interface, not to mention that a significant deal of concentration is demanded, which makes it unfeasible while ambulating. An example of this interface is [40] that uses the P300 wave that is an event-related potential. The algorithm distinguishes between several locations in a list (familiar environment) in order to command the wheelchair's control that drives it autonomously and smoothly to the desired destination. There is also the option of stopping the wheelchair.

In summary, the wheelchair framework is a different paradigm from the walker, since the user is seated and the intention of the user can be accurately inferred from one hand movement. The walker, on the other hand, has the user standing and actively moving around the environment, pushing the device. A lot of attention has to be given to the whole-body posture.

The literature on robotic walkers presents two main approaches to HMIs. The direct HMI has the user actively exerting a force on the walker, while the indirect HMI interprets user's motion to infer the desired walker's movement.

2.2.1 Direct Human-Machine Interfaces

Direct HMIs typically depend on force-sensing technologies, either underused 6 degree-of-freedom expensive force/torque sensors, or unprecise low-cost options with low repeatability. Besides this, force-sensing technologies degrade rapidly with time. The walkers PAMM and VA-PAMAID [41][42], MARC walker [43], the platforms in [44], [45], and the forearm support-based Simbiosis walker, that also efficiently combined feet mounted ultrasonic sensors [46][47], all implemented force/torque sensors. On the other side, there are walkers like the ones presented in [48][49], which used force-sensing resistors and strain gauges, respectively. Another approach the CAIROW walker [50] equipped the support bar with several force resistors. Compared to these previously mentioned works, the approach proposed in this thesis replaces force-sensing, entirely, by a vision-based solution. This also allows the introduction of integrated safety measures, while the previous works had to implement a

complementary system to address safety. Another interesting work is the ASBgo walker [51], where forearm supports are coupled to a low-cost joystick and springs, providing a safe HMI due to its body weight support topology, complemented with a body distance safety system. Comparing this approach to the ones mentioned in this state of the art chapter, the use of springs is an interesting solution, serving the same purpose of avoiding force-sensing and defining a neutral position. Since the user is supported by the forearms the need for a safety measure to ensure safe gripping becomes secondary. Another well-known work, the walker Guido [52], presents a combination of force sensors and switches, working in different modes.

All of the previously mentioned HMIs require some form of gripping from the user. This author considers that a mechanism to analyze the way the user grips the handles is fundamental for a correct operation of the device, namely to prevent accidents. This author notes, however, that none of the works mentioned above employ any kind of safety measure to actually perceive if the user is correctly gripping the handles.

2.2.2 Indirect Human-Machine Interfaces

The works found in the literature that follow an indirect HMI paradigm are based on the use of laser range finders (LRF). Some examples of this paradigm are the JAIST Active Robotic Walker (JARoW) in [53], its evolution the JARoW-II [54], and the work in [55], which combines one LRF with inertial sensors, which integrate a wearable belt placed on the user's waist. These indirect interfaces provide an interesting alternative, they employ LRFs to detect the legs' positions in the provided 2D plane, operating consistently no matter the gait pattern. However, an important aspect to consider is the fact that in certain scenarios, like for instance Parkinson's disease, the users require an active propulsion to start walking, a phenomenon known as freezing of gait (FOG) [56]. With these kinds of indirect interfaces alone, such assistance is impossible to provide due to the fact that an initial leg motion is required. However, the use of complementary technologies, like voice commands to order a motion from the walker, has been used to overcome this limitation.

Table 2.1 summarizes the works mentioned and provides an overview of the current HMIs on walkers. A dedicated extensive overview on robotic walkers is given in [57],[58].

Table 2.1. Overview of the literature on user's intention on assistive robotics.

Reference	Walker	HMI	Technology
[41] [42]	PAMM and VA-PAMAID	Direct HMI with parallel handles	3D force/torque sensor on the center of the HMI
[43]	MARC	Direct HMI with parallel handles	2x 3D force/torque sensors being one for each handle
[44]	Walking Helper II	Direct HMI with forearm support	3D force/torque sensor on the center of mass
[46][47]	Simbiosis	Direct HMI with forearm support	3D force sensors and ultra-sounds
[48]	XR4000 platform based walker	Direct HMI with parallel handles	Force resistors on each handle
[49]	Unnamed walker	Direct HMI with parallel handles	Strain gauges on each handle
[50]	CAIROW	Direct HMI with support bar	Force resistors along the bar
[51]	ASBGo	Direct HMI with forearm support	Springs and joystick
[52]	Guido	Direct HMI with collinear handles	Force sensor and switches
[53][54]	JARoW	Indirect HMI	LRF extracting 2D plane of the shins
[55]	UFES Smart Walker	Indirect HMI	LRF extracting 2D plane of the shins and IMU placed on the user's waist

2.3 Gait Analysis on Assistive Robotics

The other major topic of research addressed in this thesis is the introduction of gait analysis on board robotic walkers. Taking into account the rehabilitation scenarios where walkers are employed, the author believes that there is a potential interest in the development of tools for the analysis of gait that can assess gait pattern classification and evolution tracking on board mobility devices. Such tools could help healthcare professionals in improving patient follow-up procedures and in elaborating more accurate diagnostics. This section presents works regarding human motion tracking and modeling strategies, which involve body parameters analysis and monitoring, more specifically, gait parameters like stride, balance, and other relevant parameters. Part of the works presented are not directly related to the walker

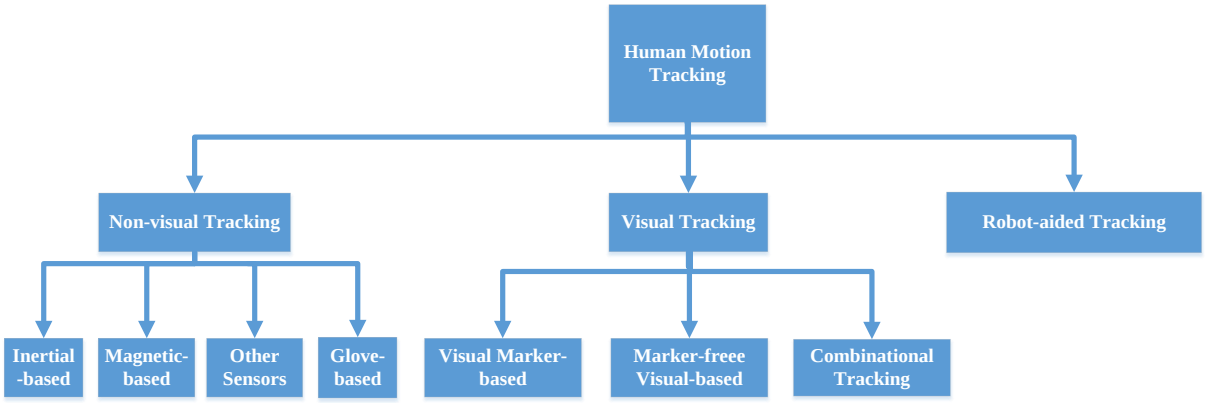

Figure 2.1. Taxonomy of human motion tracking.

framework, but are of important mentioning to understand the existing approaches that have a potential application for this particular scenario.

Looking at the literature, woks regarding human motion analysis, with particular interest to the robotic walker context, can be divided into four groups, according to the technologies used to capture data relative to the human motion. These groups can be derived from the observed ones in Figure 2.1 and are as follows:

1. Use of fixed cameras pointing to the subject that wears markers on specific body parts (visual tracking group);
2. Use of fixed cameras pointing to the subject, without the use of markers (visual tracking group);
3. Use of wearable sensors on body parts, like accelerometers and gyroscopes, as well as, sensors on the shoes or floor (non-visual tracking group);
4. Use of an instrumented moving platform (robot-aided tracking group).

The first group is the most commonly found approach to study the human body's motion, and it was the pioneering approach as well. In this approach markers, that can be passive if they simply reflect light, or they can be active if they produce a light signature, are strategically placed on body parts that represent the degrees-of-freedom of the human body, more specifically, joints or limb segments. Cameras are used to track these identifiable markers so that the body motion can be modeled. Visual marker-based tracking systems, e.g. VICON or Optotrack, are quite often used as a ''golden standard'' in human motion analysis due to their accurate position information (errors are around 1mm). This accuracy optimistically motivates popular applications of visual marker-based tracking systems in medicine and rehabilitation. A widely cited work is the Roy B. Davis III, *et al.* [59], where a visual-tracking system is used to assess human locomotion to address pediatric gait disorders. Another work uses markers solely

on the upper-body for gesture recognition [60]. There is also a well-established work performed by Sigal *et al.* [61], which led to a public dataset for gait analysis studies. They use a visual-tracking system with markers as ground truth, and multiple cameras for a multi-view perspective, to allow the development and testing of image-based tracking and pose estimation methodologies. These kinds of visual-tracking systems are expensive [62]. Besides this fact, this approach also requires a considerable amount of experience to correctly place the markers.

The second group appeared motivated by some of the drawbacks of marker-based visual-tracking systems. These drawbacks include the occlusions of markers when joints rotate or body parts overlap, along with markers drifting or wobbling. These alternate systems use cameras to collect data without the need for marker detection. However, this comes at a high computational cost, due to the complexity of the algorithms that are required to extract the right information from sampled data. These newer approaches have been proposed using other technologies, like Muro-de-la-Herran *et al*. [63] summarized. The use of visual-systems like time-of-flight cameras [64] and stereoscopic vision [65] have been proposed for gait recognition in biometrics applications. On the other hand, structured-light cameras, have been used for full-body motion analysis, as in the work [66], where the authors use the well-known Kinect camera from Microsoft, a cheap camera created to track body motion for the gaming industry. On that particular work, besides standard stride information, the authors also measure arm kinematics, demonstrating the wide range of information that can be extracted. In another work the Kinect camera is compared with a professional system for computation of precision of joint angles [67]. The precision of the Kinect is smaller than the professional motion capture system, but evidence other advantages like price, portability and it is markerless. Even so, the precision performance obtained for the main joints of the body, using the Kinect, reveals that this is currently a technology to take into account in the rehabilitation domain. Hence, for some applications the solutions in this group allow the replacement of the marker-based visual-tracking systems, offering less expensive solutions.

All the previous groups rely on visual-tracking systems that are positioned in a room with a controlled environment, and the subject has to perform the activities within the field of view of the system. Alternatively, the third group introduces the use of wearable sensors. Visual-tracking systems usually have the problem of line-of-sight, which means if an object is not in the field of view of the camera or is occluded, it cannot be tracked. Inertial sensors on the other hand, can sense relative movement or displacements. They have to be in contact with the body

part that needs to be tracked, measuring its accelerations and orientation. An example of gait analysis using inertial sensing is the work [68]. Here, the authors use inertial sensors placed on the feet to measure spatiotemporal gait parameters like stride time and relative stance. This approach is not constrained to a room, but implicates a certain degree of discomfort for the user. Besides that fact, it also requires some experience to correctly place the sensors and these may shift in position due to motion.

The fourth and last group resorts to using a platform with which the user interacts or supports the body weight while moving. This platform is instrumented with several sensors like cameras and/or force sensors in order to extract the most relevant information to describe gait parameters. This approach is the most appropriate for the concept of onboard gait analysis considered in this thesis. The robotic walker framework being a mobile platform naturally needs gait monitoring solutions that can be deployed on board. Very few works can be found in the literature, further supporting the motivation of the author of this thesis. A relevant work was performed using the MARC smart walker, where the forces/moments exerted on the handles from 22 subjects were analyzed against the information captured from a motion capture system from VICON, served to assess gait parameters [43]. This work combined both visual-tracking systems and instrumented platforms, to provide a validation of the force/moment approach to extract gait parameters. Several navigational scenarios were used and the gait characteristics extracted were heel's initial contact, toe-off, and stride time. Some other preliminary works can be found, specifically with robotic walkers. The proposed instrumented rollator walker of Wang *et al.* [69] estimates gait parameters, like gait cadence, walking speed and stride cycle, based on the readings from encoders, a gyroscope, and an accelerometer, fitted to the walker's frame. Lim *et al.* [70] uses a depth camera on a robotic walker to perceive the user's lower parts of the legs, and provide assisted rehabilitation by projecting footsteps on the floor. Some other examples, also using depth cameras, are the works which take into consideration only feet and shins, modeling them for a future disorders diagnosis application [71], or pose estimation [72]. While in [73] an approach just for feet pose estimation is proposed, without any kind of quantitative or qualitative analysis.

2.4 Automatic Gait Analysis on Assistive Robotics

The goal of modeling human motion on board the walker is a relevant contribution. However, it also paves the way to develop intelligent methods to analyze the modeled parameters. In this, section the works in the literature that provide some form of automatic classification of gait patterns are presented. The interest is in works that employ machine learning techniques to classify gait patterns. This can be either supervised or unsupervised. The supervised approach trains with different classes of gait patterns related to different pathologies. On the other hand, the unsupervised approach trains with a single class to distinguish an observable gait pattern, which in this thesis is called "normal", from unseen and untrained patterns, labeled as "novel" which are characteristically distinct from the trained one. Unsupervised learning methods are particularly interesting in the robotic walker scenario since rehabilitation, beyond merely gait analysis, is the process of determining if there is a progression in the gait pattern over time [74]. It analyzes the patient's gait with the goal of identifying perceptible changes that may indicate a positive or negative progression. This approach is conceptually identical to the traditional and most common method based on the professional's subjective visual perception, a procedure which is dependent on his accumulated experience, as described by Baker *et al.* [75], but with the goal of providing an automatic and objective tool. In this literature review, the focus is given to what has been done with gait tracking data obtained from motion tracking (points' trajectories and joints' angles over time).

Beginning with supervised approaches and looking into the literature, works suggesting the application of machine learning techniques to classify specific gait patterns can be found. For instance, Mezghani *et al.* [76] try to discriminate between an asymptomatic gait and an osteoarthritis knee conditioned gait, based on the 3D ground reaction forces. Another example, Djuric-Jovicic *et al.* [77] proposed an automatic identification system to detect disturbances in normal strides, using inertial sensors on the shank, based on a naive rule-based classification.

Considering the unsupervised approach, the one the author believes to be of interest when taken into account the nature of rehabilitation, in the literature, to the best of the author's knowledge, a single work was found, using a belt-wearable inertial sensor [78], proposes a method capable of detecting events related to gait drifts through a simple clustering technique. The author did not find any work that implemented unsupervised approaches, in the rehabilitation context, considering more complex visual features acquired from the lower limbs.

However, in the medical applications domain, there are works addressing unsupervised approaches, specifically, novelty detection techniques using more sophisticated learning

methods to detect deterioration or raise alarms, particularly in the health monitoring field. Just to mention a few examples, Gardner *et al.* [79] use energy-based statistics to extract features from intra-cranial EEG data that fed to a OC-SVM, detects the early stages of a seizure. Another example, also using OC-SVM, is the work by Clifton *et al.* [80], that identifies deterioration in vital-signs in hospitalized patients in order to generate alarms for medical staff. Another approach using multivariate Gaussian process regression, is the work by Pimentel *et al.* [81] that models vital-signs trajectories and then applies a similarity measurement to identify "abnormal" trajectories, signaling deterioration of the vital-sign data of patients recovering from gastrointestinal surgery. Table 2.2 provides a summary of the above-mentioned works.

Table 2.2. Overview of the presented literature on automatic gait analysis.

Reference	Category	Methods
[76]	Supervised	Nearest-neighbor rule
[77]	Supervised	Rule-based classification
[78]	Unsupervised	k-means clustering
[79]	Unsupervised	One-class SVM
[80]	Unsupervised	One-class SVM
[81]	Unsupervised	Multivariate Gaussian process regression

2.5 Conclusions

Robotic mobility devices, in particular robotic walkers, are envisioned as a daily life device to serve those that are afflicted by some form of gait disorder. These individuals are usually debilitated and frail, requiring a customized and reliable assistance to ensure safety.

Previous works with robotic walkers have tried to solve some of these issues but still face many challenges. The author believes that there are many areas where additional research can improve the performance of robotic walkers. This is certainly the case of user-centered robotic walker approaches. The implementation of approaches that take the user's condition (knowledge of user's posture and motion) can offer a more reliable aid. Knowing the way the user interacts with the device provides a means to design customizable and responsive devices, that lead to better HMIs in terms of natural interaction and user's effort reduction, and may lead to safer devices on which the user can trust. User-centered approaches also open new pathways

for walker applications, such as onboard diagnostics and rehabilitation therapy tracking systems. This scenario paves the way for the introduction of walkers in the medical field as devices that not just provide rehabilitation but assess the user's rehabilitation progress.

The challenges of a user-centered approach change the paradigm of looking to the robotic walker as a separate entity from the user, making it mandatory to think of the two entities as a binomial. The interaction being of permanent physical proximity, requires the safety of the robotic walker to be more than a simple safe robotic navigation. It requires the introduction of user's condition knowledge, which introduces specific constraints. The user's condition modeling is in itself a challenge. The paradigm of close proximity in the interaction's topology requires a different approach of sensor modality to properly capture the user's posture and motion.

The work developed during this thesis addressed the presented challenges, in an effort to push the robotic mobility aids domain forward. The author presents several contributions to different areas of research within this context, which led to scientific publications.

Chapter 3

Robotic Walker Framework

This chapter describes the robotic walker framework designed for the development of the methodologies proposed in this thesis. The design of the mechanical and sensorial components of the walker were influenced by the intended goals already discussed. This design stage was a crucial part of this thesis. The resulting framework is the basis for the testing and validation of all the methodologies. The following sections describe the architecture of the walker, along with the rationale behind its specific part. For a reference a video of the walker's systems can be found at: https://1drv.ms/v/s!AhZ9gZ8ru9DPiG2aDS4drjMjMdeW. This video presents the sensorial setup and each visual sensor output. It was captured at an earlier stage of implementation.

3.1 Architecture

This section describes the general architecture of the robotic walker, highlighting its main components. The architecture of the robotic walker is divided in three main components as follows:

- Robotic platform: It is responsible for the active driving of the walker through the motors. It also holds the power components to power the whole walker. This is the bottom part of the robotic walker.

- Interaction frame: It holds both the HMI and the gait analysis setup. It is composed by an array of sensors each one focused to a specific goal. This is the upper part of the walker.

- Processing unit: It is responsible to acquire data from the sensors and perform the computation for the mobility assistance and gait analysis modules.

These components make the robotic walker device was named ISR-AIWALKER. A walker prototype for the implementation of mobility assistance approaches and gait perception and analysis. Figure 3.1 shows the walker from an isometric rear perspective.

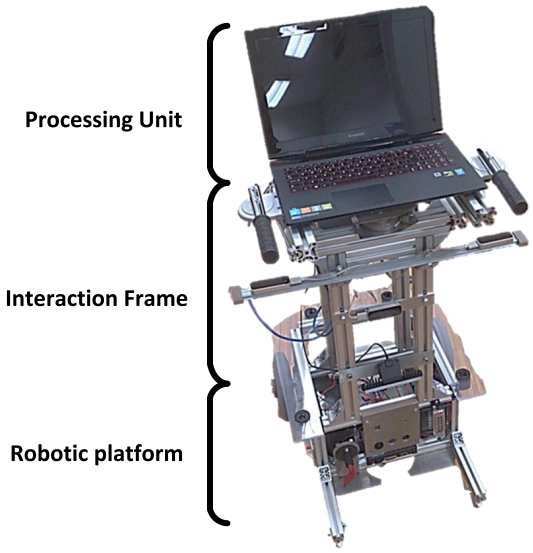

Figure 3.1. ISR-AIWALKER's architecture.

3.2 Robotic Platform

The robotic platform used to drive the robotic walker was entirely built at the Mechatronics lab of ISR – UC. It is composed by a differential motorized platform with two rear castor wheels for an improved stability when users support their body weight. The platform was designed to drive a nominal load at 80 kg, while structurally it can support higher loads. It is equipped with two motors from Maxon, integrating a gearhead and encoder on each. The motors are driven by a power controller from Roboteq, on which a PID controller was designed and implemented for a fast response from the motors. The platform is powered by lithium-ion batteries which are managed by a Battery Management System also developed at ISR – UC. The mechanical design and assembly had the technical contribution of lab members André Lopes and Daniel Almeida.

3.3 Interaction Frame

The interaction frame is the structure that is supported by the robotic platform. It holds both the HMI and the multimodal sensor setup for human motion capturing. In this section, its architecture is presented exposing the several decisions made for each chosen component according to the intended goals.

3.3.1 Human-Machine Interface

The proposed HMI follows an architecture similar to a conventional walker, with a parallel handle configuration. The sensor technology employed to estimate user's intention replaces the use of the traditional approach with force sensing technologies. This solution is inexpensive and does not degrade with time. The sensor used is the vision-based hand tracker device from Leap Motion. The Leap Motion sensor is equipped with two infra-red (IR) cameras and three IR light emitting diodes (LED) to illuminate the scene. The side-by-side cameras capture the scene at 100 Hz. The sensor outputs the position of each hand's points relative to its reference. In the proposed setup two sensors were used one for each handle, positioned under them at a distance of 15 cm and perpendicular to the handle's longitudinal axis (see Figure 3.2).

Since the Leap Motion is a vision-based sensor, the interaction of the user with the interface requires a displacement of the handles to infer a command. Each handle will slide forward and backward, returning to the center position, due to the use of springs. The sensors capture this sliding displacement when the user grasps the handles. The stiffness of the springs is dimensioned to offer a small resistance, giving the impression of pushing a light device.

The displacement of the hands when gripping the handles is directly related to the compression distance of the springs, making it possible to determine the user's push or pull force and infer a continuous range of commands instead of simple binary ones (forward, stop, turn right, etc). The schematic representation of the proposed interface is shown in Figure 3.2.

The inputted signal that refers to the user's intention to the system is the displacement of each hand given by the respective sensor, specifically the Z-axis variation of each hand's palm position, when the user grasps the handles, which is the parallel axis to the handle's

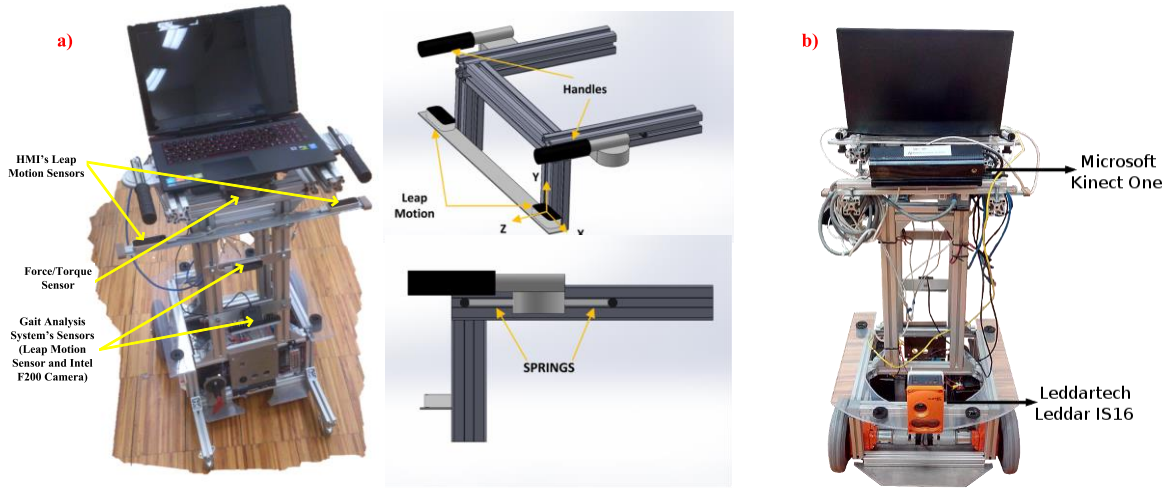

Figure 3.2. ISR-AIWALKER's sensor setup: a) rear view and the HMI's schematic, b) front view.

displacement, as seen in Figure 3.2. The development of the HMI is detailed in Chapter 4.

As a means to validate the proposed HMI and a future work perspective, the interaction frame was equipped with a 6-axis force/torque sensor from ATI. In the future, this may be used to study the support forces exerted on the walker by the user, while walking.

The interaction frame is also equipped with a mounted Microsoft's Kinect One for the perception of the environment. The RGB-D camera facing the front of the walker captures the surroundings in order to detect the walkable path possibilities and constraints, as seen in Figure 3.2. A Leddartech's Leddar was also placed on the walker to monitor the immediate close proximity in front of it, as an additional safety feature to avoid collisions.

3.3.2 Multimodal Human Motion Capturing Setup

For the design of the lower limbs perception system, several constraints had to be respected. First, the use of any form of sensor that would require any physical contact with the user to eliminate any possible discomfort was discarded, which invalidates the use of both inertial sensors or marker-based tracking systems. Taking this into account, the biggest challenge was the fact that the user's lower limbs move within a very short distance from the walker's platform. Hence, to capture their motion, the use of a single sensor is not viable. This suggests the need to adopt a multimodal approach. Furthermore, since it is necessary to deal with short-ranges, not every sensor system is applicable. For instance, if the use of 3D approaches is desired, then the used cameras need to have a very short effective minimum range, which excludes cameras like Microsoft's Kinect or Asus' Xtion.

Two body regions were identified for this multimodal strategy. Waist and legs were divided into one region and feet into another. To capture waist and legs the walking kinematics was considered. While walking the user's knee joint can typically get closer to the sensor, at distances shorter than 100 mm. To be able to use a 3D approach in this work, the only sensor that was able to cope with such short-ranges was once again the Leap Motion Controller.

Figure 3.3. Raw data of the sensors and multimodal setup on board the ISR-AIWALKER: a) raw IR images of the Leap Motion sensor, b) shows on the left the RGB image and on the right the colored depth map, and c) presents the multimodal setup on board the ISR-AIWALKER and the sensors' regions of interest.

Describing the sensor more specifically it is a sensor composed by two side-by-side IR cameras, which can be used as a stereo sensor, with a minimum effective range of 25 mm, with a resolution of 640x240. It was placed approximately at the height of the knees, facing the legs. The sensor's provided raw data from both of its IR cameras can be seen in Figure 3.3. For feet capturing, the effective minimum range is greater than for the legs. As such, the option was to use a system that could provide a broader range of data, instead of just an IR pair of images. So, an RGB-D approach was opted for, which is a commonly used sensor in motion tracking. However, even in this scenario, the minimum effective range is a constraint. The only viable RGB-D sensor found, was the Intel's F200 front facing camera, with a depth sensor's effective range starting at 150 mm and 640x480 pixels. In this case, it is possible to have access to a depth map created through IR structured-light projection and RGB image, as well. The sensor was placed facing the feet from a top-down tilted perspective. The raw data from this sensor can also be seen in Figure 3.3.

A panoramic of the proposed setup can be seen in Figure 3.2 and Figure 3.3, showing where the sensors are integrated on board the ISR-AIWALKER platform.

Chapter 4

Mobility Assistance

In this thesis, mobility assistance is assumed to be the combination of both user's intention estimation and safe navigation assistance. This chapter presents the proposed HMI encompassing user's intention estimation, safe navigation, and safe walker handling.

4.1 Human-Machine Interface

From the analysis of the state of the art, this author defined to develop an HMI with the specification goal of following a user-centric strategy. A cost-effective solution with the constraint of not hindering performance was also considered. The final design followed an all-in-one approach, that integrates both interaction and safety capabilities, in a compact and versatile solution. This section describes the development of the Human-Machine Interface implemented on the ISR-AIWALKER, as outlined in Figure 4.1. The user's intention input signal is the position of the hands of the user given by the Leap Motion sensors. Three modules are responsible for the HMI's operation as shown in Figure 4.1,. The first module filters the Leap Motion sensors' signals to remove noise and outliers, as soon as the user starts to perform a reach-to-grasp gesture . The second module is responsible for guaranteeing that the user is correctly gripping the walker's handles. This module determines if the performed reach-to-grasp pattern is safe for the operation of the walker, providing the "clear for operation" signal. If safety conditions are not met, the motors are locked and a warning auditory cue is triggered. The last module, the interface's command generator, is responsible for translating the hands' displacements into a range of navigational commands. These modules operate continuously in a loop.

4.1.1 Inferring User's Intention

The purpose of any HMI is to translate an intention, which is expressed by an interaction

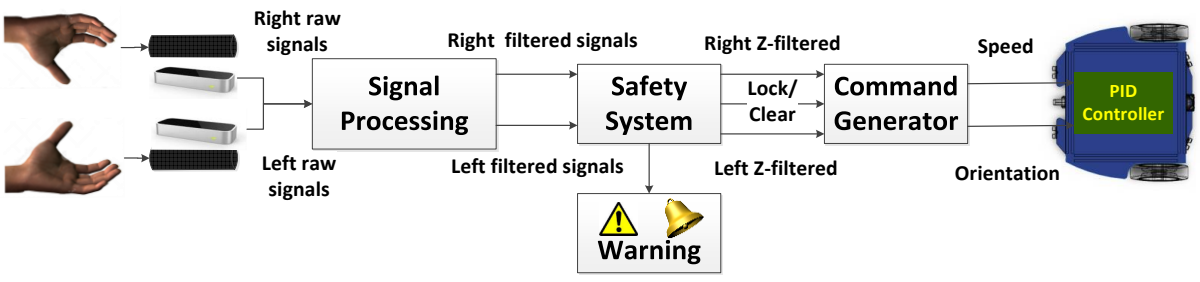

Figure 4.1. Human-machine interface's flowchart.

behavior or action, into a command. This interaction should be as intuitive as possible for a good acceptance from the user. During the interface's design, a study was performed motivated by the desire of accurately estimating the user's intention. This involved, determining the most suitable combination of handles' displacements that directly relate to specific maneuvers (navigational commands). This is a crucial study for the appropriate implementation of the chosen controller's strategy used in the HMI. In this thesis the author opted to use a fuzzy controller (command generator), due to its suitability in translating expert knowledge that take the form of rules, into accurate commands. The result from this study provide the definition of rules that govern the controller's operation. This allowed to focus the design of the HMI toward an intuitive and accurate user's intention estimation.

First, the aim of this study was to understand the correlation between the forces/moments exerted by the user on the walker with the corresponding linear velocities and curvature angles, involved in each walker maneuver (turn left, walk forward, etc.). The next step was the analysis of the correlation between the relevant forces on each maneuver and the handles' displacements. The linear velocity and curvature angle were calculated from the motor encoders at every sample, considering that the platform is actually a differential robot. The linear velocity and curvature angles are calculated at every sample, from the motor encoders, according to (4.1), respectively. Where V_L and V_R are the velocities at the left and right wheel respectively. The constant d is the distance between the two driving wheels.

$$V = \frac{V_R + V_L}{2}, \theta = \frac{(V_L - V_R)}{d} \tag{4.1}$$

Five healthy volunteers between 25 and 35 years old were invited to collaborate in this experiment. They were asked to perform specific maneuvers with the walker, like walk forward, turn left/right 90º and walk backward. The device was passive at this point, which required the

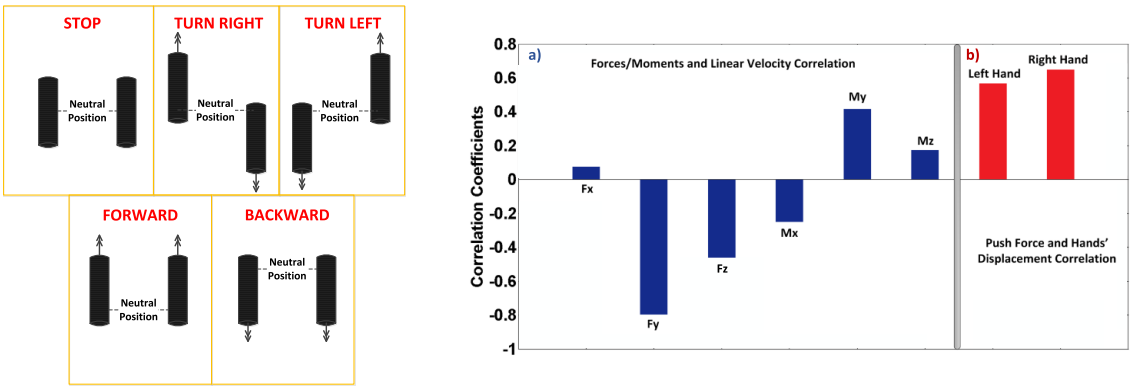

Figure 4.2. HMI's combination of commands, and the correlations for a forward maneuver a) between forces/moments and linear velocity, (b) between push force (Fy) and hands displacements.

user to maneuver the full weight of the device. A dataset was collected and all the post-processing was done offline.

Considering the force/torque sensor shown in Figure 3.2, its coordinates system is composed by the up vertical axis which is the positive Z, followed by the forward positive Y (pointing towards the front of the walker) and right positive X. The results from this experiment revealed that for a linear motion the force in Y is highly correlated with the linear velocity and poorly correlated with the curvature angle. For forward and backward maneuvers, the set of handles displacements is characterized by both handles being either pulled or pushed towards or from the user, respectively. In the case of sharp turns, the relevant variable is the moment around the Z axis, which is highly correlated with the curvature angle and poorly correlated with the linear velocity. Both handles slide in opposite directions, depending on the side of the turn. The combination of possible commands implemented on the HMI, derived from this study, is represented in Figure 4.2

As an example, Figure 4.2 also shows a forward maneuver from a standing still point to a total halt, showing the correlations between forces/moments and the linear velocity, as well as, the observed relevant force for this specific maneuver, the push force (Y axis), and the handles displacements. As a result of this experiment a set of decision-making rules was obtained. This set of rules was then integrated into a fuzzy-logic command generator.

4.1.2 Signal Processing

The first processing stage is related with the acquisition of the Leap Motion sensors' signals. Each sensor outputs the positions of several hand points with a precision of millimeters.

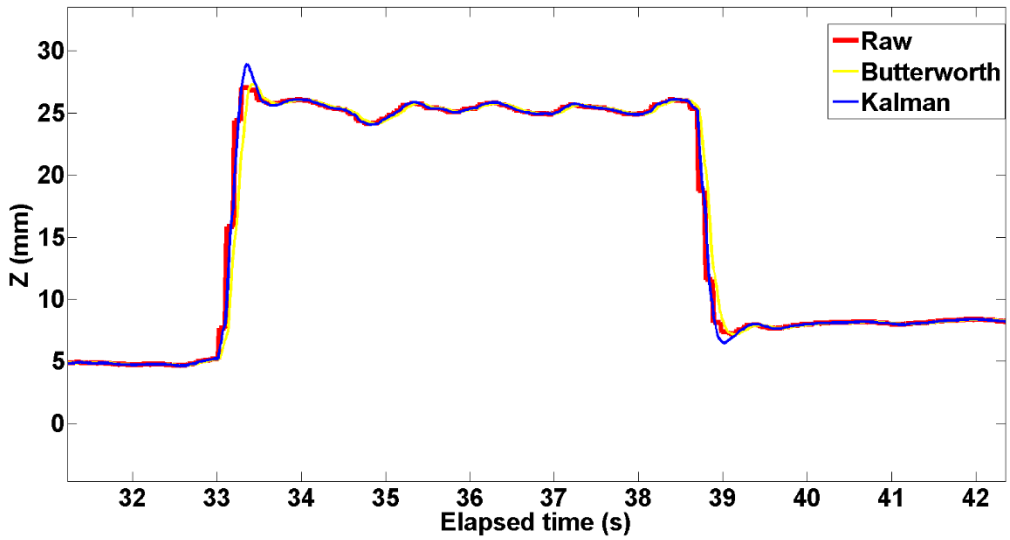

Figure 4.3. Command signal filter comparison.

For this work the relevant point for navigational command is the hand's palm's position, particularly, the Z-axis variation. Although several other points are used for feature extraction (addressed in the safety system) and the definition of the neutral position of the user's hands (addressed in the command generator strategy).

The processing of the signal represents the implementation of filters to remove possible outliers and noise from the measurements that can be affected by the vibrations of the structure (irregularities of the ground or user's involuntary hand movements). An important factor to take into account when addressing this kind of applications is the delay time between the user's command and the actual walker's response, the filter has to be designed so that the response time is less than the perception of the user, which for this kind of applications it is known to be around 200 ms [82].

A Kalman filter was used to eliminate high-frequency components in real-time. For evaluation purposes, a comparison was made between the implemented Kalman filter and an offline Butterworth filter, which is considered the ideal case scenario. Figure 4.3 presents the variation of the Z coordinate of the left hand, processed through different filters, during a turn right maneuver. It is perceptible that the Kalman filter smoothens some of the noise and offers a fast response. The delay time is much lower than the perception time aforementioned. The slight overshoot of the filter can be neglected since it rapidly settles with no real noticeable abrupt acceleration changes.

4.1.3 Gripping Safety System

The safety of the user is the purpose and motivation of this complementary system. Frail and debilitated individuals are highly susceptible to falls if they do not properly support their weight. Walking aids, traditionally, are recommended to those with lower limb disorders, such as lack of proper strength or gait impairments. For such individuals, walking aids provide a way to support their body weight by imposing their weight on the upper limbs. If the upper limbs are not properly placed on the grips of the walker or any other support structure, a fall is very likely to occur. An issue indirectly addressed in this work is the fear of falling (FOF) [83][84]. Individuals that are aware of their condition, often, discard the use of walking aids, fearing that their inexperience with them will lead to falls. With this proposed system, a reinforced feedback to the user is provided. In this manner, the user has the knowledge of his performance, potentially increasing the sense of confidence.

To ensure a safe operation of the robotic walker, the system detects if the handles are being correctly gripped (both hands' palms facing each other). Analyzing the reach-to-grasp

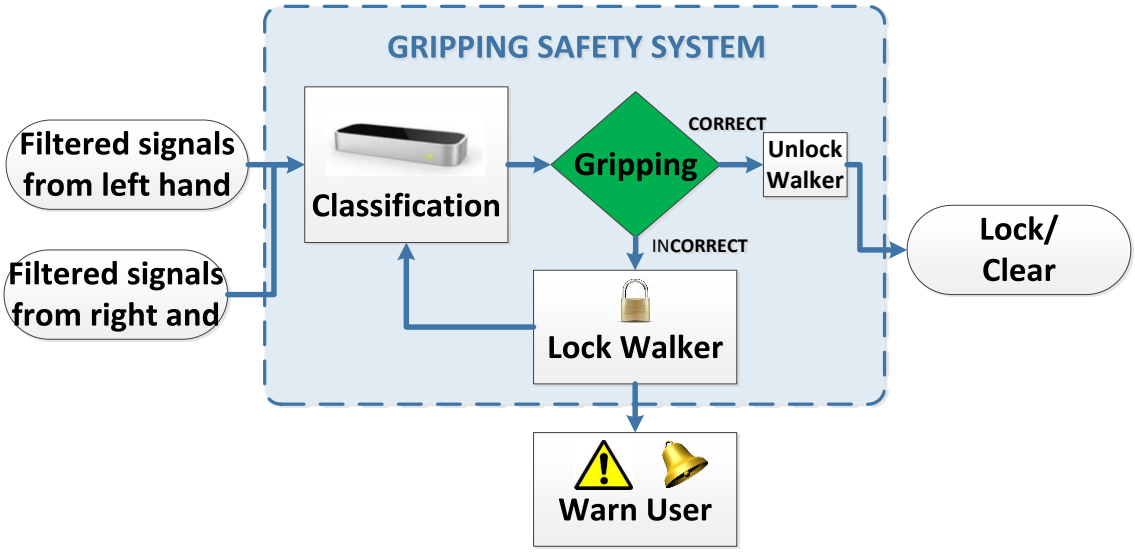

Figure 4.4. Human-machine interface's safety system's functional diagram.

gesture, the adequateness of the gripping pattern can be indirectly inferred. Each gripping is classified as suitable for operation or as unsafe.

The safety system follows the functional diagram of Figure 4.4. This system has a higher priority than the command generator, only allowing the robotic walker to move if safety conditions are met. The following paragraphs describe the development of the safety system. A contact solution was not an option, like a resistive or capacitive sensor, due to the fact that these sensors do not provide enough data to discriminate between gripping patterns neither do they have the capability to capture the reach-to-grasp gesture in all its trajectory. In this sense, the Leap Motion Controller provides an all-in-one solution.

When a hand enters the sensor's field of view the tracking of the hand and its fingers starts. A spherical region of interest with a radius of 5 cm around the center point of the grip was considered for the classification of the reaching and gripping quality, as Figure 4.5 illustrates. From the moment, the sensor identifies a hand until that hand enters the region of interest, tracking is the only task. When the hand enters the region of interest, feature extraction begins. The hand is assumed as being inside the region of interest when the center point of the hand's palm is at a distance equal or inferior to the radius from the grip's center point. At every frame this Euclidian distance is calculated by (4.2). All points refer to the sensor's coordinate reference system. The grip's center point (center point of the spherical space) is determined by physically measuring the distance between grip and the origin of the sensor's frame of reference.

$$d = \sqrt{(g_x - p_x)^2 + (g_y - p_y)^2 + (g_z - p_z)^2} \tag{4.2}$$

Where:

- g_x, g_y and g_z are the coordinates of the grip's center point.
- p_x, p_y and p_z are the coordinates of the palm's center point.

The radius of this region of interest can be explained by the morphology of a typical reach-to-grasp binomial. By observation, two stages were identified. At the first stage, the reaching movement is focused on the forearm, leaving the hand's shape unchanged. Then at a close distance from the walker's grip, the actual gripping is performed. The hand is positioned in the correct position for gripping and fingers contract to grab hold the grip. This second stage is of crucial importance to qualify the gripping, while the first is crucial to ensure a correct lock onto the hand and a precise tracking of the reaching.

Considering the second stage and since a classification of the gripping pattern is intended to be performed, the system requires a feature extraction process, which occurs for each frame of data received from the sensor. Considering the hand object, the features selected were the radius of the sphere that fits the curvature of the hand, palm position and the palm's unitary direction vector. The selection of these features were influenced by the analysis of the several points of interest tracked by the Leap Motion sensor. From that analysis, the selected three most relevant features were considered to completely define the shape and movement of the hand.

For the calculation of the sphere's radius two hand's points are projected to the horizontal plane. As illustrated by Figure 4.5 the palm's center point and the middle finger's tip, are projected to the sensor's XZ plane. The distance between these two points in this plane is the radius of the sphere that fits the hand's curvature calculated by:

$$r = \sqrt{(\mathrm{f}_x - p_x)^2 + (\mathrm{f}_z - p_z)^2} \tag{4.3}$$

Where:

- f_x and f_z are the projected coordinates of the middle finger's tip point.
- p_x and p_z are the projected coordinates of the palm's center point.

The second feature that was considered was the center point of the palm. The palm's position is automatically provided by the sensor. This point was also used for the calculation of the last feature, the palm unitary direction vector. The vector is defined by a middle finger's base point, which separates palm from finger, and the palm's center point, as in:

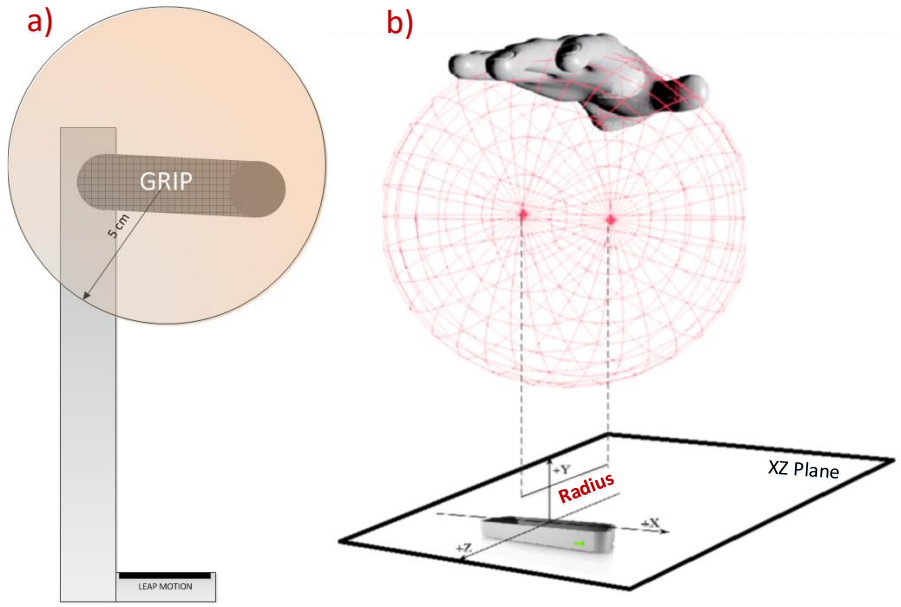

Figure 4.5. Safety system's a) gripping region of interest and b) hand's sphere radius feature.

$$\vec{d} = \frac{< F_x - P_x, F_y - P_y, F_z - P_z >}{\sqrt{(F_x - P_x)^2 + (F_y - P_y)^2 + (F_z - P_z)^2}} \tag{4.4}$$

Where:

- $F_{(x,y,z)}$ is a middle finger's base point
- $P_{(x,y,z)}$ is the palm's center point.

The resultant vector is the palm's unitary direction vector.

For classifying the gripping quality, a supervised learning model was adopted. The goal was to recognize different gestures and get a binary output. The binary output corresponds to adequate or inadequate gripping. A support vector machine (SVM) classifier was used [85].

4.1.4 Command Generator

The Command generator system developed and implemented in this work is based on fuzzy logic, which obeys the premise that precise outputs can be obtained from imprecise or vague inputs [86].

The proposed algorithm is described by the following operators: Takagi-Sugeno fuzzy inference, Gaussian fuzzifier, minimum *t*-norm, Mamdani minimum implication, maximum aggregation and centroid defuzzifier.

The inputs of the controller are the right and left Z-axis hands' displacements, that are described by the linguistic terms $T_{left} = T_{right} = \{A_1, A_2, A_3\}$ (**B**ackwards, **N**eutral and **F**orward)

Left Hand	Right Hand						
		F		N		B	
	F	Front	Straight	None	Straight	None	Right
	N	None	Straight	None	Straight	None	Straight
	B	None	Left	None	Straight	Back	Straight

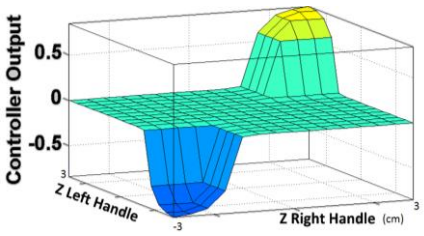

Figure 4.6. Command generator's fuzzy logic a) decision-making rules, b) Resulting fuzzy controller output for the linear speed command.

with universe of discourse of [-3,3][cm]. The fuzzy membership functions associated to A_1, A_2, A_3 are defined by Gaussian shapes.

The outputs of the controller are the linear and angular speed commands. The linear speed command is described by the linguistic terms T_{linear} = {A_1, A_2, A_3} (Back, None and Front) with universe of discourse of [-100,100][%]. The fuzzy membership functions associated to A_1, A_2, A_3 are also defined by Gaussian shapes. On the other hand, the angular speed command is described by the linguistic terms $T_{angular}$ = {A_1, A_2, A_3} (Left, Straight and Right) with universe of discourse of [-100,100][%]. The fuzzy membership functions associated to A_1, A_2, A_3 are again defined by Gaussian shapes.

The decision-making rules for the system were determined taking into account the several combinations of hands' displacements needed to infer a motion command. All the statements are summarized in Figure 4.6.

The outputs are a range of commands, which means that the higher the force exerted by the user on the handles the higher is the compression of the springs and as such the longer the displacement of the hands will be. This will result in continuous speed command curves rather than binary commands that would take the walker from a stop to a forward or turning motion without speed control. In this approach, the user's intention is reflected on the adjustment of the walker's speed. A dead-zone, where the user's motions do not cause involuntary motor commands was defined to prevent accidents when the user stops to rest or when the user performs the initial hands' approach and gripping adjustments. Figure 4.6 exemplifies the behavior of the linear speed command output of the command generator's controller given the two inputs, left and right hands' displacements.

4.2 Assisted Navigation

4.2.1 Background

This proposed method for assisted navigation is a collaborative work developed within the Mechatronics lab at ISR – UC. The contribution of this assisted navigation method, in comparison to the literature, resides in the manner the user's control power is handled, and in the behavior of the platform's outputted motion, which emphasizes a social behavior by navigating as close as possible to walls. The robot-assisted navigation combines the user's intention provided by the HMI, and the perception of the environment (inputs), to produce a safe and smooth navigational behavior of the walker (output). The decision is never taken from the user, which controls the walker at all times. A full description of the method can be found in [87]. In this thesis, a brief description of the method is provided.

The proposed method is the result of the combination of several modules summarized in Figure 4.7. At every sample, the user's intention derives from the HMI. The available navigational commands for the user have been divided into either linear motion or rotational motion. This means that during a translational motion there is no orientation decision from the user. Each time the user wants to take another orientation, the walker has to be stopped and reoriented, a behavior explained in the HMI's section. During translations, the angular velocity is controlled by the assisted navigation method. At each sample, the method perceives the environment and analyzes the possibilities (candidates) for safe navigation. If the user's intention does not present an unsafe navigational option, no assistance is provided. On the other hand, if presented with an unsafe user's intention, the proposed method will provide an adequate linear and angular velocity to preserve safety, resolving the conflict.

To better understand the contribution of the overviewed method, the relevant works performed using walkers are presented. There have been several works along the years that address robotic walkers. However, not all of them address assisted navigation. In this section,

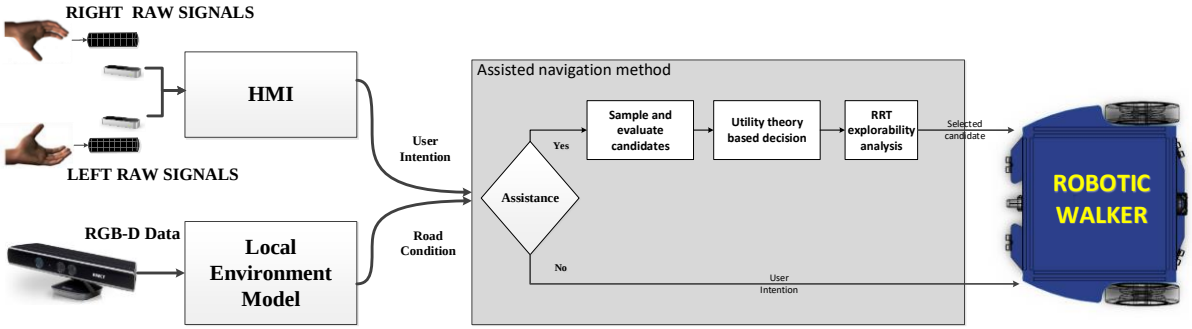

Figure 4.7. Robot-assisted navigation's functional diagram.

focus will be given to the works that have implemented some form of robot-assisted navigation in the context of robotic walkers.

A precursor in the robotic walkers domain is the PAM-AID walker [42], designed to augment the independence of visually impaired people and sufferers of mobility problems. The walker is not motor driven for locomotion, but employs an actuator to control the orientation of the front wheel. Equipped with an ultrasonic array on the front, the navigation assistance involves the detection and avoidance of obstacles. There is no assistance with an active propulsion of the motion and no assistance with trajectory corrections considering the environment, to follow straight paths like in corridors. Another work, the PAMM smart walker [41], employs motorized locomotion as well as a sonar array and a camera. This system allows the user to define a destination within a previously provided map, and from this point the walker takes the control of the navigated path, using marks on the ceiling (structured environment) and the sonar array to navigate and avoid obstacles. These previously mentioned works receive the user's input through the use of a force/torque sensor on the handles. The assistance is either just an obstacle avoidance approach or a structured environment and map dependent one, making the devices not very versatile for new scenarios. Similar to these approaches other works were published [88],[44] and [89]. An even simpler approach, the work described in [90] with the JARoW device, detects obstacles but does not avoid them.

More robust navigational approaches have been proposed resorting to simultaneous localization and mapping (SLAM) techniques. This kind of approaches suggest a direction to avoid obstacles and keeps the device's motion adequate in accordance with the perceived environment, always taking into account a map. The walker Guido described in [52] and the ARSO walker presented in [91], are two examples of this approach.

The previously mentioned works rely on the principle that the user controls the platform at a higher level. The user determines goals, but does not control the navigation process at all times. They guide the user, knowing the goal *a priori*. The proposed system provides an assistance which helps the user navigate, but does not take the power of navigation from the user. It empowers the user with the decision of navigating the environment, but with an abstraction layer which offers safety against collisions and maintains smooth trajectories considering the traversable possibilities within the perceived environment.

4.2.2 Methodology

In this section, the approach of the robot-assisted navigation method for the ISR-AIWALKER is overviewed, and can be diagrammatically seen in Figure 4.7. The method

includes a utility based decision step and a safety stage based on a rapidly exploring random tree (RRT). The methodology presented in this thesis belongs to the family of semi-control approaches, known as direct user control [17]. The platform's operator maintains most of the motion control duties and is aided when a critical or predefined situation is detected based on the provided user's intention. The proposed method has two main input variables, the user's intention and a local environment model.

Chapter 5

Human Gait Tracking and Modeling

The second main topic addressed by this thesis is human motion analysis. As previously stated, human motion analysis on board mobility assistive devices is a challenge and it is still an open field of research. This fact by itself represents an opportunity and motivation to contribute to this field of gait analysis empowered by mobility devices.

To be possible to analyze human motion, or more specifically human gait, first, it is necessary to model it. Human gait analysis has a predominant focus on the lower limbs. However, the upper body is also important to analyze posture and weight distribution that ultimately affect gait. As mentioned in Section 2.1.3, the proposed modeling strategies focus only on the lower limbs, because in the considered application scenario, the user is supporting his body weight on the walker's handles. This support automatically compensates any posture imbalances of the upper body, so the upper body analysis was not considered relevant. To model the lower limbs, data from the multimodal sensor setup, presented in Figure 3.2, were used. It is important to note that in this thesis, the term lower limbs refers to waist, legs, and feet.

Two modeling strategies were developed to model specifically waist and legs:

- Skeletal Approach: This approach considers the fitting of a linked kinematic model with joints and segments fitted to the waist's and legs' projection.

- Shape-based approach: The waist and legs are segmented by their parts and fitted using 3D ellipsoid shapes, which are linked through the anatomic joints.

The development of two modeling strategies was meant, in a first stage, to acquire expertise in this domain, and in a second stage to evaluate the potential of each strategy.

For feet segmentation and modeling a single strategy that combines depth and RGB data was used. The feet modeling serves to estimate the feet's position. However, it is also used to determine heel strike events. Heel strike events divide each gait cycle and it is an important parameter used in gait analysis.

This chapter also includes the description of two safety systems that use the output of the user modeling strategies. The author opted to include them in this chapter due to their dependency on the modeling methods. These systems are directly connected with both the modeling strategies and the motion controller. They use the information of the user's posture to adequately adjust the walker's motion to guarantee safety.

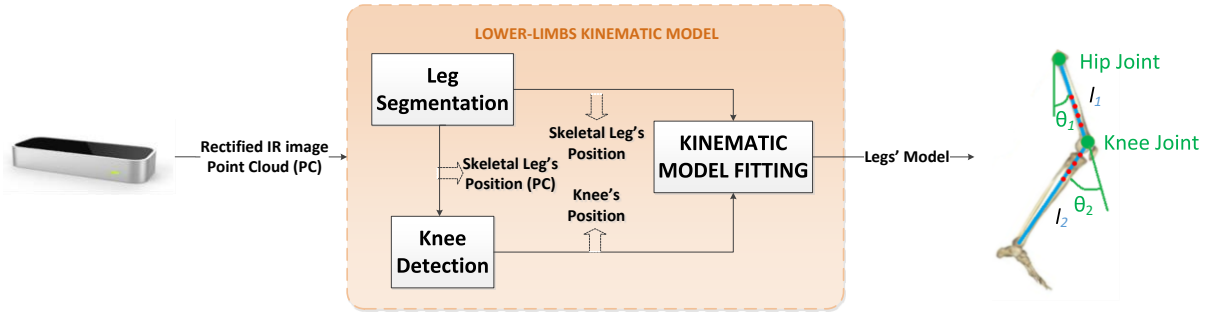

Figure 5.1. Skeletal modeling's functional diagram with kinematic model limb where red dots represent fixed distance points to the knee joint.

5.1 Skeletal Modeling Strategy

The functional diagram represented in Figure 5.1 presents the different modules that compose the proposed skeletal modeling strategy taking advantage of the considered sensor setup. This section presents a detailed description of the techniques used to implement it. The sensor responsible for the perception of the waist and legs is the Leap Motion sensor, as explained in Section 3.3.2. It is placed facing the coronal plane of the user (frontal view), but the data are handled so that it is possible to have a projection in the sagittal plane (side view). The waist and legs are modeled as a two-link robotic arm model, seen from the sagittal plane perspective. The model has two links, with the hip and knee as two joints, as shown in Figure 5.1. To build this kinematic model the following sequence of steps is required.

5.1.1 Raw Data and 3D Point Cloud Reconstruction

This subsection is transversal to both of the above-mentioned skeletal modeling strategies, since they both rely on the same sensor setup and data representation. The Leap Motion sensor, although specialized for hand tracking, also provides access to the raw data obtained from its two IR cameras, as seen in Figure 5.2 a). The objective of this first processing step is to project the perceived waist's and legs' points into the sagittal plane. To achieve this, it is necessary to obtain the point cloud from the Leap Motion's stereo images. This involves the offline calibration of both cameras to estimate their intrinsic parameters and the estimation of the translation and rotation of one of the cameras relative to the other (base image). This was achieved with the help of the toolbox presented in [92].

The remaining steps are addressed at each new frame and are as follows:

1. The parameters from the calibration are used to rectify the stereo pair of images to make

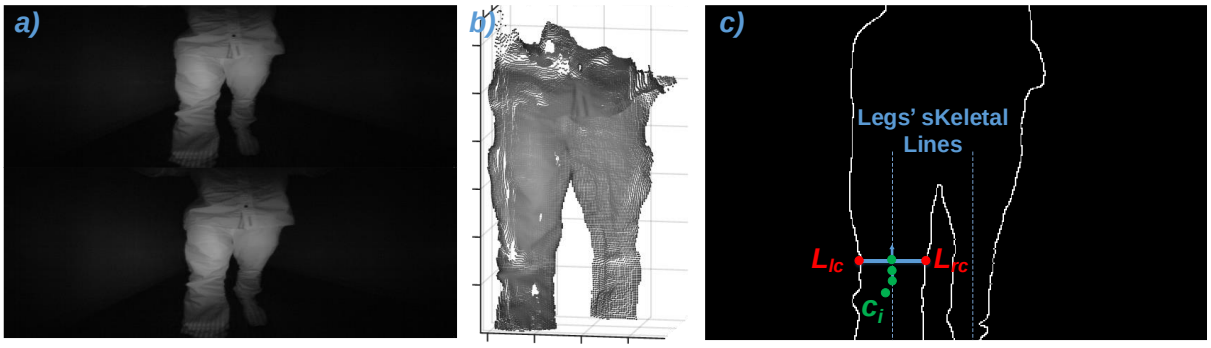

Figure 5.2. Lower limbs' modeling method. a) presents the stereo raw data, b) 3D point cloud reconstruction, c) waist and legs contour where the skeletal line of each leg is determined.

them appear as though the two image planes are parallel, reducing the 2D stereo correspondence problem to a 1D problem.

2. Then the disparity map is computed through a semi-global matching technique [93], this computes the distance in pixels between corresponding points in the rectified images. Disparity is proportional to the distance between the cameras and the 3D world point.
3. The final step is the reconstruction of the 3D scene using the outputs from the previous steps. As a result of this step a 3D point cloud is provided (see Figure 5.2b for an example of the resulting point cloud).

5.1.2 Leg Segmentation

In this step, both legs are first segmented by identifying the two vertical lines that are equidistant to each leg's contours in the frontal plane (left and right contour). Using the image with registered pixels corresponding to the points in the point cloud (base image described in the previous step), a Canny edge detector is used to extract the contours of the waist and legs. Figure 5.2 c) shows an example of the resulting waist and legs contour. The process of extracting each leg's vertical line consists in computing the set of center points between the left and right contour for every horizontal line in the leg area (points c_i in Figure 5.2 c). This set is then used to compute the average v-axis coordinate that will define the vertical line that passes through the leg. Algorithm 3 describes this process which is performed at every frame.

A limitation of this approach is that for individuals with gait patterns like scisor patterns, that present lateraly bended legs below the knees, which can cause each leg's frontal view not to be modeled as a vertical line, the result of the legs' segmentation can become unreliable.

5.1.3 Knee Detection

To build the kinematic model of the lower limbs it is imperative to find the position of

Algorithm 3: Legs Segmentation

Input : $\{I_C=(u,v)\}$

1 $L_{cp} : L_{cp} \leftarrow \{\}$ (set of v-coordiantes of left leg's between contour points)

2 $R_{cp} : R_{cp} \leftarrow \{\}$ (set of v-coordiantes of right leg's between contour points)

3 $N : N = 0$;

4 **for** each row of I_C **do**

5 **if** $(numberofcountours == 4)$ **then**

6 $L_{cp} := L_{cp} \cup \{middle(I_C(i, contour(1)), I_C(i, contour(2)))\}$;

7 $R_{cp} := R_{cp} \cup \{middle(I_C(i, contour(3)), I_C(i, contour(4)))\}$;

8 $N++$;

9 **end if**

10 **end for**

11 $L_{cp\_final} := \Sigma L_{cp} / N$;

12 $R_{cp\_final} := \Sigma R_{cp} / N$

Output : $L_{cp\_final}, R_{cp\_final}$

the knee (one of the model's joints). In the previous step a vertical line that passes through the center of each leg is determined. The points laying in these two lines in the image have a direct correspondence to points in the point cloud. These points' projection in the ZY-plane (sagittal plane), correspond to the legs' surface profile (red dots on Figure 5.3 a).

Considering the projection of each line in the ZY plane, to find the knee's position the process is divided into two steps. In the first one, a Y-value for the knee's height position (y_{det}) is naively estimated. This value is most probably in the vicinity of the position where the knee is actually located. In the second step, a curve interpolation is used in the vicinity of that Y-value to find the accurate knee's height. This final step only uses points that belong to the part of the leg where the knee is most likely to be. As shown in Figure 5.3 a), each projection is divided into two halves ($y_0/2$). For each half, a line is fitted using a least-squares approach. The intersection of the two lines provides the y_{det} point of each knee.

Next, a fourth-degree Fourier curve is fitted to each leg's projection, only concerning a band of points within the vicinity of the knee's position. The vicinity is defined by the points in the gate $(y < y_{det} + \tau) \wedge (y > y_{det} - \tau)$, where τ denotes the limits of the gate. The band of points is defined by points belonging to lines parallel to the line used during leg segmentation.

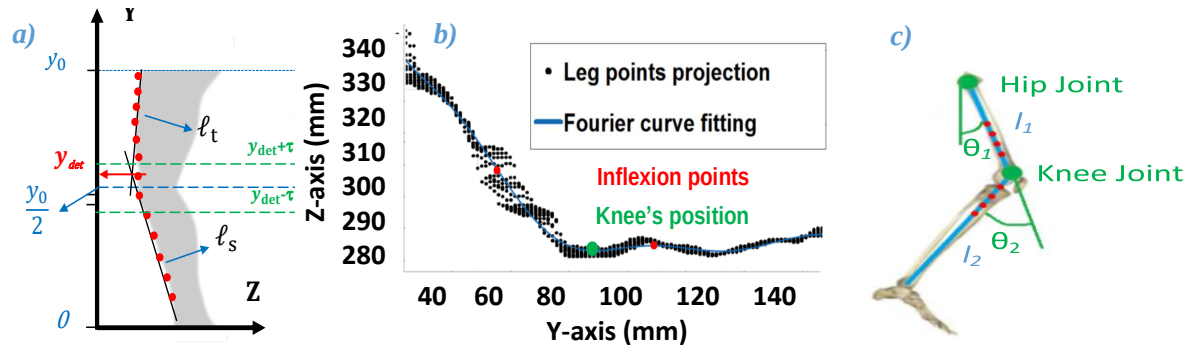

Figure 5.3. Continuation of the lower limbs' modeling method. a) presents the knee's Y-interval estimation, b) the fitting to the leg's point cloud interval projection to determine the vertical knee point, c) kinematic model for each lower limb where red dots represent fixed distance points to the knee joint.

Analyzing the resulting curve for each leg, as exemplified in Figure 5.3 b), one can realize that the knee's position lies between two inflection points of the fitted curve. To determine this position, the second derivative of the curve is computed. The knee's position is the global minimum in the Z-axis between the inflection points. The output of this step is each knee's point position's height (Y-value). With the Y-value computation each knee's position is completely defined by its 3D position, by combining it with the already determined X-value and Z-value.

5.1.4 Kinematic Model Fitting

The kinematic model employed is a two-link robotic arm model (thigh and shin) with two joints (hip and knee). This model is fitted into the 3D points that belong to the sagittal plane described in the previous step. The basic problem that needs to be solved is the identification of the angles of each leg joint. Considering Figure 5.3 c), the forward kinematics equations that rule this model are given by:

$$\begin{aligned} x &= l_1 \cos(\theta_1) + l_2 \cos(\theta_1 + \theta_2) \\ y &= l_1 \sin(\theta_1) + l_2 \sin(\theta_1 + \theta_2) \end{aligned} \tag{5.1}$$

The model in the right part of Figure 5.3 c), clarifies the equation's variables. To minimize the complexity of the minimization problem, which scales up with the number of considered points, only a subset of equally spaced points along the two lines were taken into account, as illustrated in Figure 5.3 c) (red dots). The angles are determined by a least squares minimization of the respective model points' positions against the points' positions with the same Y-value given by the sensor's points projections in the sagittal plane. The error function is given by (5.2), where N is the number of fitting points used.

$$E(x) = \frac{1}{N}\sum_{i=1}^{N}(x_{imodel} - x_{isensor})^2, i = 1, ..., N$$
$$E(y) = \frac{1}{N}\sum_{i=1}^{N}(y_{imodel} - y_{isensor})^2, i = 1, ..., N \quad (5.2)$$

The goal is to minimize it taking into account several combinations of joints' angles as in:

$$\min_{\theta_1,\theta_2} E(x)+E(y) \quad (5.3)$$

5.2 Shape-based Modeling Strategy

The shape-based strategy intends to find a 3D model of the lower limbs through the segmentation and modeling of the several lower limbs' parts, fitting them to 3D ellipsoid shapes (at the point cloud level). These interconnected ellipsoids define the lower body model. The shape-based strategy can be summarized by the functional diagram represented in Figure 5.4. The segmentation of each lower limb part is achieved by consecutively finding the plane that divides the left and right leg regions followed by the segmentation of the thigh and shin regions on each leg.

The first step determines the YZ plane which segments the left and right leg regions. For this purpose, a wKDE technique is used. This segmentation is not straightforward, due to the bouncing movement of the waist during walking, so the separation point cannot be set using a fixed-point location in the frontal plane. However, the wKDE solves this problem since it provides a density function of the distribution of the point-cloud points along the X-axis. The separation point of both legs (which corresponds to the crotch) can be identified in the density function as a local minimum of the distribution (see Figure 5.5 d).

With each leg segmented, the goal is then to find the XZ plane that passes though the knee and divides each leg into thigh and shin regions. The next step is to fit 3D ellipsoids (defined by center, length of axes and Euler angles) to each segmented region. From the 3D ellipsoids, the 3D lower limbs' parameters corresponding to joints' angles and positions can be determined, specifically, knees' positions, crotch's opening angle, hips' joints' angles (the angle of each thigh to the perpendicular line to the ground), and each joint angle of the knee. This is a basic problem of determining ellipsoids' axes intersections.

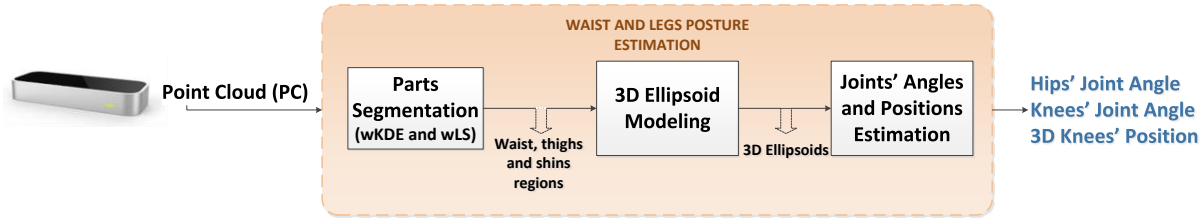

Figure 5.4. Shape-based modeling strategy's functional diagram.

5.2.1 Waist and Leg's Part Segmentation

To segment each part, there is the need to estimate the positions of the points that link them. These points are the legs' joints (crotch and knees). A method based on a wKDE followed by a wLS applied to the point cloud is proposed to achieve that, as described in the following sections.

5.2.1.1 Crotch's Position Estimation:

Assuming the crotch's position located at $P_0=(x_0,y_0,z_0)$, a wKDE is used to find in the point cloud the x-intercept (x_0), seen in Figure 5.5, of the crotch's point position, and which also determines the YZ plane which divides each leg's region allowing the segmentation of the left and right legs. As mentioned above, the x-intercept (x_0) of the crotch's position is identified as the local minimum between the peaks in the wKDE's outputted density function, where each peak represents the x-intercept, points x_l and x_r shown in Figure 5.5 a), of the left and right legs, respectively. The wKDE is computed along the X-axis, weighting the points according to their respective Y-values. The rationale for this assumption is based on the fact that the upper points in the Y-axis (waist region) have a lower potential of discriminating each leg than the points on the lower end (shins). For the points' Y-values-based weighting, a set of weights (W_{legs}) are defined as being linearly decreasing with the Y-values (decrease of height) and normalized to the range of [0, 1], as shown in Figure 5.5. Let $X = \{x_1,x_2,\ldots,x_n\}$ denote a set composed by the univariate measurements on X-axis for the point cloud, and $W_{legs} = \{w_1,w_2,\ldots,w_n\}$ are the defined weights. Given X and W_{legs}, the univariate wKDE estimate is obtained using:

$$f(x) = \frac{1}{\sum_{i=1}^{n} w_i} \sum_{i=1}^{n} w_i \, K_\sigma(x - x_i) \tag{5.4}$$

where $K_\sigma(.)$ is a Gaussian kernel function with bandwidth σ. To estimate the crotch's position y_0, the average of the Y-values of the points in the point cloud with X-values within

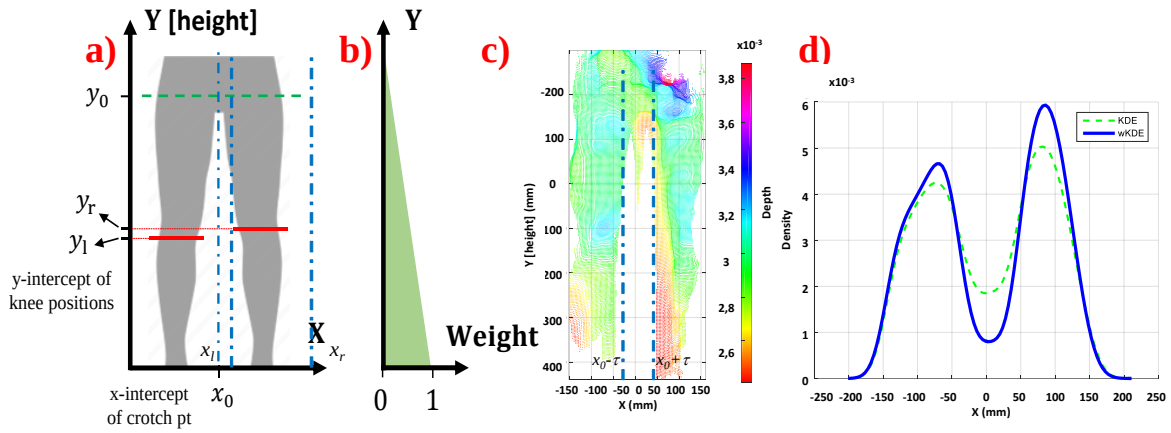

Figure 5.5. Legs segmentation a) the joints' positions with red line segments showing left and right knees' locations. The dashed blue line represents the division boundary between left and right legs. The area under the green line indicates the region where the four leg segments are located. b) The distribution of the weights used in the wKDE related with Y-axis values. c) An example of the inputted point cloud, where points are colorized based on their estimated depths (z values). d) The corresponding computed KDE (dashed-green) and wKDE (blue), with the wKDE evidencing a more expressive density distribution of points along the X-axis.

the interval $(x < x_0 + \tau) \wedge (x > x_0 - \tau)$ is computed, where τ is a fixed threshold that prevents this computation to be affected by noise or outliers (see Figure 5.5 c). The y_0 and its y-intercept define the XZ plane's Y-value which separates the region of waist and legs.

5.2.1.2 Knees' Positions Estimation:

With the determination of each leg's region (left and right) one can estimate the Y-value of each knee's position. Finding the knee's Y-value is important to divide each leg into its two segments. This is a two-step process. First, a naive separation of each leg region in the sagittal plane is computed by dividing it into two halves on the Y-axis (see Figure 5.6 a). Then, by fitting a line to the upper and lower halves of each leg, a more accurate knee's height is determined, resulting from the intersection point of the two lines. The accurate knee's Y-value determination can be further improved by considering a weighted-base line estimation. Since the initial separation of the upper and lower parts of the legs is performed using a naïve approach, the use of a weighting scheme can reduce the influence of points around the first estimation of the knee (see Figure 5.6 b), because they most probably do not belong to the associated leg's segment. On the other hand, points farther away from the legs' middle (up and down extremities) are more reliable because they have a higher probability of belonging to the correct leg segment. The line fitting is carried out on the projection of the point cloud of each leg (in the YZ plane), computing the lines ℓ_t and ℓ_s using wLS (see Figure 5.6 a). The

intersection of these lines is considered as the knee position's Y-value. Given sets of $Y = \{y_1, y_2, \ldots, y_n\}$ and $Z = \{z_1, z_2, \ldots, z_n\}$ measurements of each segmented leg on the Y-axis and Z-axis, respectively, LS fits a line, $z = my + b$ to the considered points, by minimizing the sum of squared distances of the actual points to the estimated line. By replacing n points in the line's equation, it gives an over-constrained system that can be expressed in matrix form as:

$$\underbrace{\begin{bmatrix} y_1 & 1 \\ y_2 & 1 \\ \vdots & \vdots \\ y_n & 1 \end{bmatrix}}_{Y} \underbrace{\begin{bmatrix} m \\ b \end{bmatrix}}_{\ell} = \underbrace{\begin{bmatrix} z_1 \\ z_2 \\ \vdots \\ z_n \end{bmatrix}}_{Z} \tag{5.5}$$

Considering this definition, the wLS solution, which allows dedicated contribution of each individual point to the overall error, is given by.

$$\ell = (Y^T W Y)^{-1} Y^T W Z \tag{5.6}$$

where W is a diagonal $n \times n$ weighting matrix with diagonal elements w_i corresponding to the weights associated with the points in the projection with coordinates (y_i, z_i).

To increase the robustness of the knee's Y-values positions over time (y_l and y_r values in Figure 5.5, a Kalman filter with Constant Acceleration (CA) model is used. A gating strategy is also applied as a data association tool to eliminate outliers. For each of the leg's knee, let the state of the filter be $y = [y, \dot{y}, \ddot{y}]$, where $\dot{y}$ and $\ddot{y}$ are velocity and acceleration of the knee's y-intercept position in Y-axis, respectively. The discrete time process model is given by:

$$\begin{bmatrix} y \\ \dot{y} \\ \ddot{y} \end{bmatrix}_t = \begin{bmatrix} 1 & dt & 0.5 \times dt^2 \\ 0 & 1 & dt \\ 0 & 0 & 1 \end{bmatrix} \cdot \begin{bmatrix} y \\ \dot{y} \\ \ddot{y} \end{bmatrix}_{t-1} + w_t \tag{5.7}$$

And the system's measurement model is given by:

$$z_t = \begin{bmatrix} 1 & 0 & 0 \end{bmatrix} \cdot \begin{bmatrix} y \\ \dot{y} \\ \ddot{y} \end{bmatrix}_t + v_t \tag{5.8}$$

Where w_t and v_t represent the process and measurement noise, respectively, and dt is the sampling time.

To increase the robustness of the knee tracking, the knee search area is limited to a gate in the vicinity of $y_0/2$ (as in Figure 5.6): $(y < y_0/2 + \tau) \wedge (y > y_0/2 - \tau)$, where τ is a given threshold,

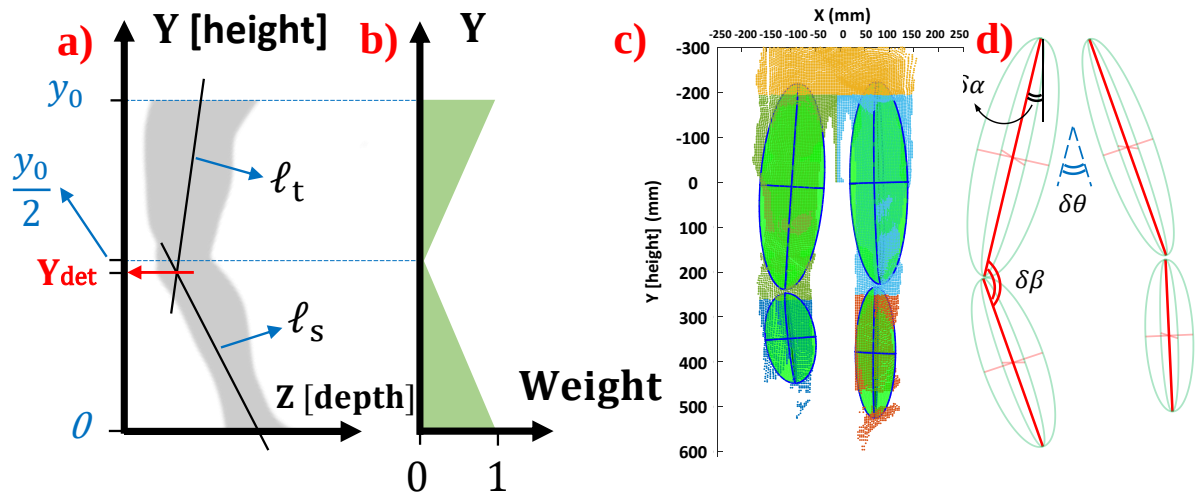

Figure 5.6. Knees' positions and 3D ellipsoids fitting. a) the lines ℓ_t and ℓ_s represent the wLS-based fitted lines to upper and lower halves of the leg's region in the point cloud, and Y_{det} indicates the intersection of the lines. b) The weights applied to the fitting of each line considering the Y-axis. the 3D ellipsoidal model of the lower limbs. d) the extracted joints' angles from the model of the lower limbs.

defined empirically to be one third of the length of ℓ_t and ℓ_s. If no measurement is available inside the gate area, the predicted Kalman filter value is used. The Kalman filter predicts each knee's y-intercept in the next scan using:

$$\begin{bmatrix} y \\ \dot{y} \\ \ddot{y} \end{bmatrix}_{t+1} = \begin{bmatrix} 1 & dt & 0.5\times dt^2 \\ 0 & 1 & dt \\ 0 & 0 & 1 \end{bmatrix} \cdot \begin{bmatrix} y \\ \dot{y} \\ \ddot{y} \end{bmatrix}_t \tag{5.9}$$

From the estimation of the Y-values of the knees' positions (y_l and y_r), the segmentation of each leg in thigh and shin regions in the point cloud is achieved.

5.2.2 3D Ellipsoidal Modelling

This method is applied to each one of the previously mentioned segmented regions. A 3D ellipsoid is fitted to each region, using Principal Component Analysis (PCA). Assuming each region's point cloud is centered (the average of X, Y and Z are equal to zero), the 3 × 3 covariance matrix of the points in each segment is given by a symmetric matrix $C = P^{T}P/(n-1)$. C can be diagonalized *as* $C = VLV^{T}$, where V is a 3 × 3 matrix of eigenvectors that represents the principal directions/axes of the ellipsoid, and L is a 3 × 3 diagonal matrix, with eigenvalues λ_i on the diagonal that is related to the length of each semi-axis of the ellipsoid.

The output of this step is a set of ellipsoids, where each one is represented by a center, length of semi-axes, and Euler angles (obtained from the principal axes and representing the

ellipsoid orientation). The 3D ellipsoidal model of the legs is presented in Figure 5.6.

5.2.3 Joints Angles and Knees' Position Estimation

As stated before, the goal of the proposed method for Waist and Leg's Part Segmentation is to obtain each joint angle of the legs (crotch, hip and knee) and knees' positions, so that a linked 3D model of the lower limbs can be created. Using the computed 3D ellipsoids, defined by their principal axes as seen in Figure 5.6, it is possible to determine joints angles and positions. These angles and positions are in the 3D space (XY, YZ and XZ planes) since it is possible to work with the principal axes' vectors. The desired parameters are then computed as follows:

- Legs' opening angle (crotch's angle): The legs' opening angle is computed by:

$$\delta\theta = \arctan\left|\frac{\vec{\ell}_t^{\,left} \times \vec{\ell}_t^{\,right}}{\vec{\ell}_t^{\,left} \cdot \vec{\ell}_t^{\,right}}\right| \tag{5.10}$$

  Where $\vec{\ell}_t^{\,left}$ and $\vec{\ell}_t^{\,right}$ are the principal axes of ellipsoids and are extracted from eigenvector matrices of the left V_{left} and right V_{right} thighs.

- Thighs' angle: These angles are computed between each thigh and the perpendicular line to the ground, using:

$$\delta\alpha = \arctan\left|\frac{\vec{\ell}_t \times \vec{z}}{\vec{\ell}_t \cdot \vec{z}}\right| \tag{5.11}$$

- Knees' angles: These are the angles between the principal axes of thigh's and shin's ellipsoids extracted from eigenvector matrices of the thigh V_t and shin V_s, using:

$$\delta\beta = \arctan\left|\frac{\vec{\ell}_t \times \vec{\ell}_s}{\vec{\ell}_t \cdot \vec{\ell}_s}\right| \tag{5.12}$$

- 3D Knees' position: The knee's Y-value was previously obtained in Section 5.2.1.2. The 3D position of the knee for each leg is estimated by computing the remaining coordinates that result from the average of the X-value and the Z-value of all the points with Y-values within the gate of the detected knee ($y < Y_{det} + \tau$) $\wedge$ ($y > Y_{det} - \tau$).

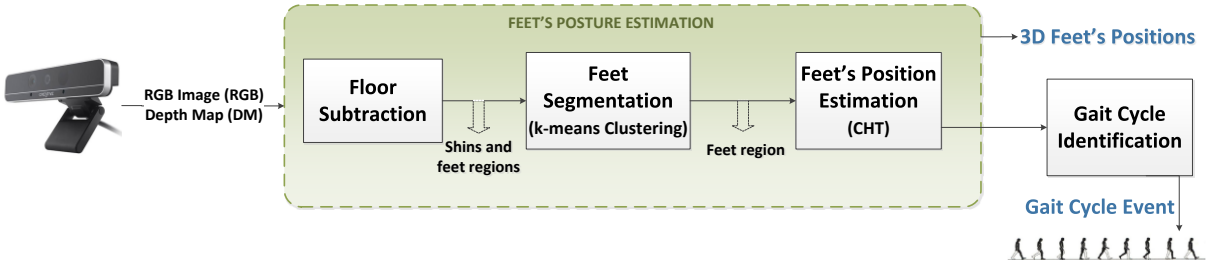

Figure 5.7. Feet's position estimation functional diagram.

5.3 Feet and Heel Strike Detection

From Section 2.1.3, it is clear that the heel strike detection is a fundamental feature when performing gait analysis. It provides the separation point between each stride and defines the window where feature extraction to classify the gait pattern should occur. The sensor that monitors the feet is an Intel F200 camera, as seen in Figure 3.2. The data that will be considered are both the RGB image and the provided depth map. The methods proposed to achieve heel strike detection through feet detection are represented in Figure 5.7 and are described next.

5.3.1 Feet Detection

5.3.1.1 Raw Data

Figure 5.8 a) and b) shows the RGB image and depth map obtained from the Intel F200 camera. It gives a perspective of the raw data collected from this sensor. Each pixel of the RGB image has a correspondence to a pixel in the depth map.

5.3.1.2 Floor Subtraction

As a basic technique in computer vision, the background subtraction allows separating the relevant data from the rest of the environment. In this context, the relevant data are the feet and the background is the floor plane, which is at a constant distance from the camera and at a certain inclination angle. The expected result is to have an image with only the feet and part of the leg, as seen in Figure 5.8 b). To reduce the computational cost, this step is done in the first frame of the image sequence and the estimated parameters are used in the subsequent frames.

The process is divided into several consecutive steps enumerated by Algorithm 4 which

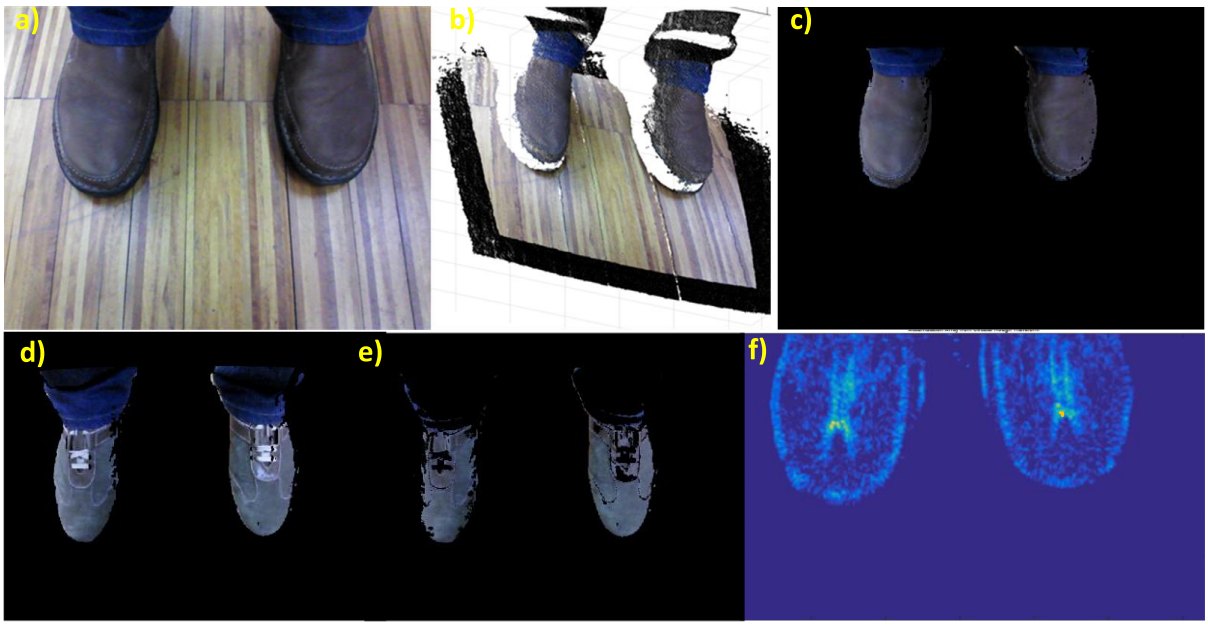

Figure 5.8. Feet detection procedure: a) and b) raw data from the Intel F200 camera, RGB image and colored depth map, respectively, c) the result of the floor subtraction on the RGB image, d) and e) the subtracted image and the result of the clustering technique used on that image on the left resulting on an image without the shins, f) the accumulation vector resultant from the Circular Hough Transform with a temperature gradient which is applied to the clustered image where the two brightest points identify left and right foot.

uses the RGB image and depth map (DM) as inputs are seen in Figure 5.9.

5.3.1.3 K-means Clustering

This clustering is performed on the RGB image, with the intention of getting a separation between the feet and the legs by color clustering. The final RGB image will only contain pixels from the region of the feet, being the remaining pixels discarded. This technique is used on the assumption that the footwear color distribution is most probably distinguishable from pants, socks, or even skin.

The K-means clustering is an unsupervised clustering method. It classifies data points

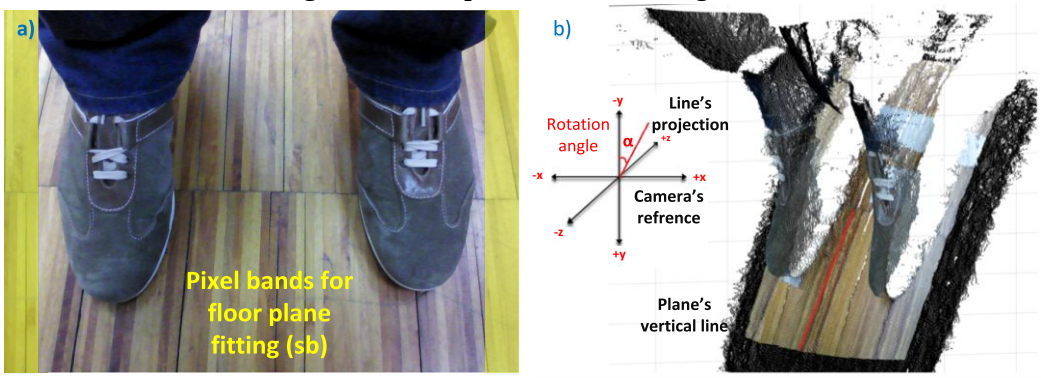

Figure 5.9. Visualization of the parameters for the floor subtraction method.

Algorithm 4: Floor Subtraction

Input : $\{RGB=(u,v), DM=(x,y,z)\}$

1 $sb : sb \leftarrow$ extracted side bands from DM, Fig 8 a)

2 $floorplane := fitplane(sb)$;

3 $l_y : l_y \leftarrow$ projected plane's line on the camera's Y-axis, Fig 8 b)

4 $\alpha : \alpha = tan^{-1}\left(slope(l_y)\right)$;

5 $DM_{rot} := rotate(DM, \alpha, camerareference)$;

6 **for** each DM_{rot} pixel **do**

7 **if** $(DM_{rot,z} > dist(floorplane, imageplane)$ **then**

8 $DM_{rot,(x,y,z)} =$ Null ;

9 **end if**

10 **end for**

11 $DM_{clean} := rotate(DM_{rot}, -\alpha)$;

12 **for** each RGB pixel **do**

13 **if** $(DM_{clean,z} == Null)$ **then**

14 $RGB_{(u,v)} = 0$;

15 **end if**

16 **end for**

Output : RGB, DM_{clean}

into classes based on the distance from each other. This distance is taken depending on the chosen metric. Points are clustered around centroids $\mu_i, \forall i=1..k$ which are found by minimizing the objective function:

$$V = \sum_{i=1}^{k} \sum_{x_j \in S_i} (x_j - \mu_i)^2 \tag{5.13}$$

Where k is the number of clusters and μ_i is the i^{th} centroid [94]. In this case, two clusters and a metric based on the Euclidian distance are considered. The result from this processing step is visible in Figure 5.8 c).

5.3.1.4 Circular Hough Transform

The Circular Hough Transform is an extension of the Hough Transform specialized in

finding circles in input images. The circle candidates are obtained from a voting process in the Hough parameter space, followed by finding the local maxima from an accumulator matrix. This technique was proposed due to the fact that the footwear's tip shape typically resembles a semi-circle.

By applying the Circular Hough Transform to the image resulting from the previous step, an accumulator matrix is obtained. This matrix has the dimensions of the RGB image, where each pixel has a value corresponding to the number of circles that pass through it. Finally, the two global maximum points of the accumulator are considered, since they will typically correspond to the feet's tip's center point. Figure 5.8 f) shows the accumulator matrix where the brightest points in the image are the maximums, allowing the visual perception of the result of the feet detection algorithm.

5.3.2 Heel Strike Detection for Gait Cycle Identification

A gait cycle or stride is defined by two consecutive heel strikes of a left or right foot., as described in Section 2.1.3. In this processing stage, the global maximum points from the accumulator matrix, obtained in the feet detection method (feet's position), are mapped into the corresponding depth map. The detection of the heel strike is a time dependent process, that basically tracks the depth variation of the swinging foot, being the most important part of the motion when it is closest to the robotic walker (see Figure 5.10). A heel strike event occurs

Algorithm 5: Heel Strike Detection

Input : $\left\{Foot_{left}=(x,y,z), Foot_{right}=(x,y,z), Leg_{left}=(x,y,z), Leg_{right}=(x,y,z)\right\}$

if ($isclosestleft(Foot_{left}, Foot_{right})$ & $isclosestleft(Leg_{left}, Leg_{right})$)

  if ($findpeaks(Foot_{left}, [T-1:T])$

    $\text{Heel}_{left\_T} := T$; ← left heel strike event

  end if

else

if ($isclosestright(Foot_{left}, Foot_{right})$ & $isclosestright(Leg_{left}, Leg_{right})$)

  if ($findpeaks(Foot_{right}, [T-1:T])$

    $\text{Heel}_{right\_T} := T$; ← right heel strike event

  end if

end if

Output : $\text{Heel}_{left\_T}, \text{Heel}_{right\_T}$

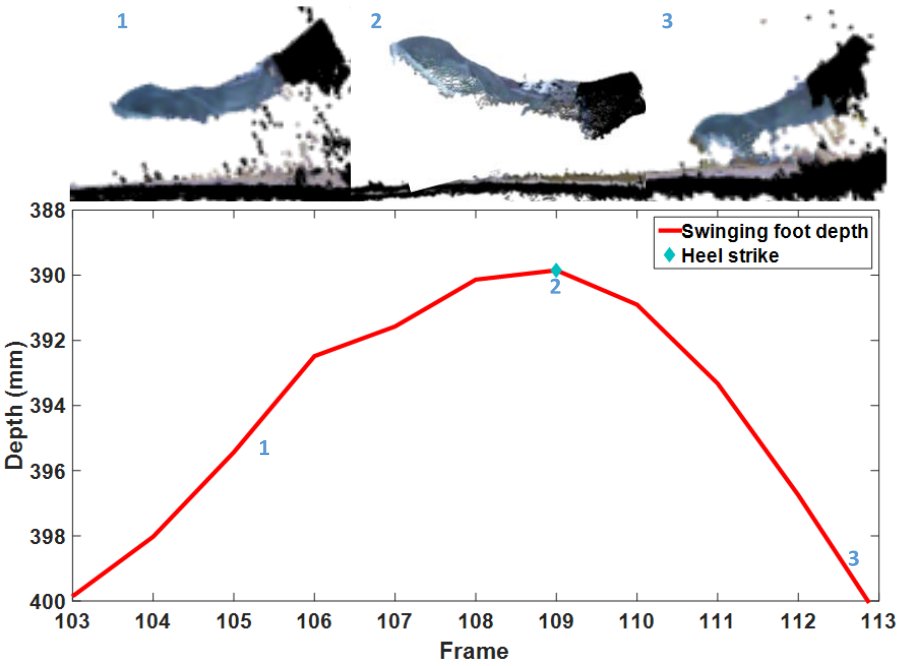

Figure 5.10. Heel strike detection during the swinging foot depth variation (sagittal plane). Point 2, gives the heel strike, which is when the foot's tip is closest to the camera and the depth evidences the lowest value.

when the considered foot's depth transitions from a rising state to a descent state. The detection process is performed on every frame, in order to identify the occurrence of a heel strike.

In this approach, gait cycles related to the right foot's heel strike were considered. At every frame, the system checks which one of the feet is closer to the walker, by taking into account its position (*x*,*y*,*z*) determined by the obtained maximum accumulator points. As a redundancy, it also checks if the corresponding side limb is the closest, because if that is not the case, then the data are unreliable. If the previous condition is met, the system checks for peak events on the depth variation using the current frame and the previous frame. If there is a peak in the depth data a heel strike is registered. This process is summarized in Algorithm 5.

5.4 User-centered Safety

When dealing with mobility devices safety is fundamental. The user of such devices typically presents impairments that affect gait and stability, and an inadequate interaction with the assistance device may prove to be hazardous. Safety needs to be user-centered and not a byproduct of the platform's navigation safety mechanism.

Looking at the literature, in one of the first works with robotic walkers A. Morris *et al.*

[88] considers some safety features in the form of navigational corrections avoiding obstacles. Most of the other research in this domain does not give special interest to the user's posture and direct the effort to the navigational challenge, discarding the manner in which the user navigates the walker [95][96][50][52][46]. Safety is, most of the time, reduced to the avoidance of possible dangerous paths (stairs, obstacle collisions, wall collisions, etc.). Other works like [97][98] provide a system for seating and standing assistance, focusing not on the navigation, but on the approach to the platform. The focus, so far, has been directed to the robotic walker as a smart platform, and not so much to the interaction between the user and the assistive device.

Taking advantage of the generated models of the human motion suggested in this thesis, two complementary safety systems are proposed. Both stability and adaptive speed control are addressed, taking into account the user's gait patterns. These additional safety systems allow the walker to move adequately according to the user's characteristics, thus avoiding accidents. These systems in combination with the safe navigation method and safe gripping system, proposed in this thesis, create a closed loop user-centered safety system. It accounts for both environment and user's condition, making the assistive device user-friendly and reliable, empowering the user with confidence in the assistance. This confidence translates itself in a more natural gait and reduces the fear of falling.

5.4.1 Stability Safety System

Taking advantage of the lower limb's kinematic model, a system to check if the user's issued motion commands are consistent with the user's pose was developed. This system brings together the HMI and the human motion modeling modules, adding an extra safety feature to the walker.

When a motion command is issued by the user, the extracted feature of the user's detected knees' positions is leveraged, to determine if the user is operating the walker within a safe region (between $dist_{min}$ and $dist_{max}$). The average position of the user's knees is considered to determine the user's distance to the walker, as proposed in (5.14). If this position is not within the safe region the walker is stopped to prevent hazardous situations.

$$dist_{\min} < \mathrm{dist}(\mathrm{average}(knee_z^{left}, knee_z^{right}), walker) < dist_{\max} \tag{5.14}$$

5.4.2 Adaptive Speed Control

The safety system here proposed takes advantage of the Weighted Kernel-Density

Estimation function computed on each frame as described in Section 5.2.1. In this method, the purpose is to use the wKDE to analyze the gait pattern using the information from the whole density function generated at each frame. The system uses the data from the Leap Motion Controller which captures waist and legs to infer partial knowledge about the conditions the user is operating the walker (normal or other type of gait pattern). If a normal gait pattern is observed then the speed profile of the walker is adjusted accordingly.

Giving the whole pipeline, as previously mentioned, the Leap Motion Controller provides two side-by-side IR images, as seen in Figure 5.11. From these images, the method reconstructs a 3D point cloud of the scene. The 3D point cloud is used to model the lower limbs as follows: (i) Following the same method as in Section 5.2.1, at every frame, Weighted Kernel-Density Estimation (wKDE) is applied to the 3D point cloud. The output is a curve of the density of the points belonging to the waist and legs along the X-axis of the image plane. (ii) A sliding window approach is used to group density functions belonging to the same gait cycle. The sliding window's step represents the duration of a gait cycle, extracted using the method in Section 5.3.2. Since the wKDE computes a fixed number of points, considering all density function within each sliding window, a set of spatial features can be extracted for each respective point

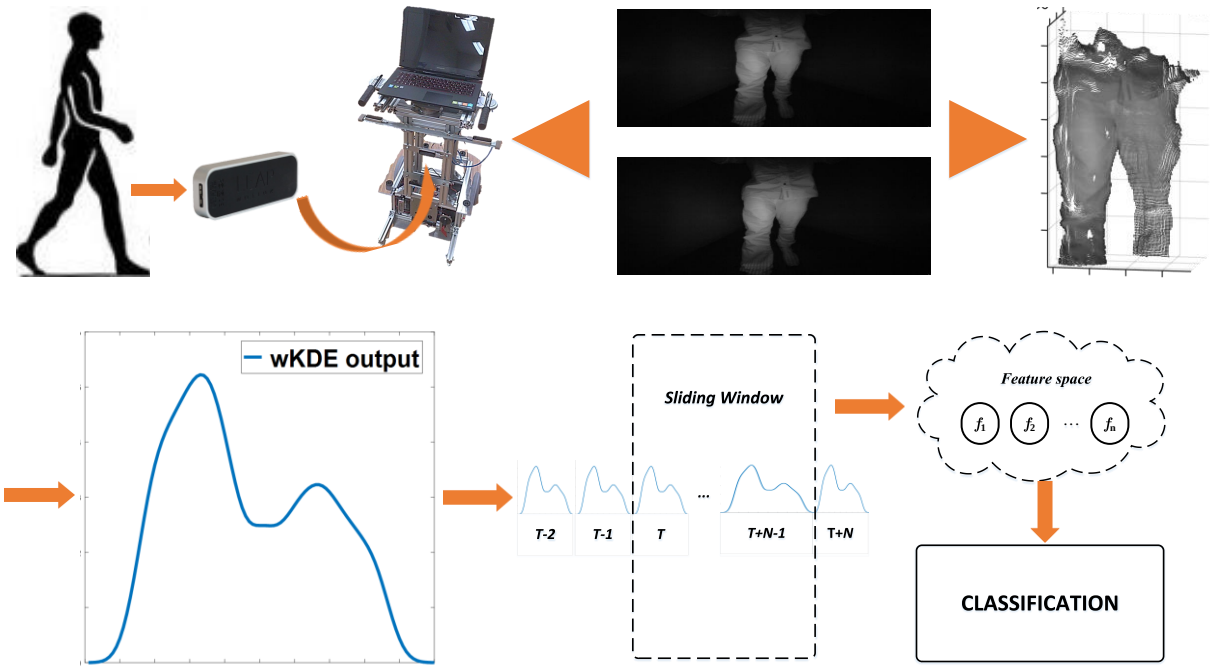

Figure 5.11. Adaptive speed control system's functional diagram: The Leap Motion on board the robotic walker captures the user's lower limbs, a 3D point cloud is reconstructed from an image stereo pair, being applied a wKDE algorithm that allows to process a density function by frame that are grouped in a sliding window to extract features and perform classification to identify gait patterns. The probabilistic output of the classifier's normal gait pattern class is fed to the fuzzy controller which adapts the speed profile according to the user's gait pattern.

of the densities. (iii) The generated feature space is fed to a classifier to label the currently observed gait pattern as one of the previously trained classes. (iv) The final step is the use of the probabilistic output of the normal class, which provides the similarity of the observed gait pattern to the distribution of a normal gait pattern. This output is inputted to the command generator which was redesigned to integrate another set of fuzzy rules. Step (i) was already described in Section 5.2.1.The proposed method is summarized in Figure 5.11.

5.4.2.1 Feature Extraction

At each frame, a density function is obtained as in Figure 5.5, the feature extraction process uses these curves to extract relevant information. From the biomechanical perspective of gait, as mentioned in Section 2.1.3, the gait pattern is divided into consecutive gait cycles, which in turn are defined by heel strike events of the same reference foot [34]. The proposed method uses a sequence of frames to extract features instead of a single frame. This sequence of frames belongs to a sliding window with a variable width, which is related to each gait cycle's duration.

Within each window, since all the sampled density functions have the same number of points, these are automatically aligned, being each point easily tracked from one function to the

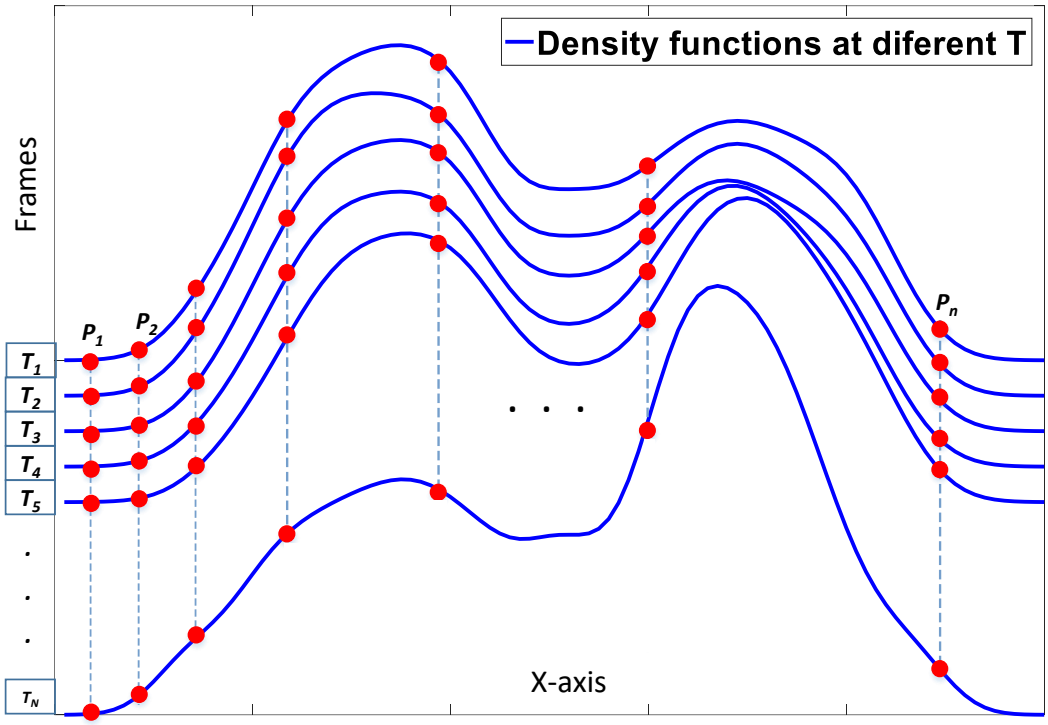

Figure 5.12. A representation of a sliding window with width N of density functions where the extracted features are computed for each respective point of the consecutive density functions, from P_1 to P_n, where T_i is the time period of each gait cycle.

other, as seen in Figure 5.12. Hence, it is possible to track each point's variation over time within the sliding window. As such, using a point-by-point approach, for all the corresponding points of the density functions, spatial features can be computed. The proposed spatial features are considered to be able of completely representing the gait cycle's variability, being time-independent. The considered features, for every P_i, $i \in \{1,\ldots,n\}$, are as follows:

- Average value;
- Root mean square value;
- Standard deviation;
- Third order moment;
- Fourth order moment.

5.4.2.2 Gait Pattern Classification

In this work, a classification strategy that could efficiently classify gait in terms of distinct gait patterns is used. Each specific gait pattern has its own gait cycle characteristics with specific variations in the gait parameters. The implemented classifier handles the obtained feature space from the previous subsection, and labels posteriorly observed gait patterns dependent on the number of trained classes.

The classifier used is a support vector machine (SVM) [99]. The feature set is normalized to guarantee that the minimum and maximum values obtained during the training stage are applied on the testing set. The SVM was trained according to the strategy "one-against-all", using a soft margin (Cost) parameter set to 1.0. The chosen kernel is a cubic kernel. For this classification strategy the training was considered to be user-independent. The data collected, only considers walking in straight lines. At this point, angular velocity and stops are not being considered for training.

5.4.2.3 Fuzzy Set Rules

An extension to the fuzzy command generator described in Section 4.1.4 was introduced, resulting in the inclusion of a new input variable representing the user's gait pattern (T_{gait} corresponding to a posterior probability), an update to the linear velocity linguistic variable (T_{linear}) and consequently an update on the fuzzy rules set. This extension provided the control

of the velocity profile of the walker taking into account the gait pattern of the user. More precisely, it affected the linear velocity of the platform, by taking into account the probabilistic output of the classifier (T_{gait}).

Considering the classifier's model described above, it is possible to obtain the posterior probability from the SVM's output. This probability is the observed instance's probability of belonging to the normal gait pattern class, which is computed from the classifier's outputs by applying the method described by Platt *et al.* [100]. The linguistic variable T_{gait} is described by the linguistic terms T_{gait} = {A_1, A_2, A_3} (Impaired, Limited and Normal) with universe of discourse of [0,1] and defined by Gaussian shapes. The outputs of the controller are the linear and angular speed commands. The linear component was updated in order to provide a finer control for smaller linear speeds. The updated linguistic variable is given by T_{linear} ={ A_1, A_2, A_3, A_4, A_5} (Back, Slow Back, Slowest Back, None, Slowest Front, Slow Front and Front) with the respective universe of discourse of [-100,100][%]. The updated fuzzy rules are given by:

- If T_{left} is Back, T_{right} is Back and T_{gait} is Limited, then T_{linear} is Slow Back and $T_{angular}$ is Straight;

- If T_{left} is Front, T_{right} is Front and T_{gait} is Limited, then T_{linear} is Slow Front and $T_{angular}$ is Straight;

- If T_{left} is Back, T_{right} is Back and T_{gait} is Impaired, then T_{linear} is Slowest Back and $T_{angular}$ is Straight;

- If T_{left} is Front, T_{right} is Front and T_{gait} is Impaired, then T_{linear} is Slowest Front and $T_{angular}$ is Straight.

If the input T_{gait} is Normal or is not defined in the previous rules, then the rules defined in Section 4.1.4 take precedence.

The evaluation of the proposed methods in this chapter (modeling strategies and safety system), as previously mentioned, is presented in Chapter 7. This was the strategy adopted for the whole thesis, and which is followed in the remaining chapter.

Chapter 6

Automatic Gait Analysis

Gait analysis is a process widely used in the rehabilitation field. It has been performed by healthcare providers for decades, mainly relying on their experience and on subjective observation techniques. In this chapter, the focus is given to the introduction of machine learning strategies to automate this process. With the introduction of machine learning methods, an alternative to subjective analysis is intended to be presented, by using automatic tools that analyze the human motion tracking data and that could give consistent and unbiased results. This machine learning approach opens the way for both, an auxiliary diagnostic technique to identify previously trained gait pattern classes, and to the identification of changes over time of a single user's learned gait pattern, which might indicate either a positive or a negative evolution.

The work proposed follows two application scenarios. The first one is motivated by the goal of identifying asymmetries in the gait pattern to help diagnose several gait disorders at an early stage. The discrimination between normal and asymmetrical gait patterns is based on the use of supervised machine learning techniques. The second scenario intends to identify changes in a single user's gait pattern over time. This goal is motivated by the focus of rehabilitation therapies, which aim to promote gradual change and identify it, to determine progress or deterioration. For this purpose, unsupervised machine learning techniques were implemented. For this second scenario, this thesis proposes two methodologies.

The use of machine learning methods relies on features. In this chapter, features to analyze gait are also proposed. Spatiotemporal features were extracted based on conventional gait parameters used in the gait analysis literature. However, the work in this chapter also goes beyond those. Features taking into account the biomechanical aspects of the human motion are also introduced.

The following sections describe the proposed methodologies in detail. The use of unsupervised machine learning in this context is one of the major contributions of this thesis. It is a particularly unexplored approach that the author believes to have huge potential when applied to gait analysis techniques.

6.1 Gait Pattern Classification

A supervised approach was the strategy used to address gait pattern classification. The focus was given to the discrimination between normal asymptomatic gait patterns and

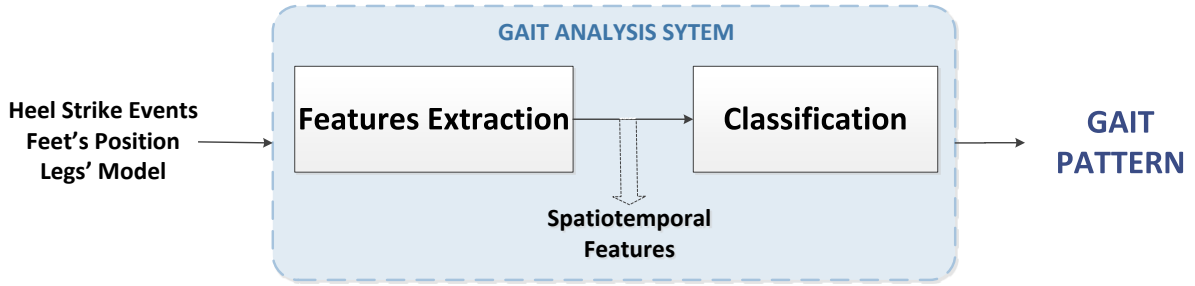

Figure 6.1. Supervised learning approach's functional diagram.

asymmetrical gait patterns. The detection of asymmetries is of significant importance since it can help to identify gait disorders at an early stage [101].

As illustrated in Figure 6.1, a set of potentially discriminative features is identified and used to classify different gait patterns. These features are fed to a classifier that learns a model of each considered gait pattern.

6.1.1 Spatiotemporal Features

For this supervised technique, the considered features were based on the studies of Section 2.1.3. In [34] spatiotemporal gait and joints' parameters are identified as relevant features. Furthermore, they describe that the spatiotemporal features are considered for each stride, which is defined as the time period between two consecutive heel strikes (hs). These features are obtained from the feet detection method and from the kinematic model. The considered features are summarized in Table 6.1.

Table 6.1. Selected features for gait classification.

Feature	Definition
Step length (at heel strike)	$dist(foot_{left}, foot_{right})$
Step time (hs to hs)	$T(hs^{T}) - T(hs^{T-1})$
Δ, μ of hip's joint's angle (hja) of swinging and support leg	$\Delta = \max(hja) - \min(hja), \mu = \frac{\sum_{i=hs^{T-1}}^{hs^{T}} hja}{N}$
Δ, μ of knee's joint's angle (kja) of swinging and support leg	$\Delta = \max(kja) - \min(kja), \mu = \frac{\sum_{i=hs^{T-1}}^{hs^{T}} kja}{N}$
Δ of knees baseline separation	$\Delta = dist(knee1_{hs}, knee2_{hs})$
Maximum swinging foot's rise ($foot_z$)	$\max(foot_z)$
Δ of the swinging foot's rise	$\Delta = \max([foot_z]_{hs-1}^{hs}) - \min([foot_z]_{hs-1}^{hs})$

6.1.2 Classification Strategy

In this approach, a classification strategy that could efficiently classify gait in terms of normal gait and asymmetric gait was used. In an asymmetric gait, right and left stride present different variations in the gait parameters, thus each stride is classified against two possible classes, normal stride and impaired stride. An asymmetric gait pattern is identified when at two strides, at least one is classified as impaired.

The classifier used is a binary-class SVM, which was implemented using the LibSVM package [102]. The feature set is normalized to guarantee that the minimum and maximum values obtained during the training stage are applied on the testing set. The SVM was trained according to the strategy `one-against-all', using a soft margin (Cost) parameter set to 1.0. The chosen kernel is the cubic kernel because it was the kernel that provided the best results during the experimental evaluation that was performed.

6.1.2.1 Support Vector machines

Since this method is based on the Support Vector Machines (SVM) classifier it is of relevance to introduce it. SVM is a discriminative classifier which maximizes the margin between classes [103], [104]. Assuming training samples x_k with class labels $y_k \in \{+1,-1\}$, then equation (6.1) can be rewritten as:

$$y_k(\mathrm{W}.\varphi(\mathrm{x}_k)+b) \geq 1-\xi_k \tag{6.1}$$

where $\xi_k \geq$ is a slack variable to cope with overlapping classes (soft constraint). The margin is given by $2/\|w\|$, therefore to maximize the margin, the SVM optimization problem is given by:

$$\min_{\mathrm{w},b} \frac{1}{2}\|\mathrm{w}\|^2 + C\sum_k \xi_k \tag{6.2}$$

$$\text{subject to } y_k(\mathrm{W}.\varphi(\mathrm{x}_k)+b) \geq 1-\xi_k \text{ for } k \in \{1\cdots K\} \tag{6.3}$$

where C is a tradeoff parameter (regularization parameter) that controls the compromise between having a large margin with more misclassifications, or having a small margin with less misclassifications, and K is the number of training samples. A strength of SVM is that it can be transformed into a nonlinear classifier in an effective way. To construct nonlinear boundaries, Kernels can be used transforming input features to a new features space [99]. A commonly used

Kernel is the Gaussian Kernel (radial basis function, RBF):

$$K(X_k, X_j) = e^{-\frac{\left\|X_k - X_j\right\|^2}{2\sigma^2}} \tag{6.4}$$

This results in a nonlinear discriminant function

$$g(\mathrm{x}) = \sum_{k}^{K_s} y_k \alpha_k K(\mathrm{x}, \mathrm{x}_k) + b \tag{6.5}$$

where K_s is the number of support vectors, and α_k are the Lagrangian multipliers used to solve the SVM optimization problem. The parameters C and σ were selected through grid search and checked with cross-validation. The learning algorithm to find the optimal hyperplane was the sequential minimal optimization (SMO) [100]. Solving these problems can be very time consuming, especially when a large number of training examples is used.

6.2 Gait Pattern Novelty Detection

Looking at the gait rehabilitation field, one can realize that the main goal of any rehabilitative therapy is to promote progress. This progress is translated in the form of a motor function evolution. The healthcare professionals devise therapies to stimulate the lower limbs in order to train them to regain lost abilities. However, an essential part of this process is the analysis of the therapy's progress. The professional observes the patient daily, during several hours, and tries to identify evolution to better adapt the therapies and assess its effectiveness. This evolution manifests itself through the change of the motion patterns of a predefined set of gait parameters. In conventional gait analysis, these parameters are obtained from the several lower limbs parts listed in Table 6.2.

With the idea of developing automatic tools to identify gait pattern changes in mind, this section proposes an approach using machine learning techniques to address this use. From the set of techniques available in machine learning, the unsupervised methods seem to be an adequate fit in this case. Analyzing progress is based on the fact that what is currently observed can be modeled, and progress is something that moves away from that model and which is unknown at a first stage. The goal in novelty detection is to model a single class with examples exclusive from that class, and determine if new observations are novel against that trained

Table 6.2. Example list of gait parameters tracked for gait analysis scenarios.

Gait Parameters	
L/R greater trochanter of the femur	L/R anterior of the tibia
L/R thigh	L/R heel
L/R lateral epicondyle of the knee	L/R toe
L/R lateral malleoulus of the ankle	L/R 5th metatarsal

model. A novelty is something that falls outside of the trained class.

6.2.1 Implemented Methods

Over the years several methods have been proposed for novelty detection. They can be categorized according to the used methodologies [105]. They can be probabilistic [106], distance-based [107], regression-based [108], and domain-based [109]. There is no optimal method for novelty detection.

The following subsections present a brief summary of the implemented methods used in the proposed novelty detection stategies in this thesis.

6.2.1.1 One-class Support Vector machines

Among the several methods proposed in the literature, for this work, the OC-SVM was chosen since it is a robust and well-known method used in novelty detection [105]. The OC-SVM is a method with good performance [110] and widely used for novelty detection in the medical field as mentioned in Section 2.4.

The OC-SVM implementation that was followed in this thesis was the one presented in [110]. In the referenced implementation, considering a *d*-dimensional dataset $\{X_1, \dots, X_l\} \in \mathbb{R}^d$, a quantity *l* of data points is mapped into a (potentially infinite-dimensional) feature space $\mathbb{F}$ by some non-linear transformation $\Phi: \mathbb{R}^d \rightarrow \mathbb{F}$. The dot-product between pairs of transformed data in $\mathbb{F}$ is provided by the kernel function k:

$$k(X_i, X_j) = \Phi(X_i) \cdot \Phi(X_j) \tag{6.6}$$

A Gaussian kernel is used to allow any data-point to be separated from the origin in $\mathbb{F}$:

$$k(X_i, X_j) = e^{-\frac{\|X_i - X_j\|^2}{2\sigma^2}} \tag{6.7}$$

where σ is the width parameter of the Gaussian kernel.

The decision boundary is determined by minimizing the weighted sum of a support vector-type regulariser and an empirical error term depending on both an overall margin variable ρ and individual errors ξ_i,

$$\min_{w\in F,\xi\in\mathbb{R}^l,\rho\in\mathbb{R}} \frac{1}{2}\|w\|^2 + C\sum_{i=1}^{l}(\xi_i - \rho) \tag{6.8}$$

$$\text{subject to } w\cdot\Phi(X_i) \geq \rho - \xi_i, \xi_i \geq 0 \tag{6.9}$$

where w is a weight vector in the feature space, and C is a user-specified penalty parameter. Higher C values lead to a higher penalization of errors. [110].

The decision function in feature space $\mathbb{F}$ is:

$$z(X) = w_o \cdot \Phi(X) - \rho_o \tag{6.10}$$

With parameters

$$w_o = \sum_{i=1}^{N_S} \alpha_i \Phi(s_i) \tag{6.11}$$

$$\rho_o = \frac{1}{N}\sum_{j=1}^{N_S}\sum_{i=1}^{N_S} \alpha_i k(s_i, s_j) \tag{6.12}$$

where s_i correspond to the support vectors, summing up to a number of N_s, and where k is the Gaussian kernel defined in (6.7). The element $w_o\in\mathbb{F}$, $\rho_o \in \mathbb{R}$, and α_i are Lagrangian multipliers used to solve the dual formulation.

6.2.1.1 Autoencoders

When looking at motion tracking data from therapy sessions, professionals analyze the graphical representation of the evolution of several gait parameters over time (typically curves) and compare their evolution [111]. It is an analysis strongly sustained on shape-based curve comparisons. The autoencoder used in this work was motivated by the way it learns a model, which the author believes is suitable for gait analysis, due to how gait parameters are analyzed by healthcare professionals. Autoencoders, although being a method that has not been found as a novelty detector in the literature, were chosen since they output a reconstruction of inputted data according to a trained model, allowing a comparison of similarities. The autoencoder is a neural network constructed with a narrow hidden layer, which causes redundancies in the input

to be compressed, while retaining and differentiating non-redundant information generating a modeled representation of the input [112].

In this approach, the autoencoders are trained to reconstruct as well as possible a training set of gait cycles consisting on "normal" examples only. Hence, an autoencoder is an unsupervised neural network, whose objective is to learn to reproduce input vectors $\{X_1, \dots, X_m\}$ as outputs $\{\hat{X}_1 \dots, \hat{X}_m\}$. In the hidden layer, the inputs are compressed into a small number of neurons. Activation of unit *i* in layer *l* is given by:

$$a_i^{(l)} = f\left(\sum_{j=1}^{n} W_{ij}^{(l-1)} a_j^{(l-1)} + b_i^{(1)}\right) \tag{6.13}$$

where *W* and *b* denote weight and bias parameters respectively. In the input layer (first layer), $a^{(1)} = X$, and in the output layer (last layer), $a^{(3)} = \hat{X}$. During the t training period, the objective function shown in (6.14) is minimized with respect to *W* and *b*. The objective function includes a regularization term, and the parameter λ determines the strength of regularization.

$$J(W,b) = \frac{1}{m}\sum_{i=1}^{m}\left(\frac{1}{2}\left\|X(i) - \hat{X}(i)\right\|^2\right) + \frac{\lambda}{2}\sum_{l=1}^{n_l-1}\sum_{i=1}^{s_l}\sum_{j=1}^{s_l+1}\left(W_{ji}^{(l)}\right)^2 \tag{6.14}$$

where n_l and s_l denote number of layers in the network and number of units in layer L_l, respectively.

6.2.2 OC-SVM-based Gait Pattern Novelty Detection

The presented approach for gait pattern novelty detection is based on the gait pattern's elemental unit, the gait cycle. A OC-SVM-based algorithm is proposed to achieve novelty detection for each gait cycle. The approach is divided into training (model construction) and testing (detection). To construct the model of the observed gait cycle a training dataset is required. For this unsupervised approach, the extracted features considered went beyond the spatiotemporal approach found in the literature of gait analysis. The goal was to propose features that could enrich the method to better detect progression of the gait pattern. The novelty detection algorithm is composed by two consecutive modules, seen in Figure 6.2. In the first module, a classifier for each kinematic feature (kinematic feature space) is applied separately, to obtain an individual kinematic score of novelty of each kinematic feature by itself. The outputs from these classifiers are then fused with the spatiotemporal features resulting in a new feature space. This process basically implements a technique of early integration or fusion, contrasting with the alternative that is the fusion of the outputs of several classifiers (late

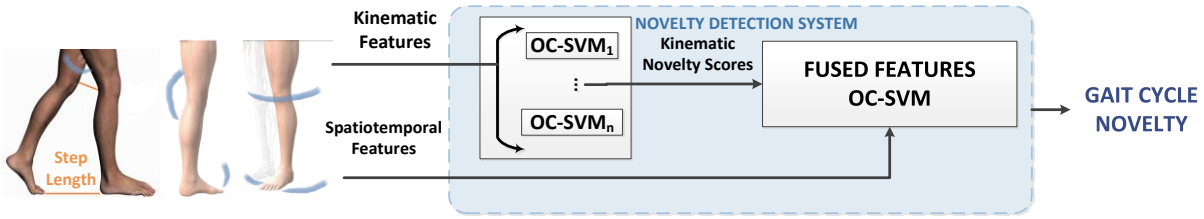

Figure 6.2. Unsupervised OC-SVM learning approach's gait cycle novelty detection functional diagram.

integration). The other module is responsible for providing a novelty detection score for each gait cycle. It performs a classification through the use of a OC-SVM, considering the previously determined new feature space.

The percentage of novel gait cycles within a sliding temporal window determines if the currently observed gait pattern is considered to be a novel one (the gait pattern changed). If that is the case, a new training stage is triggered, starting the whole cycle again.

6.2.2.1 Feature Extraction

Before addressing the novelty detection algorithm, the considered features will be described. These features derive from the lower limbs (waist, legs and feet) detection methods previously proposed in this thesis, based on the study of the rehabilitation literature reviewed in Section 2.1.3. The proposed features are extracted at each gait cycle.

The extracted features are divided into two sets of features. The first one, as mentioned, is composed by spatiotemporal features related to parameters computed from the lower limbs' tracked points positions and angles, such as mean, standard deviation, and minimum/maximum values. The other set of features is composed by kinematic features. Kinematic features are taken directly from the tracked lower limbs' points and angles, being positions, velocities, and spatial relation between some of those points and angles over time.

Spatiotemporal Features

For each gait cycle a collection of parameters are computed for the lower limb's points positions and angles as presented in Table 6.3. To compute the mean and standard deviation of each tracked point or angle, the following equations are applied.

$$\mu = \frac{\sum_{t=1}^{N} p_t}{N}, \sigma = \sqrt{\frac{1}{N}\sum_{t=1}^{N}(p_t - \mu)^2} \tag{6.15}$$

Where N is the number of frames in each specific gait cycle and p_t is one of the lower limb's tracked points or angles.

Kinematic Features

The kinematic features are extracted at every frame of a gait cycle, being represented by a vector instead of a scalar as in the case of the spatiotemporal features. Since the goal is to classify each gait cycle to detect novelty, and since each gait cycle has its own period and time-dependent characteristics, first a resampling/resizing and alignment of all gait cycles is performed, so that each kinematic feature can be compared from gait cycle to gait cycle.

A resize step was decided to be implemented to resize to the shortest one, so that performing an upsampling could be avoided, which would involve resizing to a mean size or maximum size, which would artificially interpolate unseen data. This way a downsampling, which keeps the integrity of the shortest gait cycles is performed.

To ensure that similar gait cycles are well aligned, for a more reliable model construction in the training stage, and that in the testing stage the gait cycles are related to the trained model, a Dynamic Time Warping (DTW) is employed. This is a well-known technique used in speech recognition [113], that performs an alignment of curves according to the dynamic temporal behavior of their features. The DTW preprocessing is applied to each gait cycle collected during the training and testing stage of the novelty detection algorithm.

The first group of computed features is composed by the velocities and normalized position of the knees' and feet's points positions, and normalized joint angle excursions of hips, crotch, and knees, computed according to the following equations:

$$v_t = \frac{\left\| p_t - p_{t-1} \right\|_3}{T}, \; p_t^{'} = \frac{p_t - m}{M - M} \tag{6.16}$$

Where v_t is the velocity at time t, T is the period of the data acquisition, p_t is the normalized lower limb tracked feature's trajectory or excursion at time t, and M and m are the maximum and minimum values, respectively, for each lower limb feature on each gait cycle.

The remaining computed kinematic features are intra and inter leg geometric parameters.

Table 6.3. Spatiotemporal features.

Feature	Definition
Stride length	Sum of $dist(foot_{left}, foot_{right})$ at each heel strike
Stride period	Number of frames
μ, σ, max and min of joint angle of the hip (hja) of each leg	μ(*hja*), σ(*hja*), max(*hja*), min(*hja*)
μ, σ, max and min of joint angle of the knee angle (kja) of each leg	μ(*kja*), σ(*kja*), max(*kja*), min(*kja*)
μ, σ, max and min of knee's position of each leg	μ(*knee*), σ(*knee*), max(*knee*), min(*knee*)
Maximum knees' baseline separation	$\max(dist(knee_{left}, knee_{right}))$
μ, σ, max and min of foot's position of each leg	μ(*foot*), σ(*foot*), max(*foot*), min(*foot*)

The intra and inter leg features provide important geometrical information about each leg as well as the geometrical relation between both legs. The extracted training set is normalized using the minimum and maximum values.

6.2.2.2 Gait Cycle Novelty Detection Strategy

The novelty detection algorithm proposed is based on a OC-SVM approach, as represented in Figure 6.3. This subsection addresses the steps necessary to achieve novelty detection considering the described features.

From the feature extraction stage two feature spaces are obtained, $\mathcal{K}$ kinematic and $\mathcal{S}$ spatiotemporal. Each feature space has a different dimensionality. In the $\mathcal{K}$ feature space, each instance of the feature vectors represents a time instant *t*, while in the space $\mathcal{S}$, vectors are composed by instances related with a single gait cycle. Hence, $\mathcal{K} \in \mathbb{R}^{NG \times d_K}$ and $\mathcal{S} \in \mathbb{R}^{G \times d_S}$, where *N* is the number of instants *t* on a preprocessed gait cycle, *G* is the number of gait cycles of the dataset, and d_K and d_S are the dimensionality of the features of each space.

For each gait pattern learning stage (model construction stage) a training set of gait cycles is captured. The kinematic features are obtained from trained classifiers that output novelty scores, as seen in Figure 6.3, as described before. For this purpose, the training dataset is divided into two equal parts. The first is used to train the classifiers and the second to obtain the novelty scores. The dataset is divided purposely to avoid overfitting by not computing the final kinematic novelty sore per feature using the same training data. Hence, for the kinematic features a OC-SVM classifier is trained for each feature separately. The result from this step is a novelty score (novelty or not) for each time instant *t*.

To fuse the novelty scores with the spatiotemporal features, which are correspondent to each gait cycle, all time instances *t* within a gait cycle are processed to obtain a single kinematic score of the detection of novelty per feature. This score is determined, using equation (6.17), which directly maps the novelty scores at each instant within a gait cycle to a new feature space where kinematic features by gait cycle (kinematic novelty scores) and the spatiotemporal features can be fused.

$$\phi(f_1,\ldots,f_n) = \phi\left(\sum_{i=1}^{N}\frac{Y(f_1=-1)}{N},\cdots,\sum_{i=1}^{N}\frac{Y(f_n=-1)}{N}\right) \tag{6.17}$$

Where *Y* is the novelty score at each instance of a gait cycle. Equation (6.17) is applied

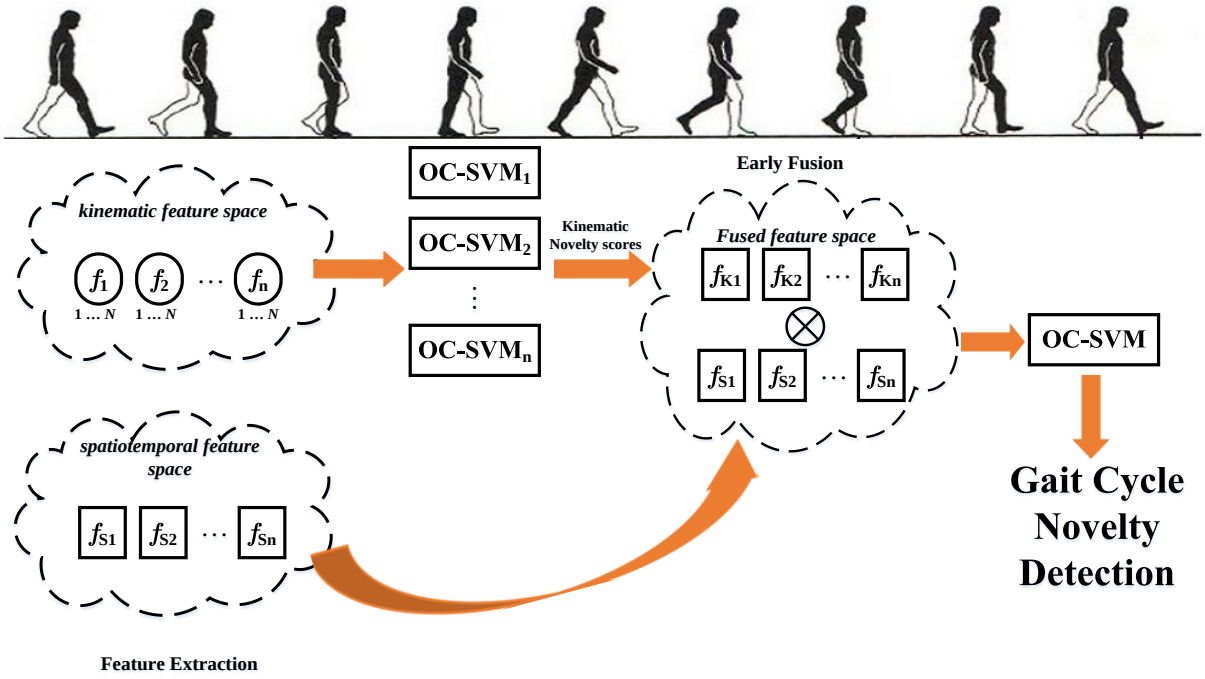

Figure 6.3. Novelty detection strategy for gait cycle analysis.

per kinematic feature. This process can be compared to an early fusion or integration at the feature-level [114]. The fused feature space is now represented by $\mathcal{F} \in \mathbb{R}^{G \times (d_K + d_S)}$. The new feature space $\mathcal{F}$ has a higher dimensionality than the previous feature spaces.

The OC-SVM is particularly suited for these cases [115]. In this approach, the classifiers use a Radial Basis Function (RBF) kernel. To achieve the classification for each gait cycle, a global OC-SVM is employed on the fused feature space.

At the testing stage (detection), each observation (gait cycle) is processed to extract the considered kinematic and spatiotemporal features. Then, the same steps are taken as in the learning stage, percentages of novelty are computed per kinematic feature and fused with the spatiotemporal features. The final step, is the computation of the novelty score for the observation, using the trained model of the OC-SVM.

6.2.2.3 Gait Pattern Shift Detection and Relearning Decision

The previous Subsection addressed novelty detection at each gait cycle. However, the goal is to detect gait pattern shifts based on the gait cycle's novelty. A new gait pattern is considered to be present if the percentage of gait cycles labeled as novel is above a certain threshold for a group of observations. Specifically, for a temporal sliding window of observations (gait cycles), if the threshold of novel gait cycles is reached, the system triggers a

new learning stage. This means another training dataset of gait cycles is collected. After training the system starts rechecking for novelty again.

6.2.3 Autoencoder and OC-SVM Gait Pattern Novelty Detection

In this subsection, the second approach for a gait pattern shift detection method is presented. The analysis, like in the previous method, is done on each gait cycle.

The proposed approach focuses on the analysis of the gait tracking data using two complementary ideas. One is the extraction of spatiotemporal parameters from the data retrieved during each gait cycle, as in the previous method. This provides a perspective of the behavior of the lower limbs in a quantifiable manner, allowing to understand statistical values and limits. The other idea was to use the information present in the curves of the variation of gait parameters over time, as it is inherently performed by healthcare professionals [111]. By comparing these curves, a measure of similarity can be obtained. Hence, the proposed method fuses both spatiotemporal features and similarity rates to assess novelty of each individual gait cycle, as summarized in Figure 6.4.

A classification strategy which combines the mentioned features is performed. This classification addresses novelty detection at the gait cycle level. To detect novelty in the gait pattern, like in the previous method, a temporal analysis of the occurrence of novelty in the gait cycles is performed.

6.2.3.1 *Gait Cycle Model Construction*

The objective is to use reference gait cycles, which are labeled as “normal”, to construct a model, in order to detect novelty in the posteriorly observed gait cycles. A model of the “normal” gait cycle is constructed using a OC-SVM applied to the combination of spatiotemporal features and similarity rates. The similarity rates are computed using autoencoders, which also need to be trained. A similarity rate is computed for each gait parameter used from the gait tracking data. This model construction workflow can be seen in Figure 6.5.

A dataset of “normal” gait cycles, which are the ones belonging to the gait pattern being trained, is collected. Once more the dataset is divided in a way similar to the previous method. Half of this dataset is used only to create a representation of each curve of the gait parameters (training the autoencoders). The remaining part of the dataset is used to compute similarity rates from the trained autoencoders, using data from different gait cycles than the ones used to train

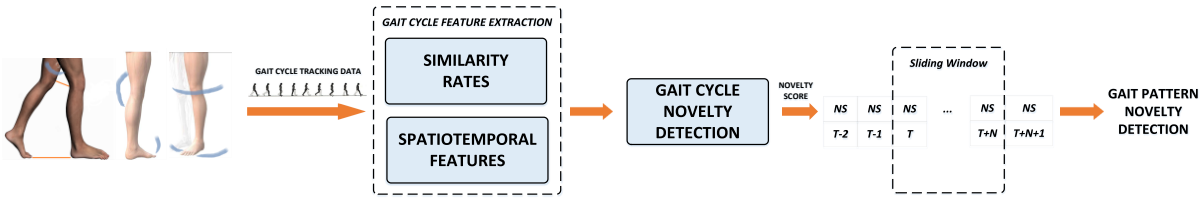

Figure 6.4. Proposed method's schematic overview, with the gait pattern novelty assessment being computed within a sliding temporal window from the individual gait cycles' novelty detection.

them (to avoid overfitting), and to compute spatiotemporal features. The combination of these computed values, constitute the feature space fed to the OC-SVM, which constructs a model of the reference or "normal" gait cycle.

Similarity Rates Definition

Autoencoders are used to learn a representation of the curves associated to each considered gait parameter. To efficiently create such curves a preprocessing of every gait cycle is required. This preprocessing serves to guarantee that all curves are equally sampled and aligned. This process is identical to the process of the previous method, and it corresponds to the module of preprocessing shown in Figure 6.5.

In addition to using positions and angles excursions, one also computed their respective velocities. In this approach, the considered lower limbs anatomical features are the knees' and feet's points positions, and hips' joints', crotch' joint's, and knees' joints' angles. The following equations are used to compute the velocities and normalized curves:

$$v_t = \frac{\left\| p_t - p_{t-1} \right\|_3}{T}, \; p_t^{'} = \frac{p_t - m}{M - M} \tag{6.18}$$

Where v_t is the velocity at time t, T is the sampling period of the data acquisition, p_t is the normalized lower limb's tracked feature's trajectory or excursion at time t, and M and m are the maximum and minimum values, respectively, for each lower limb tracked feature, for each gait cycle.

At the preprocessing stage, a filtering method is applied to each curve to remove noise. Kinematic Filtering was applied [116], since it computes a smooth curve representing a noisy input. It is a low-pass filtering technique especially adequate for signals/trajectories representing smooth natural behaviors such as hand movements. The next steps are identical to the previous methods, including the DTW and resampling/resizing techniques, for temporal alignment of every curve belonging to each gait parameter, and equally sampled curves.

For the computation of the similarity rates two steps are needed. Considering the above-

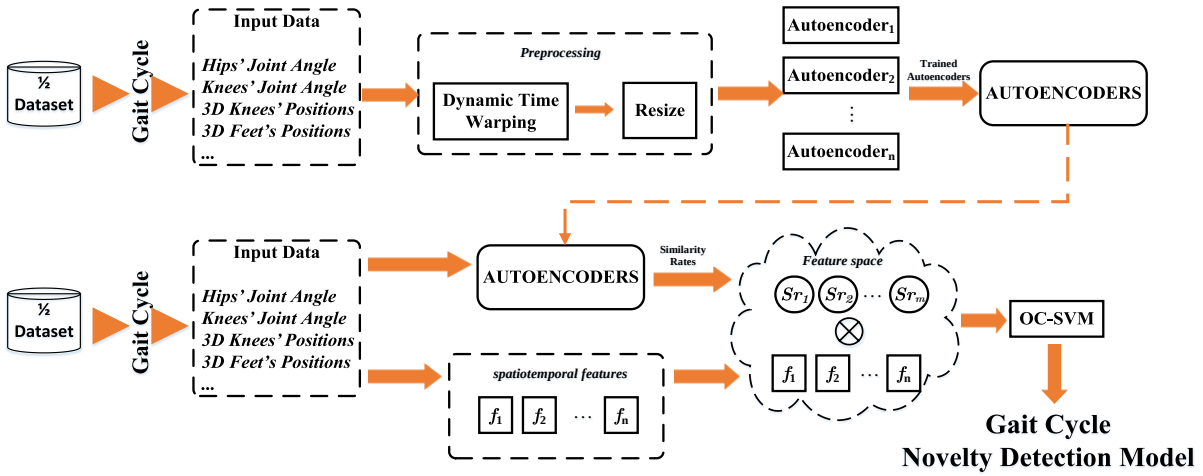

Figure 6.5. Gait Cycle model construction diagram that takes the dataset of the tracking data with which it trains the autoencoders to generate similarity rates, and it trains as well the OC-SVM that handles spatiotemporal features and similarity rates, to construct a model of the observable gait cycle.

mentioned dataset division, the first half of the dataset is used to create a representation of the gait parameter' curves. Then, the unused part of the dataset is used to compute the similarity rates. The curves are fed to the corresponding trained autoencoder, which reconstructs the inputted curves according to the learned. To compute the similarity rate, it is just a matter of comparing the inputted curve and its reconstruction using:

$$S_{rate} = 1 - \sqrt{\sum_{i=1}^{N} (X_i - \hat{X}_i)^2} \tag{6.19}$$

Where i is the ith point/sample of the curve and N is the number of points/samples of a curve (number of frames of the gait cycle).

The similarity rate is closer to one for a near identical curve to the respective autoencoder's representation. This is verified because when the inputted curve is handled by the autoencoder, it tries to reconstruct the curve according to the learned representation, outputting an undistorted curve as close as possible to that representation. The more distinct the curves are from the representation the more inaccurate the reconstruction is, thus lowering the value of the similarity rate.

OC-SVM Model Construction

The OC-SVM constructs a model of the "normal" gait cycle taking as input the feature space obtained from the combination of similarity rates and spatiotemporal features, as described in Figure 6.5.

In what regards the spatiotemporal features, for each gait cycle, these features are

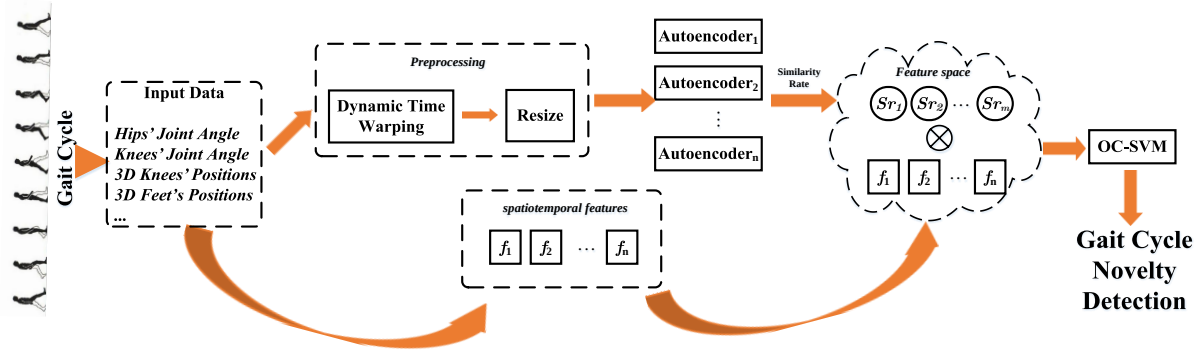

Figure 6.6. Gait Cycle novelty detection classification strategy that takes the tracking data with which computes the spatiotemporal features and similarity rates, and then assesses gait cycle novelty detection through the trained OC-SVM model.

computed from the lower limbs' points' positions and angles' excursions (gait parameters) as mentioned in the previous approach. These features are computed for each gait cycle after a filtering process as described in the previous subsection.

An important process while training the classifier is the optimization of the parameters involved in the model construction. A strategy to optimize the parameters σ and ν was adopted, using the *partial* Area Under the Curve (AUC) of the Receiver-Operating Characteristic (ROC) curve. When designing novelty detection systems, a common requirement is a low false positive rate (FRP). As such, when analyzing the ROC curve, the focus is put on the region with low values for the FPRs to evaluate the performance of the novelty detector. It is discarded how well the detector performs at higher FPRs because these correspond to thresholds that would never be used in practice. Therefore, *partial* AUC is then defined as the integral area between two false-positive rates [117]. Taking into account these previous notes, a grid search is performed to find the best parameters that maximize the partial AUC in a balanced validation dataset of "normal" and "novel" data.

6.2.3.2 Gait Cycle Novelty Detection

In this approach for the gait cycle novelty detection, to each newly observed gait cycle is attributed a novelty score. The gait cycle's data are preprocessed, then used to extract the spatiotemporal features and to compute the similarity rates. All these features are fed into the OC-SVM which outputs the novelty score that is used to assess novelty detection. The visual representation of this process can be seen in Figure 6.6.

The novelty score is restricted to the interval of [-1 1]. A gait cycle is considered to be novel if this score is above zero.

6.2.3.3 Gait Pattern Shift Detection

Much like in the previous unsupervised approach, the goal is to determine a progression or evolution of the gait pattern based on the gait cycles' novelty. Over time, this approach identifies a new gait pattern if the percentage of gait cycles labeled as novel is above a certain threshold, within a sliding window with partially overlapped step. If a "novel" gait pattern is identified, then the system triggers a new gait cycle model construction stage. This means another dataset of gait cycles is collected and considered as a new training set. After the model construction, the system starts rechecking for novelty (gait cycle novelty detection stage).

Chapter 7

Experimental Results

This chapter presents the experiments designed to evaluate all the methods and procedures described on the previous chapters. The results of this experiments are also presented.

The sequence in which the experiments are presented follows the same sequence in which the methods were introduced in the previous chapters. For each experiment both the experimental protocol and the demographic characteristics of the volunteers are presented, followed by the results. An analysis of the results is also provided for each experiment.

7.1 Human-Machine Interface Validation

The evaluation of the performance of the HMI was divided in two tests. The first test is used to assess the gripping system's performance in classifying the correctness of the user's gripping. The second test evaluates the motion command generator and user's intention estimation.

7.1.1 Gripping Safety System Test

The first experiment was designed to evaluate the performance of the gripping safety system's classifier to discriminate between an adequate gripping and an incorrect one. Several trials were made to collect a suitable dataset that could be used to classify the quality of the user's grip based on the reach-to-grasp gesture of the user's hands towards the walker's grips.

The invited volunteers were asked to repeat a sequence of reach-to-grasp gestures. Three types of reach-to-grasp gestures were defined, being one of them the correct way of reaching and safely gripping the walker, while the rest were designated as inadequate and potentially hazardous. Figure 7.1 shows the three gestures for the right hand. For each hand, a dataset was recorded. Each subject faced the walker at a reaching distance from the walker of 20 cm and then the subject performed 20 repetitions for each reach-to-grasp gesture with both hands simultaneously. Ten volunteers collaborated in these experiments, with ages varying from 25 to 35 years, 8 males and 2 females, with no prior knowledge of this work.

The dataset was divided into train and test data. The desired result was the classification of each gesture as being adequate or inadequate. The binary output accuracy was quantified as a percentage and in the form of a Precision-Recall (PR) curve and a Receiver-Operating Characteristic (ROC) curve. Accuracy alone does not qualify the quality of the classification.

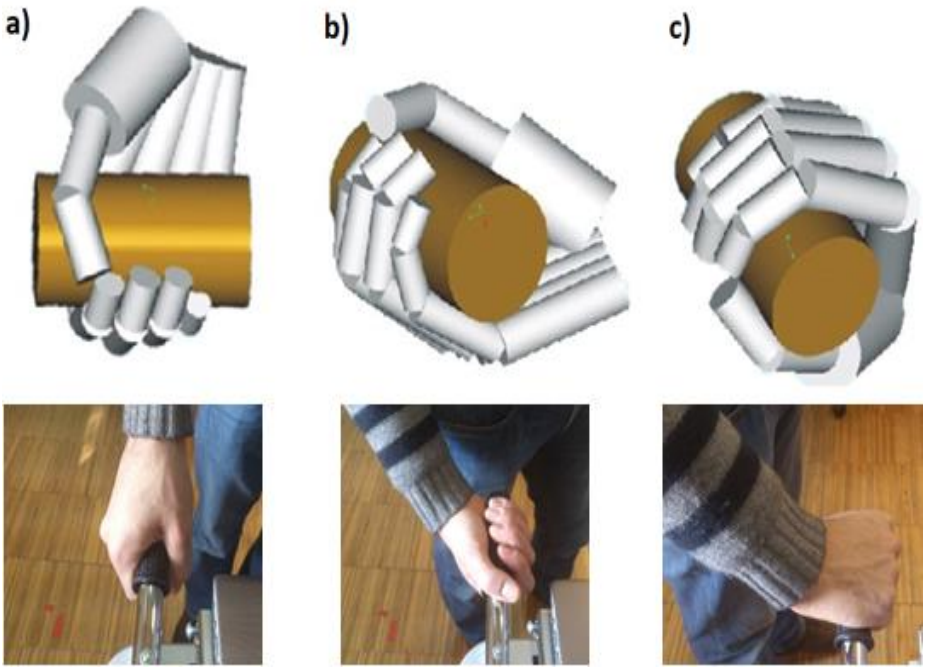

Figure 7.1. Right hand gripping gestures a) represents an adequate and safe grip b) and c) incorrect grips.

The relation between true positives and false positives is also important. Provost *et al.* [118] have argued that in classification tasks simply considering accuracy results can be misleading. They recommended the use of ROC curves when evaluating binary decision problems, because they show how the number of correctly classified positive examples varies with the number of incorrectly classified negative examples. The Precision refers to the rate of true positives in relation to the number of all positive examples, while Recall or sensitivity is the relation of true positives with the universe of true positives and false negatives. The relation between PR curve and ROC curve is also discussed in [119]. These curves are not independent and should be taken both into account when analyzing classification results

A leave-one-out cross-validation test was adopted. The learning was made with eight persons and tested with two unseen persons. To evaluate the performance of the classifier the Precision-Recall curve and the Receiver-Operating Characteristic (ROC) curve are presented in Figure 7.2. Based on the ROC curve, the quantitative parameter Area Under the Curve (AUC) was calculated, which is 0.9869. The AUC represents the probability that the classifier will rank a randomly chosen positive instance higher than a randomly chosen negative one. Other classification results can be found in Table 7.1, such as the overall accuracy of 94.76%.

During the experiments, a few limitations of the proposed method were observed. The fast and sudden erratic reach-to-grasp motions were verified to result in the inability of the system to correctly track the motion, leading to incoherent classification results. Such limitation

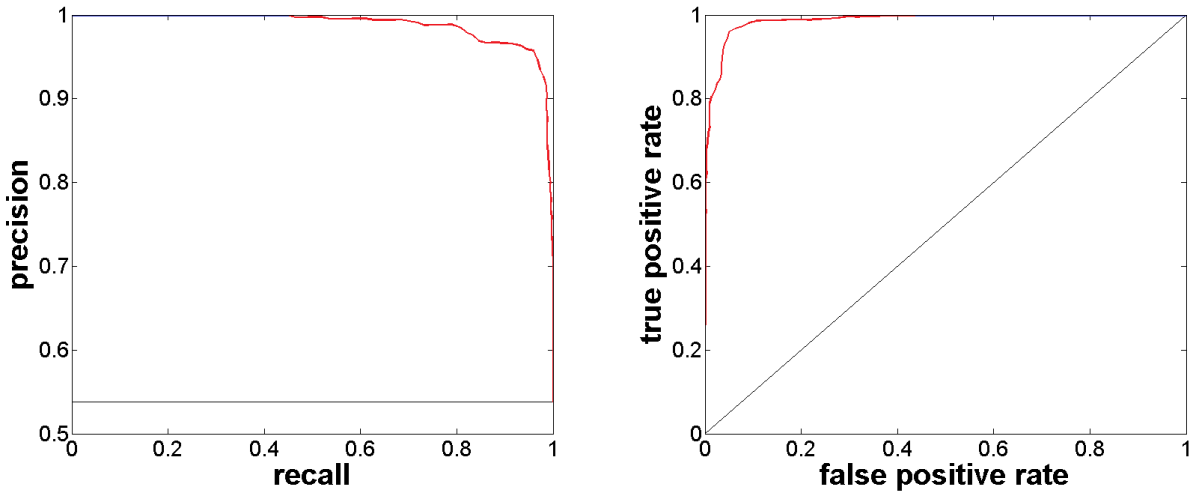

Figure 7.2. Precision-Recall and ROC curves for the safety system's classifier.

may be an issue, particularly when dealing with persons suffering from upper limbs motor coordination problems. For fist-shaped gestures, the finger tracking was verified to be compromised due to occlusions, as is the response from the classifier.

In general, results show a satisfactory generalization of the classifier. The incorrect gripping trajectories are detected with high accuracy and the system is able to prevent any walker operation whenever the grip is not appropriate. It is worth mentioning that because both handles are classified independently, the user can perform non-simultaneous reach-to-grasp gestures with each hand. However, both gestures need to result in correct gripping patterns to be classified as being adequate for operation. A possible extension to this approach might be the use of some form of force sensing in the handle to provide information regarding how tightly the user is gripping it.

7.1.2 Motion Controller Test

To validate the proposed HMI's motion controller, an experiment with five healthy volunteers was conducted. The goal was to evaluate the extent to which the proposed system would provide active assistance to users by helping them to perform the desired maneuvers, and to understand if the HMI could cope with weight-bearing conditions, which is an essential attribute of this aid for disabled individuals. The subjects' feedback about their experience with the walker was also collected through a qualitative questionnaire. The subjects were asked to maneuver the walker on a predefined track as shown in Figure 7.3 f). The shape of the track

Table 7.1. Performance results of the HMI's safety system.

	Accuracy (%)	Precision (%)	Recall (%)
Classification	94.76	96.40	93.77

involved maneuvers that completely characterize the HMI's span of operation. The data of the walked path performed by each subject was collected from the motors' encoders, force/torque sensor, and handle displacements.

The results of this experiment showed that the volunteers were able to accurately navigate through the proposed path without the need to stop to adjust their current trajectory, while being able to walk at the intended speed, as observed by analyzing both the trajectories and the handles' displacements of Figure 7.3. The subjects were able to navigate along the proposed path, imposing on the walker body weight percentage similar to the ones identified in scenarios with impaired individuals, while being able to slide the handles smoothly and accurately. As an example, Figure 7.3 a) to e) present the curves' profile for one experiment where the subjects walked down a predefined path supporting themselves heavily on the platform and were able to maneuver it as expected.

After the experiment a positive feedback was received from the users about their

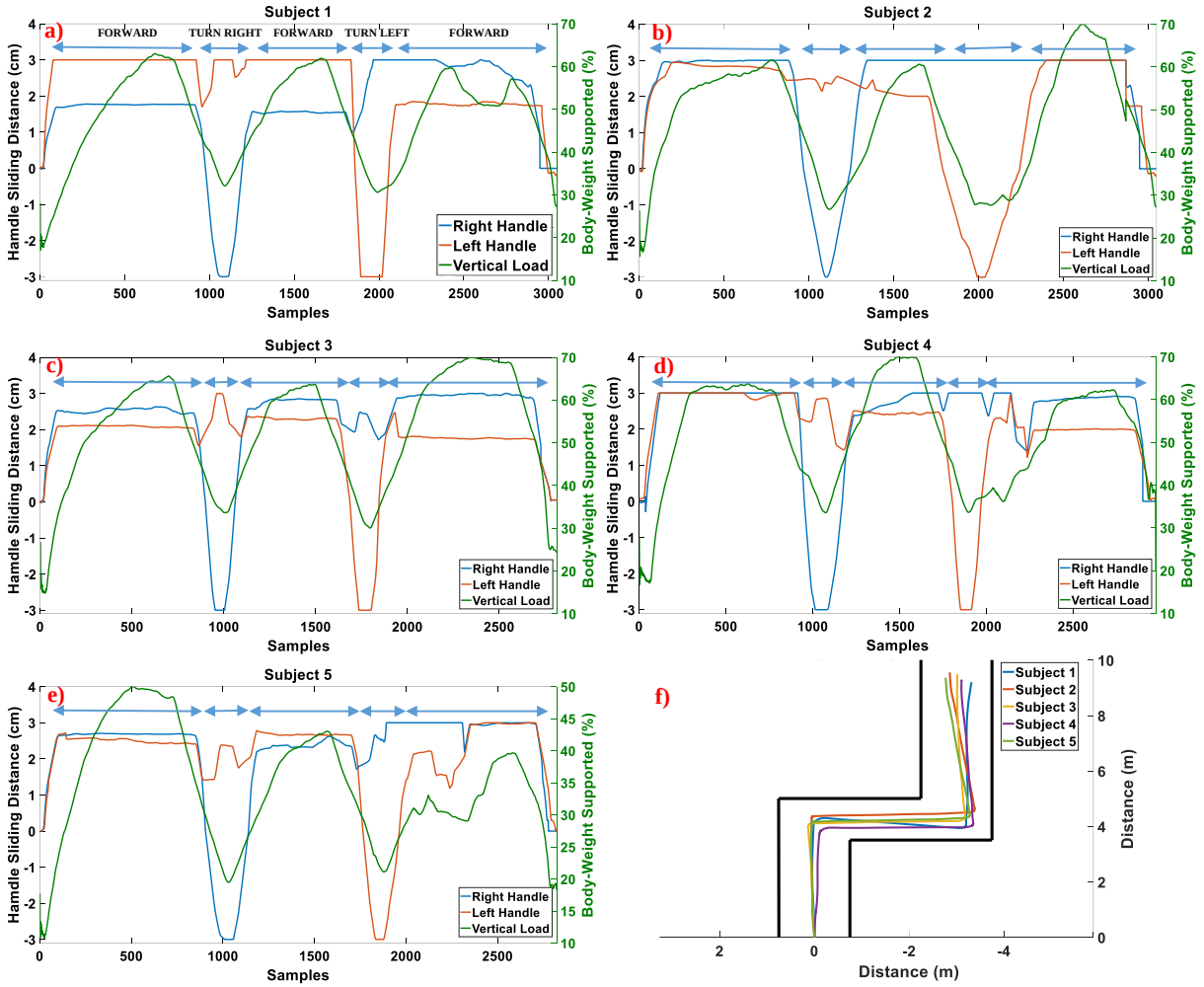

Figure 7.3. HMI's motion control system's results. a) to e) represents the body weight support of each subject on the handles accompanied by the handles displacements, and f) the obtained trajectories of each subject on the path.

maneuvering experience. All the subjects revealed that the interaction was very intuitive, allowing the platform to be easily maneuvered while supporting their body weight. Furthermore, the walker's motion was in sync with the users' intents and provided a sense of security.

It should be remarked that the interface, although operating satisfactorily with healthy subjects, can see its performance hindered when dealing with users evidencing low dexterity, such as advanced Parkinson's patients. As such it is noted that the HMI operates at its best with individuals that need to support their weight, but which maintain some upper limb control capabilities, without erratic tremors. Although the test was performed with the individuals walking at their intended speed, further testing will allow to understand the sensitivity of the HMI in terms of speed control. This is particularly important when testing the system using impaired individuals.

7.2 Assisted Navigation System Validation

The assisted navigation presented in this thesis was a collaborative effort, involving the collaboration of Luís Garrote a member of the ISR Mechatronics lab. To validate the method two tests were performed. First, a hybrid setup, which combines the physical walker's HMI and a simulated environment to maneuver a simulated walker was used to guarantee the volunteers safety, followed then, by a real-world scenario test.

7.2.1 Hybrid Setup Scenario

The first stage of the validation of the method presented in this experiment was carried out in an in-house 3D C/C++ virtual environment simulation software with a TCP/IP connection to the ISR-AIWALKER's, as illustrated in Figure 7.4. With the use of such hybrid setup, the users operated the physical HMI while ensuring they remained safe still in terms of real navigation, without the need to expose the users to real collisions during tests. The user's input was directly used, (through the HMI) and the scenarios and the local maps were virtually simulated, using a virtual 3D point cloud sensor and a differential model of the ISR-AIWALKER.

Four scenarios, seen in Figure 7.5, were defined to assess the performance of the proposed method. These scenarios intend to represent situations that can cause stress and problems to the

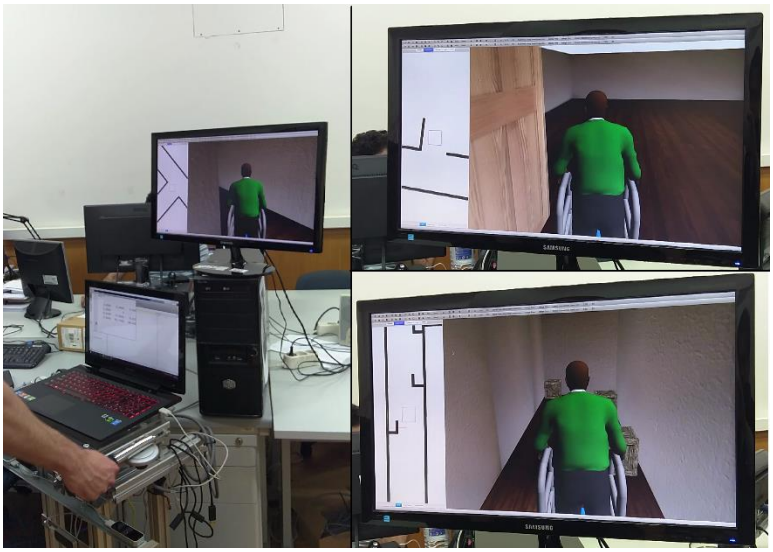

Figure 7.4. Hybrid setup with HMI provided by the ISR-AIWALKER, integrated in an immersive virtual environment.

typical walker user (e.g., narrow passages, near collisions). The first scenario has the walker following a corridor and entering a room. In the second scenario, the walker follows the same corridor but instead of entering a room follows in the same direction and turns left. In the third scenario, the walker traverses the corridors and arrives at the starting position. The last scenario includes travelling in a corridor with multiple obstacles and entering a door passage-way.

For performance comparison, the proposed method is compared with a solution where no navigational safety measure (HMI only) was employed, resulting that for each scenario two separate sets of tests were generated. The metrics evaluated in each scenario include the average minimum distance to obstacles along the generated path measured in relation to the walker's center of mass (*ANO*), occurrence of collisions or deadlocks (*D*) during the simulation (requiring outside help to fully restore walker mobility, e.g., local minimum, loss of maneuverability due to multiple near obstacles), average control effort (*CE*) and standard deviation (*CEσ*) [120], and average course speed (*AS*).

7.2.1.1 Simulation Details

The method's parameters are presented in Table 7.2. In the considered scenarios, some parameters are empirically adjusted (rapidly exploring random trees inspired algorithm parameters and object distance thresholds) and others are defined according to the walker specifications, dimensions and safety requirements. For each scenario, the virtual walker is controlled by the user, who has access to the HMI on the physical walker, and starts each scenario with the same initial conditions. After the start of each run, the user is only required to

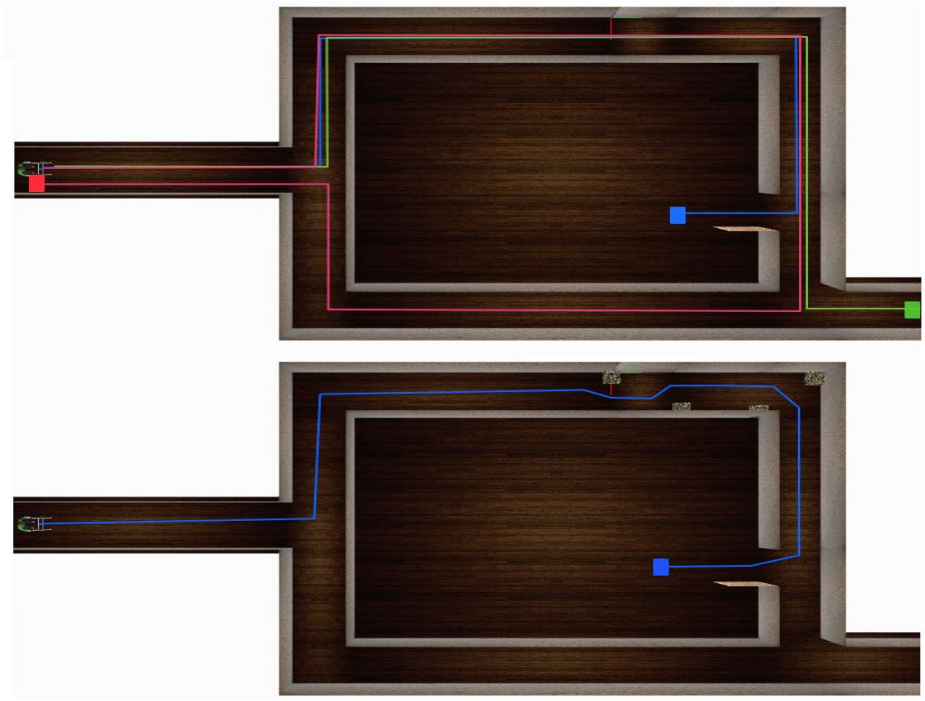

Figure 7.5. Scenarios for evaluation of the proposed method. On the top, scenarios 1-3 (blue, green and red) on the bottom, scenario 4 with pathway obstacles.

reach the goal region (green regions in Figure 7.5) as fast as possible preserving safety by avoiding collisions with the virtual walls. In case of collision or deadlock, the scenario is marked as such, and the environment is restarted until a valid result is reached. Situations where users stopped the walker before making a decision and remained still for a few moments (e.g., while resting) were not integrated in each metric, guaranteeing that idle times did not affect the final score.

7.2.1.2 Experimental Protocol

For this test, four healthy volunteers were invited to participate. The subjects were between 25 to 35 years of age, with no prior history of health conditions related to sight or locomotion. Each subject run through the four scenarios, and repeated each test twice to ensure that the data obtained for each scenario was consistent. Before the test start, an initial familiarization with the system was performed. The subjects were requested to drive safely, avoiding obstacles during free runs on a test scenario not identical to the four designed scenarios as to not bias the behavior of the subjects. During this adaptation trial no metrics were collected. This merely served to explain to the subjects how the HMI works and for them to gain some driving experience.

Table 7.2. List of parameters.

Variable	Value	Variable	Value
$\|S_v\|$	25	w_{max}	0.5
Δv_{ui}	0.1	d_{max}	2
Δw_{ui}	1.5	$d^{max}{}_O$	3
w_O	1	μ_O	0.8
w_{ui}	1	σ_O	0.25
w_t	0.8	σ_{ui}	0.3
T_{LA}	2	K	400
v_{min}	-0.3	T_r	0.5
v_{max}	0.3	h	0.1
w_{min}	-0.5	N	5

Table 7.3. Performance results of the HMI's safety system.

	CE	CE σ	ANO (m)	AS (m/s)	D
Scenario 1	0.0144	0.0571	0.7241	0.1747	No
Scenario 2	0.0195	0.0628	0.7622	0.1416	Yes
Scenario 3	0.0196	0.0664	0.7711	0.1541	No

Table 7.4. Performance results of the HMI's safety system.

	CE	CE σ	ANO (m)	AS (m/s)	D
Scenario 1	0.0036	0.0129	0.6331	0.2106	No
Scenario 2	0.0030	0.0107	0.6478	0.1832	No
Scenario 3	0.0057	0.0284	0.6401	0.1473	No

7.2.1.3 Results

Considering the scenarios in Figure 7.5, the experimental results in a virtual environment for a subject controlling a real HMI are summarized in Table 7.3 (HMI only) and Table 7.4 (HMI with proposed method). Each table represents the average values for each scenario from each subject in their two run tests except for the deadlock case where the worst result is shown from the total of runs. From the presented results, the proposed method outperforms, as expected, the HMI-only solution. The HMI-only solution shows a higher *CE* as a result of the HMI constraints. In the scenario 4 experiment, the users struggled with the narrow passage and the run had to be restarted multiple times. For the proposed method, the required control effort transitions (*CE*) were reduced as more stable control requests were achieved by the proposed method. With the use of a utility function for the object distance, the resulting distance to the walls was similar to the initial results (HMI-only), while performing the proposed social behavior of approaching the nearest wall (leaving a valid traversable path for other people) showing that the proposed framework approaches the same results provided by a human without assistance in the same conditions while providing a more tolerable control. A qualitative

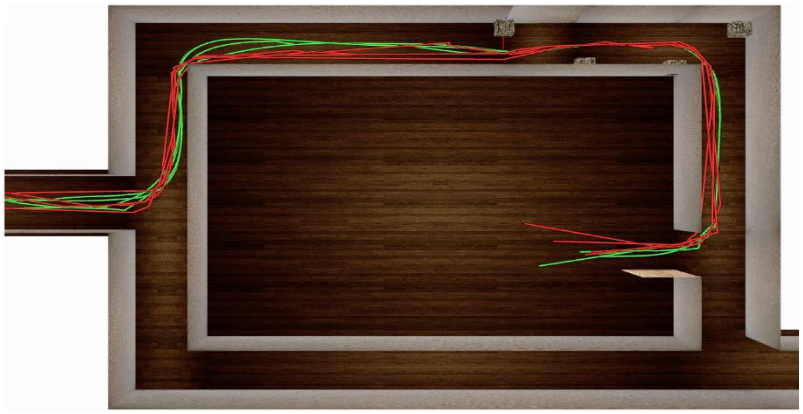

Figure 7.6. Qualitative results for Scenario 4. In red, the HMI-only, in green the proposed method.

analysis of Figure 7.6 for the scenario 4 also shows that the proposed method produces smoother trajectories.

7.2.2 Real-World Scenario

Following the promising experiments from the previous section, the deployment of the proposed method in the ISR-AIWALKER was performed in order to accurately validate a complete robot-assisted navigation pipeline. In order to deploy the proposed approach in the

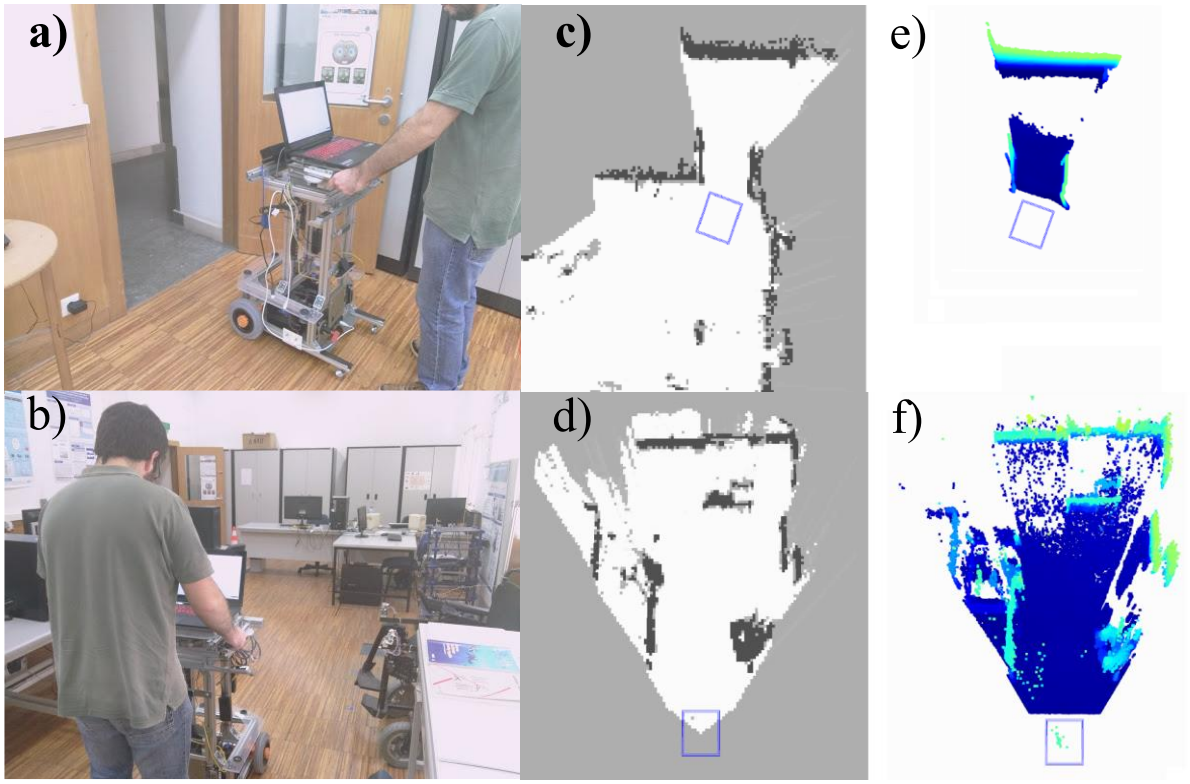

Figure 7.7. Stills with a user driving the walker, from the office traversal and door entrance a) and b). Images c) and d) correspond to the local occupancy map for both scenarios. e) and f) to the Microsoft's Kinect One point cloud in both scenes.

walker platform, a ROS-based software architecture was developed. The architecture is composed by three main modules: walker interface, local environment perception and robot-assisted navigation.

7.2.2.1 Experimental Protocol

For the real-world validation stage, one of the volunteers of the hybrid setup validation was asked to handle the walker in a new scenario with and without assistance. The scenario consisted on an office environment traversal with a final step consisting in performing a door entrance, as seen in Figure 7.7. The metrics used to evaluate the performance are the same as in the hybrid setup experiment and runs with and without assistance were also evaluated. Before the test start, a new familiarization with the system, now with a free run in a real-world setting was performed. Each volunteer was then asked to abide to the hybrid setup validation requirements (drive safely avoiding obstacles) with an additional rule. If the user feels stressed or uneasy with any type of motion he should stop and the scenario is restarted (activating the deadlock flag).

7.2.2.1 Results

Considering the scenario pictured in Figure 7.7, the experimental results in a real-world setting are summarized in Table 7.5 with and without assistance. Figure 7.8 shows on the left and on the right the linear velocity, angular velocity and walker's minimum distance to obstacles, without assistance and with assistance respectively. During the test no deadlock case occurred, with the walker's users showing signs of a comfortable driving experience. From the presented results in Table 7.5, follows a similar trend to the hybrid validation stage as the proposed method outperforms the HMI-only solution. The same discussion can be made for this experiment in comparison to the previous section. The HMI-only solution shows a higher *CE* as a result of the HMI constraints. Since the proposed approach provides smoother transitions in control command the value is higher for the HMI-only solution. Although the *ANO* values are similar for both, in Figure 7.8 on the left and right, it is noticeable a smaller variation on transitions for the minimum distance to obstacles, when compared to. In both approaches, due to the small size of the door passage, the walker is forced to operate with

Table 7.5. Performance results in a real-world scenario.

	CE	CE σ	ANO (m)	AS (m/s)	D
Without Assist.	0.037	0.0909	0.9	0.1457	No
With Assist.	0.0319	0.0860	0.8910	0.2177	No

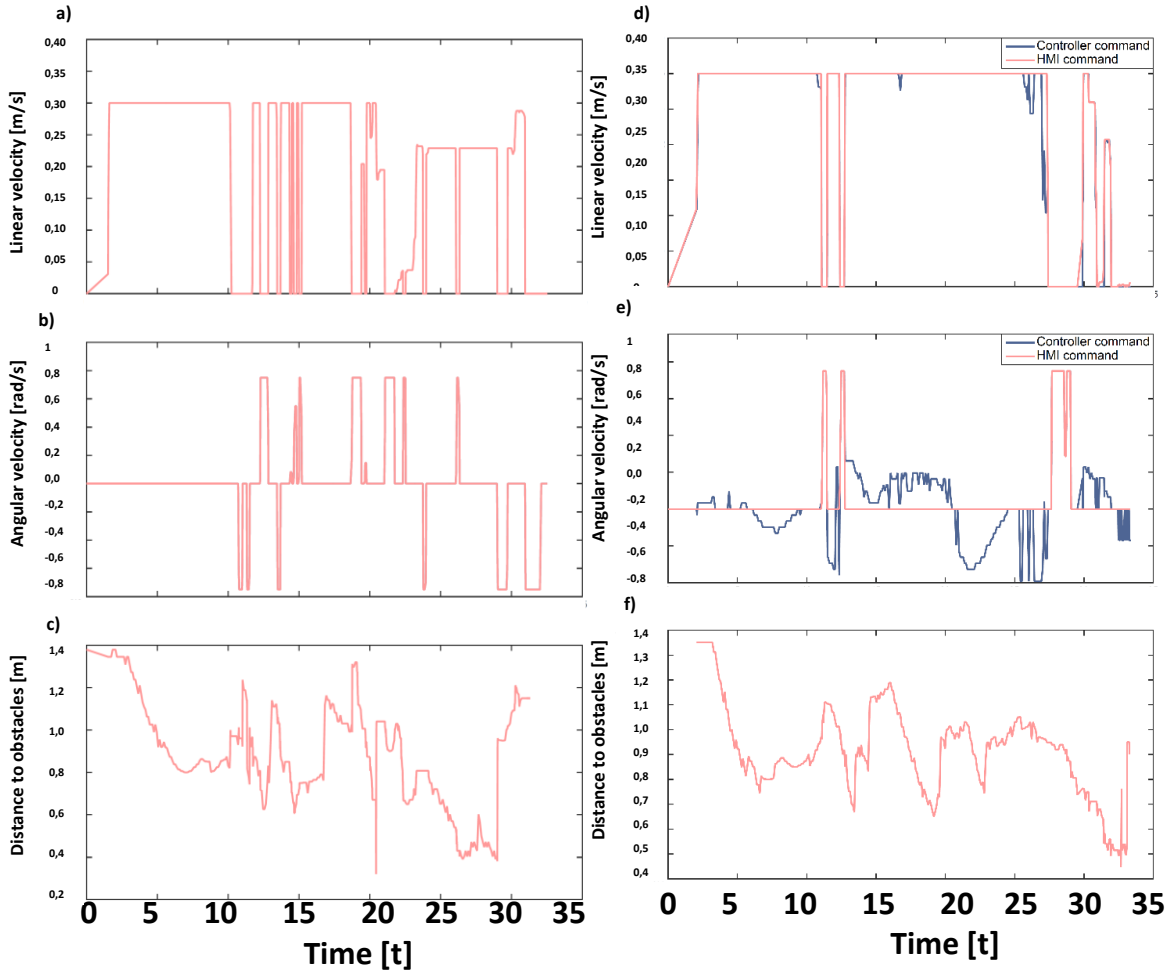

Figure 7.8. Results for an office traversal and door entrance by one user without assistance; a) user requested linear velocity, b) user requested angular velocity and c) walker's minimum distance to obstacles. And with assistance with respective scenarios d), e) and f).

obstacles as close as 10 cm apart from itself.

7.3 Human Gait Tracking and Modeling Validation

This set of experiments aims to evaluate the performance of the two proposed approaches for gait modeling against a ground truth. The tests present the accuracy in terms of the tracked features that can be extracted on both systems.

7.3.1 Skeletal Modeling Strategy Test

The proposed modeling strategy was tested considering several parameters. The objective of the implementation of the strategy is to track and record the lower limbs' specific features.

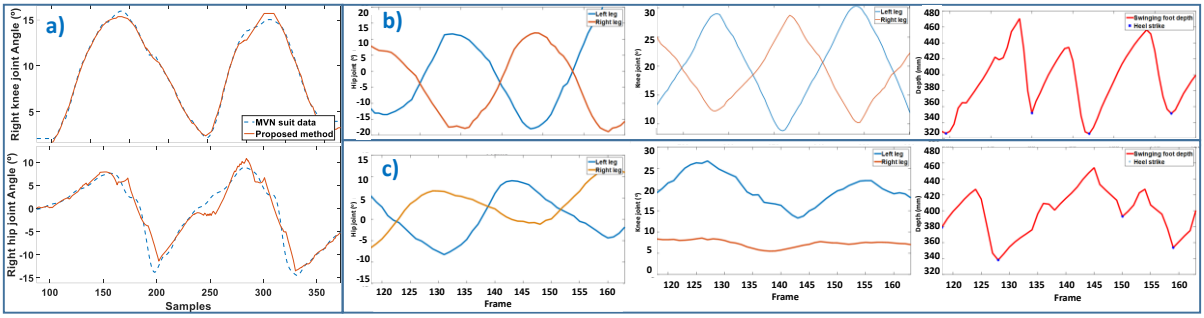

Figure 7.9. Gait analysis system's validation. a) Against ground truth. b) and c) present Tracking data for the features: hip's joint angle, knee's joint angle and swinging foot's depth with heel strike detection, seen in row b) for a normal gait pattern and c) a restricted right knee described by an asymmetrical gait pattern.

As such, the quality of the extracted features was evaluated.

For this experiment, 10 healthy volunteers with no prior history of impairments collaborated, 9 males and one female, between the ages of 25 and 35. The subjects were asked to walk in a straight line pushing the robotic walker at their self-selected speed.

The evaluation assessed the proposed system's capacity to accurately track the lower limbs. Precision is crucial in gait analysis, as such, extracted features were compared with data obtained by a XSens MVN inertial suit, which was considered as a ground truth. The system's performance was evaluated regarding the extraction of the hip's joint and knee's joint excursions, for an asymptomatic gait pattern. Figure 7.9 a) illustrates the performance of the system, providing a visual representation of the variation of each feature during a stride. Looking at the results a consistent tracking by the proposed method when compared to the Xsens's system can be observed. An average error of 1.6º was achieved, which is a very acceptable error, considering the low-cost technologies employed.

Furthermore, results for the same features as well as for heel strike detection are also provided during several strides of different gait patterns. Analyzing Figure 7.9 b) and Figure 7.9 c), a coherent tracking of each specific feature can be observed. For normal gait patterns, the motions of each leg vary symmetrically, while for a restricted knee pattern the knee's joint variation is consistent with the leg's bending restriction, where one of the leg's knee joint angle remains constant during different gait cycles.

The system evidenced, however, some misbehaviors that are related to the technical specificities of the sensors used. The Leap Motion sensor relies on IR reflection from the scene, so if the users were wearing dark and non-reflective cloths the 3D data retrieved from the sensor reveals itself unreliable. The same goes for all black footwear, where the structured light grid from the Intel's camera is not reflected. The fitting of the clothes also influences performance.

Slimmer fitted clothes offer more reliable results. However, even with regular pants, the obtained results proved to be satisfactory. these less favorable scenarios are considered to be easily avoidable by providing a set of usage guidelines and as such, they do not hinder the advantages of the proposed system. Another limitation of the system is its inability to detect gait patterns that exhibit no separation of the legs at any point from the feet up to the waist at the contour image level. If the legs completely overlap, the performance of the system is affected. It is also important to note that the approach considers gait analysis as linear motion and discards rotations. Even using a 3D approach, there is a limitation related to the turning motions of the user. If the user's body rotates and the frontal plane of the user is not considerably parallel to the walker, the proposed approach may become unreliable, due to an incorrect sagittal plane projection.

7.3.2 Shape-based Modeling Strategy Test

The other contribution in terms of modeling strategies is the shape-based one. It is an alternative approach to the lower limbs tracking, which is responsible for capturing the motions and for modeling that information. A test was performed to evaluate the system's precision against a ground truth, just like in the previous experiment. The extracted features were again compared with the data from the same XSens MVN inertial suit. The system's performance was evaluated in the extraction of the hip's joint and knee's joint angles excursions. The volunteers from the previous experiment walked in a straight path aided by the walker and wearing the inertial suit, evidencing their natural walking pattern. Figure 7.10, illustrates the performance of the system, providing a visual representation of the variation of each feature during a stride. Analyzing the lower limbs tracking system's test, looking at the plots of Figure 7.10, it is observable a coherent tracking by the proposed method when compared to the Xsens's system. An average error of 3º was achieved, which is still a satisfactory result for this proposed method, especially if the sensors' technology used in our setup, which is low-cost when compared with the Xsens system, is taken into account. The challenges faced with this specific setup were a consequence of the technical specificities of the sensors used, as in the previous experiment.

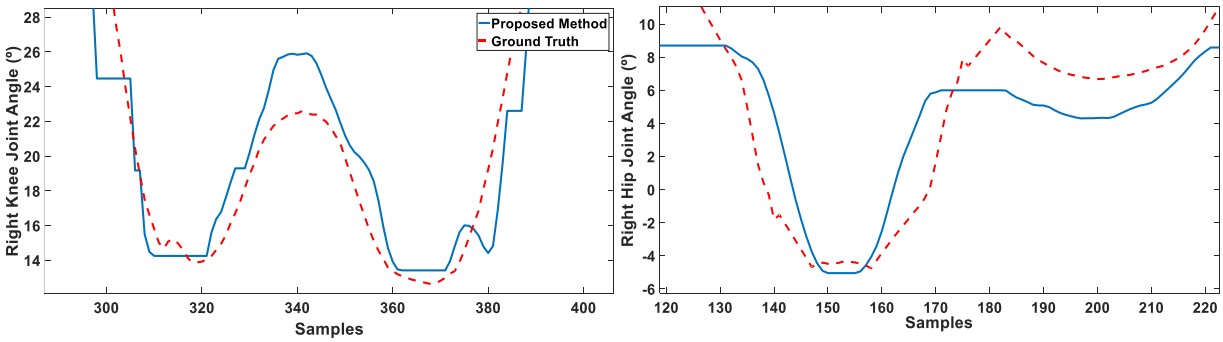

Figure 7.10. Comparison between the proposed lower limbs tracking system's performance and the MVN inertial suit for a gait cycle. Up shows the right joint angle of the knee excursion. Bottom shows the right joint angle of the hip excursion.

7.4 Adaptive Speed Control Validation

This experiment aimed to validate the proposed system's gait pattern classifier's performance. The validation of the system is performed in two-fold: (i) simulated input gait pattern normal probabilities and (ii) a real-world application on the robotic.

Considering the first test, a validation of the results of the classification strategy with a collected dataset was intended. For the dataset collection, 5 volunteers were invited to participate. This author opted to collect normal and asymmetric gait patterns for this experiment. At the time the experiment was performed, it was not possible to have pathological subjects available, with whom it could be easier to collect other kinds of gait patterns, like pathological ones. This author decided to simulate the asymmetry resorting to a physical restriction, a common practice as described in [121]. The considered normal gait pattern was collected with each subject walking naturally. The asymmetrical pattern was collected using two variations: a left knee joint bending restriction, simulated with the help of a Neo-G thigh band support wrapped around the knee, and an equivalent approach on the right knee. The Neo-G band forces the user not to flex the leg. For the two gait patterns, the subjects were asked to walk along a straight path for 10 minutes aided by the walker at a self-selected speed. The experiment considered a 30 Hz framerate.

The proposed classification strategy for gait classification was evaluated using a leave-one-out cross validation test. The learning stage was performed with four persons and tested against one unseen "new person". Results show a satisfactory classification performance, with an accuracy rate of 93.6%, and a precision and recall rate of 91.4% and 88.86%, respectively.

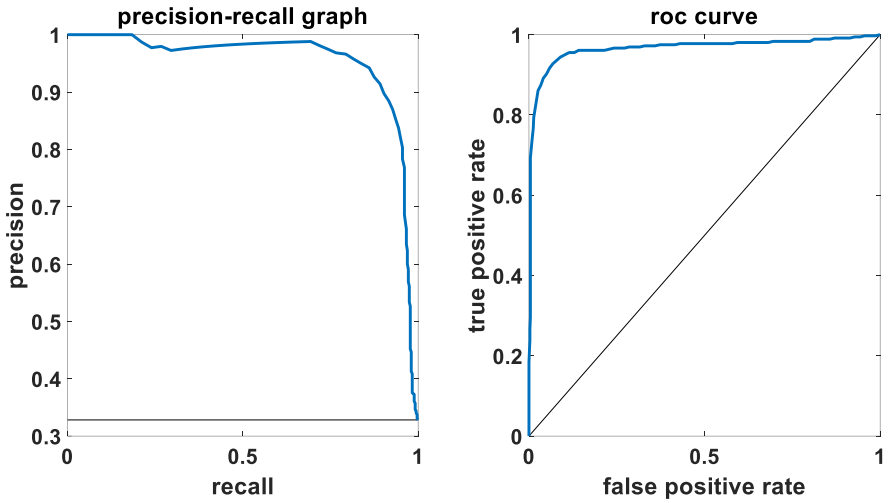

Figure 7.11. Precision-Recall curve on the left and the receiver-operating characteristic curve on the right of the classifier.

The Precision-Recall curve and the Receiver-Operating Characteristic (ROC) curve are shown in Figure 7.11, with an Area Under the Curve of 0.9428.

As an overall comment, one can identify a few challenges faced with the proposed system. Once more a reference is made that since the system is based on IR cameras, garments that are too dark to a point of not reflecting the IR light can cause a degradation of the system performance. Another important aspect, is that loose clothes, like skirts, are to be avoided. The most suited garment is pants, due to a better discriminative capacity at the 3D point cloud level, when applying density estimation. Up to this point tests only reflected constant walking speed. It is still desirable to evaluate how the speed variation of walking affects the extracted features and the classification results. However, since most of the features used are not time dependent, each gait cycle will probably be equally described as belonging to the same gait pattern, no matter the walking speed.

The second test performed intended to evaluate the system performance on a real world practical scenario. This test aimed to evaluate the specific system's applicability in the robotic walker context presented in Chapter 5.

The classifier's model used is the one trained during the previous test, and the considered posterior probability is the probability of the observed instance belonging to the normal gait pattern class, computed from the classifier's outputs.

For the experiment, the same 5 volunteers from the previous test were involved. First, an offline test of the extended controller was performed. Several linear motion commands that the user can typically perform in the platform were artificially inputted, along with artificial normal gait pattern probability inputs. The outputs were the velocities for each case, influenced by the

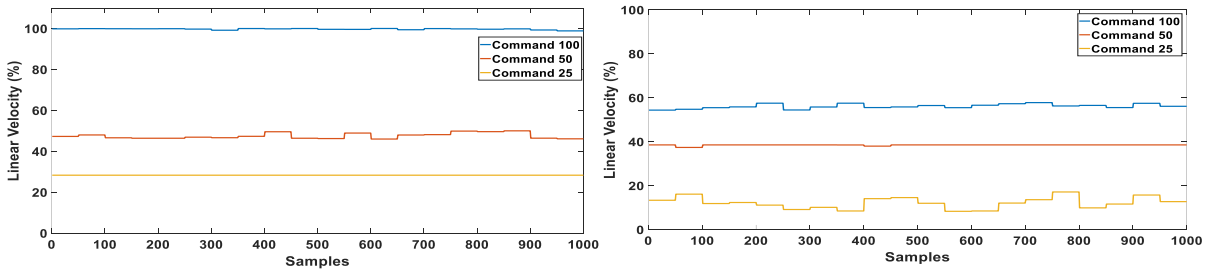

Figure 7.12. Simulation results. On the left simulated linear velocity output for a normal gait pattern for three different commands, influenced by the probability in the temporal sliding windows. On the right simulated linear velocity output for an asymmetrical gait pattern for the same three different commands.

normal gait probability. The goal was to analyze the fuzzy controller's outputs. The two distinct scenarios that were considered for the inputted normal gait pattern class's posterior probability were: the case where the user presents a normal gait pattern, which was represented by a 0.91 mean probability rate value with a standard deviation of 0.04. The second scenario was the case where the user presented an asymmetrical gait pattern. In this scenario, the probability rate was defined as having a mean value of 0.35 and standard deviation of 0.05. These values were determined on the results from the classification validation experiment using the test set from the previous experiment. The defined user commands were the ones that resulted in an output of 25, 50 and 100 % of the linear velocity, considering the previous fuzzy controller implementation without adaptive linear velocity rules.

Looking at Figure 7.12, the linear velocity commands outputted by the controller are affected by the normal gait pattern's classification's posterior probability, as observed. When the posterior probability of the gait pattern evidences values within a normal gait pattern scenario, the user can operate the walker taking advantage of the full span of velocities the platform can provide. On the other hand, when the presented gait pattern falls outside of a normal and natural gait, the system limits the linear velocity span. This way it enforces safety by avoiding linear velocities that otherwise could be hazardous for the user.

In a second stage, taking advantage of the robotic walker, an online test was performed with the system on board. The volunteers walked across the scenario pictured in Figure 7.13 a), first walking naturally and unrestrictedly, and then using the same knee restriction from the previous test. Figure 7.13 b) and c), show the controller's outputs for both linear and angular velocities, for the same user. They also show both the normal walking and the restricted walking scenarios' results, respectively. The results evidenced in this test, are coherent with the ones observed in the offline one. When the users walk naturally, the normal class posterior probability, outputted by the classifier, provides a full span linear velocity output, allowing the

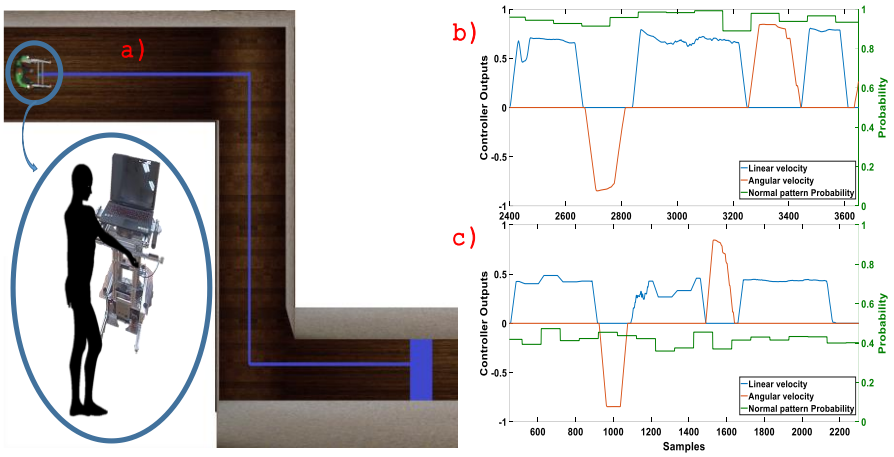

Figure 7.13. Application results. a) test path with the desired trajectory and goal in blue. b) angular and linear velocities controller's outputs against the normal pattern class probability for a normal gait scenario. c) Angular and linear velocities controller's outputs against the normal pattern class probability for an asymmetrical gait scenario.

user to maneuver the walker unrestrictedly. In the case of a restricted knee gait, the posterior probability of the normal class is lower, resulting on an adjustment of the linear velocity to guarantee a safer interval of operation. The reduced velocity allows the user to fully support his body weight on the platform safely, since the walker's velocity is adjusted to the user's gait pattern.

7.5 Automatic Gait Analysis Validation

In this subsection, the results of the proposed automatic gait analysis methods are presented. The experiment was divided in three tests that encompass the supervised method and the two unsupervised ones. The tests are focused on the assessment of the performance of the proposed learning approaches.

7.5.1 Supervised Learning Approach Test

The proposed supervised gait analysis system was tested considering several parameters. The objective of the implementation of the system is to provide an automatic classification tool of gait patterns. As such, the classification's performance was evaluated.

For this experiment, the collaboration of 10 healthy volunteers was possible, 9 males and one female, between the ages of 25 and 35. The subjects were asked to walk in a straight line

Table 7.6. Performance results of the SVM with different kernels.

	Acc. (%)	Prec. (%)	Rec. (%)
Linear	73.36	74.71	90.91
Quad.	86.14	88.99	90.44
Cubic	88.34	90.65	90.44

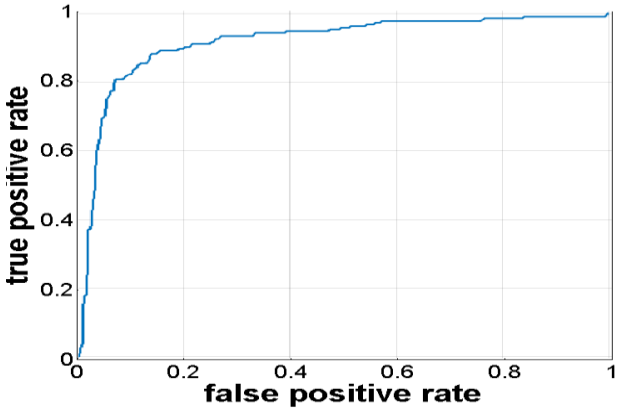

Figure 7.14. ROC curve for the gait analysis system's classifier.

pushing the robotic walker. Three gait patterns were used: (1) normal gait with no restrictions (2) restriction of the right knee preventing the leg from bending, simulating a right knee joint disorder (3) restriction of the left knee preventing the leg from bending, simulating a left knee joint disorder. Patterns 2 and 3 simulate an osteoarthritis knee condition, which presents an asymmetrical gait pattern on afflicted individuals. The subjects performed 3 repetitions of 50 consecutive steps for each pattern. Each repetition involved speed variations of 0.25 steps/s, 0.5 steps/s and 1 step/s.

The classification strategy implemented in this system was evaluated using a leave-one-out cross-validation test. The purpose was to evaluate the generalization capacity of the classifier. The learning stage was performed with 8 persons and tested against two unseen "new persons". Tests were performed with different kernel variations, linear and polynomial kernels. Table 7.6 presents the results for each kernel. The cubic kernel stands out as the best. The ROC curve shown in Figure 7.14 evidences the discrimination capacity from the SVM with a cubic kernel. The developed system is considered to exhibit a satisfactory performance, denoting an adequate an overall accuracy of the classifier for gait asymmetry pattern detection of 88.3%.

7.5.2 OC-SVM Learning Approach Test

Before validating this strategy, a test using a supervised learning strategy to validate the discriminative potential of the proposed features was performed. Using the dataset collected in the previous test, the gait patterns were labeled as "normal" or "novel", depending on the considered observed gait pattern. A user-dependent test was performed for each of the three patterns, to discriminate each one against the rest. As a supervised learning problem, such

Table 7.7. Supervised test results for each gait pattern against the others with average results for all subjects and the worst case.

	Accuracy(%)	AUC	Precision(%)	Recall(%)
		Pattern 1		
Average	98.92	0.9729	100	94.57
Worst	97.84	0.9457	100	89.13
		Pattern 2		
Average	98.57	0.9749	100	94.99
Worst	97.99	0.9661	100	93.25
		Pattern 3		
Average	98.25	0.9631	98.96	92.91
Worst	96.20	0.9155	96.88	83.98

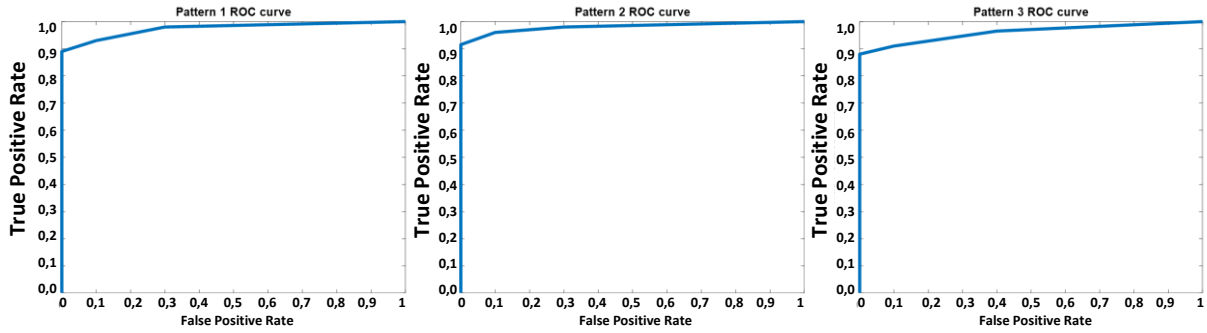

Figure 7.15. ROC curves of the supervised test for performance analysis.

Table 7.8. Accuracy values for novelty and same pattern instances detection.

	Same Pattern (%)	Novel Patterns (%)
	Pattern 1	
Average	92.31	95.47
Worst	91.34	93.61
	Pattern 2	
Average	85.24	98.83
Worst	80.65	97.66
	Pattern 3	
Average	86.89	99.37
Worst	80	98.80

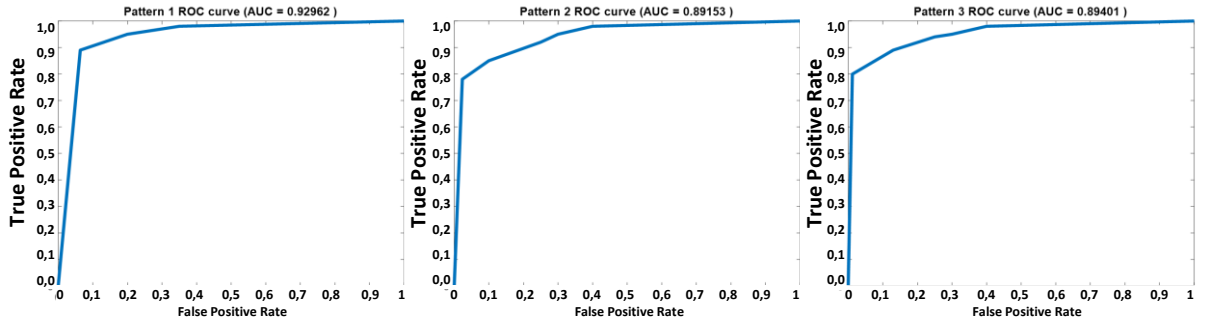

Figure 7.16. Proposed system's ROC curves of the lowest performance for each gait pattern.

classification strategy is not suitable for novelty detection. However, if the test shows a successful separation of specific gait patterns, a statement can be made about the possibility of

linear separability of the data, in the feature space. It is noted that success in this test does not imply good results of the proposed novelty detection strategy, but a failure would be a reliable indicator that no matter which technique would be used, it could not be achieved good results with the proposed strategy.

The classifier used for this test was a binary SVM with RBF kernel. The fused feature space $\mathcal{F}$ was used, representing the fusion of extracted features, both kinematic and spatiotemporal. A cross validation scheme for each test was used. The results are shown in Table 7.7 and Figure 7.15. Considering the classification performance, this supervised test evidenced a strong discrimination performance. Each pattern was classified against observations of the same pattern and against the other ones. As seen in Table 7.7, for each pattern an accuracy above 95% was reached, considering the average result from all users. The Receiver-Operating Characteristic (ROC) curves from Figure 7.15, also demonstrate the strong discrimination performance of the classification method in this test.

To test the proposed novelty detection strategy, the proposed machine learning method was trained with a single pattern for each user at a time. This is fundamental for novelty detection, where it is only possible to observe one gait pattern at a given time, and the learning is dependent on the user, not being transversal to other users. Looking at Table 7.8, it is adequate to state that the system is accurate at detecting novel gait cycles, when using the same features as the supervised test, but in a one-class learning scenario. Due its high sensitivity, some of the normal class instances are labeled as novel. This situation does not present itself as a problem since the rate of mislabeling is too low to compromise the system's capability for detecting actual novel gait patterns. This holds true because the rate of novel gait cycles is below the defined threshold to trigger a new learning step when a new gait pattern is present. This behavior is rather desirable for a novelty detection system. These kinds of approaches tend to be more sensitive to novelty than to normal events. Figure 7.16 allows the analysis of the system's performance in a generalized manner, through the ROC curves. They represent the worst-case scenario (worst subject's results) for each pattern, demonstrating that even in the worst of the three pattern scenarios, it still provides a good performance.

7.5.3 Combined Learning Approach Test

In this subsection, results from three tests to validate the proposed combined approach are presented. Tests were performed with both synthetic and real data. The real data datasets were obtained from a public dataset on human motion of subjects walking on a treadmill, and

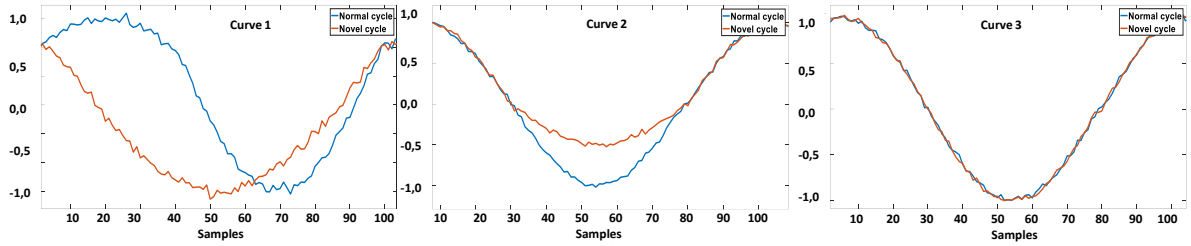

Figure 7.17. Synthetic data comparing a “normal” and “novel” gait cycle.

from the dataset captured using the lower limbs motion capturing system, located on board the robotic walker platform.

7.5.3.1 Synthetic Data

To test the strategy, synthetic data was first used to replicate the motion of the lower limbs. From the analysis of the biomechanical features of the human motion, one can approximate the motion of the lower limbs using sine waves [122]. Sine waves with a sampling rate of 10 Hz were generated and added to white noise to represent the tracking noise that is characteristic of real tracking systems. Two sets of data were generated. The “normal” data is the gait pattern used for training, as well as, testing, and “novel” data, which is used to test the created model against unseen gait patterns. Each pattern was generated using just three simulated gait parameters (features), as shown in Figure 7.17. It is a simplified approach compared to the data extracted from tracking systems, but that still allows to understand the performance of the proposed method with a reduced multi parameter dataset. The “novel” pattern, intends to represent a change in the gait pattern over time. The “novel” gait pattern was simulated, introducing a set of shifts for each respective gait parameter’s curve such as a peak time displacement, amplitude variation and purely noise variations (no change in one of the tracked parameters). The gait cycle extraction is an automatic process, considering the sine waves period. In total, it were generated 3000 “normal” cycles and 3000 “novel” ones. Three separate tests were performed using only the spatiotemporal features (SF), only the similarity rates (SR), and their combination (proposed method). This procedure allowed to evaluate if the decision of combining both sets of features evidenced a better performance when compared to their individual performances.

Analyzing the results from Table 7.9, it is observed that this approach revealed the best performance when compared to the use of the spatiotemporal features or the similarity rates alone, validating the decision to use a combined approach. Considering the results from the combined approach, this author observes that it was able to detect the “novel” gait cycles even

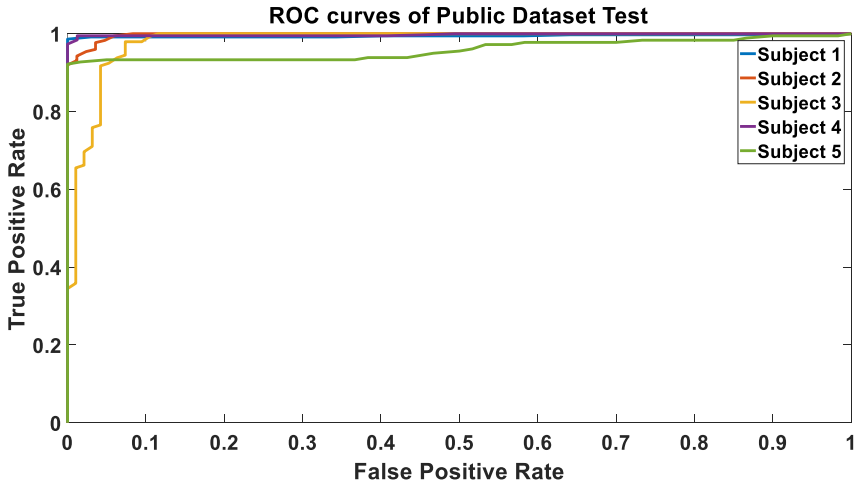

Figure 7.18. ROC curves for each subject of the public dataset test.

Table 7.10. Public dataset test results.

	Accuracy (%)	AUC (%)	Specif. (%)	Sensit. (%)	FP (%)	FN (%)
Subj. 1	97.16	97.97	86.57	99.16	13.43	0.84
Subj. 2	98.06	98.58	94.05	100	5.95	0
Subj. 3	93.75	97.04	94.74	93.10	5.26	6.90
Subj. 4	99.34	98.48	98.77	99.47	1.23	0.53

when one of the gait parameters is identical both in the "normal" and "novel" data. When analyzing the false positive rate (number of gait cycles incorrectly classified as "novel") and the false negative rate, it is demonstrated that the approach is more sensitive to the detection of novelty than to the detection of "normal" gait cycles. This is again the preferable behavior for a novelty detector. This kind of detectors should classify borderline instances as "novel" instead of "normal", providing a design more sensitive to changes.

7.5.3.2 Public Dataset

Looking at the available datasets focusing on gait analysis a public dataset [123] was found which concerns gait data collection from different subjects walking on a treadmill. The collected gait data is adequate to the intended tests since it tracks typical gait parameters used in gait analysis and it involves substantial intra subject gait variations, using three different walking speeds on an instrumented treadmill, focusing on natural walking and longitudinally perturbed walking through pseudo-random fluctuations in the speed of the treadmill belt. A total of approximately 5000 "normal" gait cycles and of 20000 perturbed gait cycles are included in the dataset. The data collected is comprised by full body marker trajectories and

Table 7.9. Synthetic data test results.

Test	Accuracy (%)	AUC (%)	Specificity (%)	Sensitivity (%)	FP (%)	FN (%)
SR	97.54	99.75	90.23	100	9.77	0
SF	98.50	99.88	94.07	100	5.93	0
Comb.	99.03	99.88	96.17	100	3.83	0

ground reaction loads along with other processed variables.

In this test, the marker trajectories were used, in particular the lower limbs' trajectories. The used data are data from five randomly chosen subjects, on which the approach was tested. A user-dependent training and testing was performed since the goal is to detect changes or shifts in the gait pattern of each user. This is particularly important since the potential use of this approach is in rehabilitation processes, where each user has its own rehabilitation progress and particular gait pattern at a given time. The learning framework was trained with normal walking gait cycles, which belong to the same distribution, and tested against the perturbed gait cycles. The goal of this test is to understand if this method is capable of detecting novelty, against a previously trained gait pattern, no matter its qualitative nature. To automatically extract gait cycles, the information provided in the dataset concerning the marked heel strike events was used.

Looking at the experimental results presented in Table 7.10 and Figure 7.18, using the combined approach, it is observable a coherent performance using the public gait tracking dataset, when compared to the synthetic data scenario. The proposed approach, consistently kept the false negative rate low, favoring the sensitivity towards "novel" score outputs.

7.5.3.3 Robotic Walker Dataset

Another experiment was performed, this time involving the robotic walker platform. Five healthy subjects were invited to participate in the dataset collection. Since the goal is to detect changes in the gait pattern it is not feasible to collect a dataset of subjects undergoing rehabilitation and expect gait pattern changes over a short period of time. Usually, these changes are only observable after months of therapy, so this author adopted a strategy of simulating gait patterns, through the use of physical restrictions as in [121][78].

The subjects, that collaborated with the experiment, performed three different sets of gait patterns, just like the protocol used in the previous experiments in this thesis and recapped here. (1) The first set considered has the users walking naturally, to evidence their natural gait pattern. (2) In the second one, users wore a Neo-G thigh band support wrapped around their left knee to simulate a left knee joint bending restriction. The band does not prevent the leg to bend entirely, offering some restriction to the usual subject's leg bending. (3) In the third and last set, a similar procedure was followed, but this time on the right knee. For each gait pattern, the subjects were asked to walk along a straight path for about 10 minutes, supported by the robotic walker.

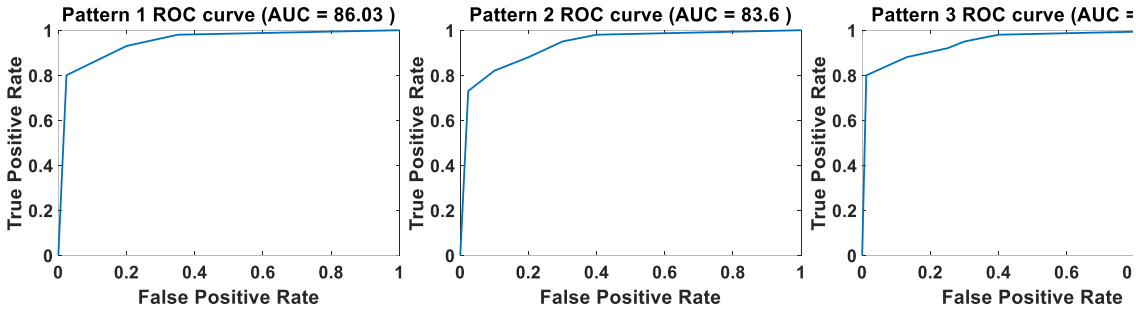

Figure 7.19. ROC curves of the worst cases for each pattern from the robotic walker dataset experiment.

Table 7.11. ISR-AIWALKER test results.

	Same Pattern (%)	Novel Patterns (%)
	Set 1	
Average	84,62	93,59
Worst case	81.25	87.23
	Set 2	
Average	85.71	100
Worst case	78.57	87.86
	Set 3	
Average	82.86	97.24
Worst case	70.83	83.23

The gait tracking data was obtained at a sampling rate of 30 Hz. The tracked lower limbs' features were:

- Left/right thigh's joint angle excursion with respect to the vertical line.
- Left/right knee's joint angle excursion with respect to the thigh's longitudinal line.
- 3D left/right knee's position.
- 3D left/right foot's position.

Since three gait patterns were acquired for each user, a test of one pattern against the other two could be performed. Table 7.11 presents the average results for all 5 subjects as well as the results for the worst case. Considering the average results, the performance for the 3 sets of gait patterns was coherent. There were no performance drops for any particular pattern. In the worst case, the proposed approach becomes more susceptible to novelties, increasing the false positive rate, resulting in the ROC curves seen in Figure 7.19. This behavior is not necessarily a limitation since, as it was discussed before, this is the desirable behavior of a novelty detector. The performance across all tests was satisfactory, however, when compared to the previous experiments, with synthetic data, and with the public dataset, it can be observed that the overall

performance is slightly lower. This performance drop is considered to may have an explanation in the fact that the tracking data of the lower limbs capturing system may have a noisier performance when compared to the professional motion capturing systems used to capture the used public dataset.

Chapter 8

Conclusions and Future Work

This thesis proposed a set of user-centered approaches for user interaction, modeling and gait analysis in the context of a robotic walker. The contributions of this thesis were twofold: (i) safe and intuitive human-machine interaction, (ii) onboard user monitoring through body motion modeling for gait analysis and gait pattern shift detection. This chapter summarizes the main contributions and draws future lines of research.

8.1 Conclusions

8.1.1 Main Contributions

In this thesis, user-centered methodologies in an assistive mobility context were developed, to improve user interaction and user's monitoring strategies. The goal was to contribute to the domain of robotic assistive devices, in particular, robotic walkers, using a user-centered approach that provides a broader understanding of the user's posture and motion, putting the user in the center of the walker's focus when dealing with safety and motion. The knowledge of the user's condition motivated the introduction of new lines of research such as onboard user motion analysis.

The first contribution that can be identified is the proposal of an intuitive and safe vision-based HMI, which moves away from the force-based paradigm. The HMI replaces the use of a force sensor, with the use of a vision-based one. With the vision-based approach, a higher level of user's state monitoring was achieved, which led to the design of a more intuitive and safer HMI, integrating user hand posture monitorization to ensure a proper interaction.

Still addressing safety, going beyond the user-centered approach, a navigation system to ensure a safer user experience was also proposed. Walkers' users may present other limitations, alongside the gait impairments for which the walker was prescribed. Such additional impairments may introduce an extra layer of difficulty to navigate in complex environments with obstacles and narrow doorways. The proposed navigation solution helps the user to avoid collisions and accidents, without taking the control from him. The system guarantees user safety by simply correcting the walker's trajectory, when appropriate. This is based on the environment's perception to understand the surroundings in which the walker is navigating.

Another contribution proposed in this thesis was the development of novel techniques for onboard user's body posture and motion modeling. These techniques allowed the introduction

of more comprehensive user monitoring methodologies to ensure both safety and progress assessment of rehabilitation therapies. To achieve this contribution, a crucial challenge had to be addressed: the challenge to cope with small distances between user and walker. For this, a novel multimodal sensorial approach was proposed to capture gait parameters while the user operates the walker. Each sensor captures specific parts of the user's body. Taking advantage of the multimodal sensor setup, novel techniques were proposed to model the user's body, using stereo and RGB-D data.

The last main contribution was onboard gait analysis. From the 3D model of the user, the use of machine learning techniques based on novel kinematic features to classify the gait pattern was proposed. One of the proposed techniques was an unsupervised machine learning method to identify changes in the gait pattern over time. The method classifies the gait pattern by analyzing its unitary element, the gait cycle, using both kinematic and spatiotemporal features.

8.1.2 Benefits

From a global perspective, the emphasis on user-centered approaches allows mobility assistance devices to offer the user a more reliable experience. The user feels safer and this is paramount to ensure a good acceptance of the device. Another advantage of user-centered approaches is the fact that the experience is more customized, making the device more intuitive, reducing the user's effort to interact with it.

The HMI coupled with the proposed navigation system, represents a holistic safety system, addressing both the user interaction and the user's navigational context. The user's safety is guaranteed by avoiding an interaction inconsistency and at the same time avoiding collisions with the environment. Holistic safety approaches are fundamental when dealing with mobility devices. The benefit of covering both the user's and the environment's context helps avoid undesirable outcomes.

The introduction of a new paradigm of onboard gait analysis using walkers allows the development of assessment tools for rehabilitation therapies. It provides a means to develop methodologies to classify how well a patient is progressing at each session, and during the whole rehabilitation period. On the other hand, it can also help to identify degenerative conditions, by identifying if the user of a walker starts evidencing gait patterns associated with known diseases, which provides a means for the early detection and intervention at an early stage of such conditions. Another important aspect of onboard gait analysis is the identification of risk factors associated with falls. Identifying the risk of falls in individuals is an important assessment to help diagnose early stage diseases or prescribe mobility aids.

8.1.3 Limitations

There are a few limitations that can be identified based on the experimental analysis of the proposed methodologies. These limitations are as follows:

- The proposed HMI's vision-based solution is based on a hand-tracking system. The performance of the system is dependent on the user's hand gesture's speed and initial hand pose. This a limitation since the system cannot properly track and detect hand features if the user tries to perform a reach-to-grasp gesture rapidly. Another issue is that if the user performs a gesture characterized by finger occlusions, like a fist-shaped pattern, the system struggles to detect the complete set of hand features.

- The HMI issued commands, without the navigation system, only provide independent translational and rotational motion. To perform a turn the user has to stop. However, this limitation can be minimized in indoor environments which are characterized by corners and not curbs.

- The multimodal sensor setup for body motion modeling is dependent on sensors that rely on IR technology, which is a limitation when the user wears non-reflective IR cloths.

- The proposed methodologies for the lower body modeling are dependent on image analysis to perform leg segmentation. If the gait pattern of the user does not provide a clear leg contour segmentation, the proposed method may output an unreliable leg segmentation.

- The developed gait analysis methodologies are constrained to gait cycles with a straight motion. During rotational motions, most of the considered gait features cannot be reliably extracted. This particular behavior may be seen as a limitation. However, in the gait analysis field much of the gait analysis is typically performed when the patient walks in a straight line.

8.2 Future Work

The proposed contributions in this thesis can potentiate several new developments. Future work is envisioned taking advantage of the designed platform and developed methodologies. It

may derive from the proposed methodologies or be a new line of research purely based on the robotic walker platform. The future work here presented focuses on increasing the performance of both the proposed methodologies, mitigating limitations, and also focuses on new methodologies that further advance the field of robotic mobility devices.

The following list presents the ideas that could be explored in the future:

- **Experimental testing with case studies**: The developed modules along the author's Ph. D. studies were tested with healthy volunteers. This is a normal step of every research, to validate the developed work. However, since the end users of this kind of devices are pathological individuals, further experiments are needed with real-world case studies. These experiments would allow the understanding of the behavior of the proposed methodologies when applied to the scenarios for which they were developed.

- **3D force fusion for user's condition modeling**: Taking advantage of the 6-axis force/torque sensor already mounted on the ISR-AIWALKER platform, one can envision the fusion of the interaction forces of the user with the 3D visual-tracking model. This fusion will allow having a more robust and complete user model, which may provide more meaningful data to healthcare professionals about the patient's balance and support. This may lead to better assessments of therapies and diagnostics.

- **Explore novel types of extracted gait features**: Using the lower limbs representation data (3D model), it is possible to further explore new features that can better characterize the gait pattern. For instance, the use of additional clinical-based descriptors may help to better describe the user's gait pattern.

- **Introduction of novel learning schemes**: The collaboration with disabled individuals, which serve as case studies, will provide the collection of a more diversified and bigger dataset with different kinds of gait patterns. This bigger dataset will allow the use of learning approaches like deep learning, which requires extensive datasets. These approaches will be studied to understand if they can outperform the proposed gait pattern classification methods. Another interesting line of research could be the use of ensembles of classifiers, which may help to better tune gait pattern classification to more specific gait pattern deviations.

Annex 1

List of Publications

[A1] J. Paulo, P. Peixoto, and P. Amorim, “Trajectory-based Gait Pattern Shift Detection For Assistive Robotics Applications,” in Journal of Intelligent Service Robotics. [under review]

[A2] J. Paulo, A. Asvadi, P. Peixoto, and P. Amorim, “Human Gait Pattern Changes Detection System: A Multimodal Vision-based and Novelty Detection Learning Approach,” in Biocybernetics and Biomedical Engineering, 2017.

[A3] J. Paulo, L. Garrote, A. Asvadi, C. Premebida and P. Peixoto, “Short-Range Gait Pattern Analysis for Potential Applications on Assistive Robotics,” in IEEE International Symposium on Robot and Human Interactive Communication (RO-MAN), 2017.

[A4] J. Paulo, P. Peixoto, and U. J. Nunes, “ISR-AIWALKER: Robotic Walker for Intuitive and Safe Mobility Assistance and Gait Analysis,” in IEEE Transactions on Human-Machine Systems, 2017.

[A5] L. Garrote, J. Rosa, J. Paulo, C. Premebida, P. Peixoto and U. Nunes, “3D Point Cloud Downsampling for 2D Indoor Scene Modelling,” in IEEE ICARSC, 2017.

[A6] J. Paulo, L. Garrote, C. Premebida, A. Asvadi, D. Almeida, A. Lopes and P. Peixoto, “An Innovative Robotic Walker for Mobility Assistance and Rehabilitation”, in IEEE 5th Portuguese Meeting on Bioengineering (ENBENG), 2017.

[A7] J. Paulo, P. Peixoto, and U. Nunes, “A Novel Vision-based Human-Machine Interface for a Robotic Walker Framework,” in IEEE International Symposium on Robot and Human Interactive Communication (RO-MAN), 2015.

[A8] J. Paulo and P. Peixoto, “Classification of reaching and gripping gestures for safety on walking aids,” in IEEE International Symposium on Robot and Human Interactive Communication (RO-MAN), 2014.

References

[1] W. H. Organization and others, *World report on disability: World Health Organization*. 2011.

[2] P. Fougeyrollas and L. Noreau, “Long-term consequences of spinal cord injury on social participation: the occurrence of handicap situations,” *Disabil. Rehabil.*, vol. 22, no. 4, pp. 170–180, 2000.

[3] E. S. Chaves, M. L. Boninger, R. Cooper, S. G. Fitzgerald, D. B. Gray, and R. A. Cooper, “Assessing the influence of wheelchair technology on perception of participation in spinal cord injury,” *Arch. Phys. Med. Rehabil.*, vol. 85, no. 11, pp. 1854–1858, 2004.

[4] B. E. Leduc and Y. Lepage, “Health-related quality of life after spinal cord injury,” *Disabil. Rehabil.*, vol. 24, no. 4, pp. 196–202, 2002.

[5] “Finance and Development,” *Finance and Development | F&D*. [Online]. Available: http://www.imf.org/external/pubs/ft/fandd/2006/09/carone.htm. [Accessed: 13-Feb-2014].

[6] I. N. Estatística, “Censos 2001-Análise de população com deficiência,” *Lisb. Destaque INE*, 2001.

[7] “Observatório das Desigualdades :: Indicadores.” [Online]. Available: http://observatorio-das-desigualdades.cies.iscte.pt/print.jsp?page=indicators&type=&lang=pt&id=80. [Accessed: 11-Jul-2017].

[8] “WHO | Rehabilitation in health systems,” *WHO*. [Online]. Available: http://www.who.int/disabilities/rehabilitation_health_systems/en/. [Accessed: 13-Apr-2017].

[9] D. Feil-Seifer and M. J. Mataric, “Defining socially assistive robotics,” in *Rehabilitation Robotics, 2005. ICORR 2005. 9th International Conference on*, 2005, pp. 465–468.

[10] S. P. Levine, D. A. Bell, L. A. Jaros, R. C. Simpson, Y. Koren, and J. Borenstein, "The NavChair assistive wheelchair navigation system," *IEEE Trans. Rehabil. Eng.*, vol. 7, no. 4, pp. 443–451, 1999.

[11] G. Pires and U. Nunes, "A wheelchair steered through voice commands and assisted by a reactive fuzzy-logic controller," *J. Intell. Robot. Syst.*, vol. 34, no. 3, pp. 301–314, 2002.

[12] T. Taha, J. V. Miró, and G. Dissanayake, "POMDP-based long-term user intention prediction for wheelchair navigation," in *Robotics and Automation, 2008. ICRA 2008. IEEE International Conference on*, 2008, pp. 3920–3925.

[13] A. Huntemann, E. Demeester, M. Nuttin, and H. Van Brussel, "Online user modeling with Gaussian processes for Bayesian plan recognition during power-wheelchair steering," in *Intelligent Robots and Systems, 2008. IROS 2008. IEEE/RSJ International Conference on*, 2008, pp. 285–292.

[14] S. S. Nudehi, R. Mukherjee, and M. Ghodoussi, "A haptic interface design for minimally invasive telesurgical training and collaboration in the presence of time delay," in *Decision and Control, 2003. Proceedings. 42nd IEEE Conference on*, 2003, vol. 5, pp. 4563–4568.

[15] J. Shen, J. Ibanez-Guzman, T. C. Ng, and B. S. Chew, "A collaborative-shared control system with safe obstacle avoidance capability," in *Robotics, Automation and Mechatronics, 2004 IEEE Conference on*, 2004, vol. 1, pp. 119–123.

[16] Y. Gao *et al.*, "Towards validation of robotic surgery training assessment across training platforms," in *Intelligent Robots and Systems (IROS), 2011 IEEE/RSJ International Conference on*, 2011, pp. 2539–2544.

[17] S. McLachlan, J. Arblaster, D. K. Liu, J. V. Miro, and L. Chenoweth, "A multi-stage shared control method for an intelligent mobility assistant," in *Rehabilitation Robotics, 2005. ICORR 2005. 9th International Conference on*, 2005, pp. 426–429.

[18] C.-H. Law and Y. Xu, "Shared control for navigation and balance of a dynamically stable robot," in *Robotics and Automation, 2002. Proceedings. ICRA'02. IEEE International Conference on*, 2002, vol. 2, pp. 1985–1990.

[19] P. Aigner and B. McCarragher, "Contrasting potential fields and constraints in a shared control task," in *Intelligent Robots and Systems, 1997. IROS'97.,*

Proceedings of the 1997 IEEE/RSJ International Conference on, 1997, vol. 1, pp. 140–146.

[20] P. Aigner and B. McCarragher, "Shared control framework applied to a robotic aid for the blind," in *Robotics and Automation, 1998. Proceedings. 1998 IEEE International Conference on*, 1998, vol. 1, pp. 717–722.

[21] K. Wada, T. Shibata, T. Saito, and K. Tanie, "Analysis of factors that bring mental effects to elderly people in robot assisted activity," in *Intelligent Robots and Systems, 2002. IEEE/RSJ International Conference on*, 2002, vol. 2, pp. 1152–1157.

[22] E. Wade, A. R. Parnandi, and M. J. Matarić, "Using socially assistive robotics to augment motor task performance in individuals post-stroke," in *Intelligent Robots and Systems (IROS), 2011 IEEE/RSJ International Conference on*, 2011, pp. 2403–2408.

[23] M. Ghosh and F. Tanaka, "The impact of different competence levels of care-receiving robot on children," in *Intelligent Robots and Systems (IROS), 2011 IEEE/RSJ International Conference on*, 2011, pp. 2409–2415.

[24] A. Tani, G. Endo, E. F. Fukushima, S. Hirose, M. Iribe, and T. Takubo, "Study on a practical robotic follower to support home oxygen therapy patients-development and control of a mobile platform," in *Intelligent Robots and Systems (IROS), 2011 IEEE/RSJ International Conference on*, 2011, pp. 2423–2429.

[25] H.-M. Gross *et al.*, "Progress in developing a socially assistive mobile home robot companion for the elderly with mild cognitive impairment," in *Intelligent Robots and Systems (IROS), 2011 IEEE/RSJ International Conference on*, 2011, pp. 2430–2437.

[26] K. Kawamura, S. Bagchi, M. Iskarous, and M. Bishay, "Intelligent robotic systems in service of the disabled," *IEEE Trans. Rehabil. Eng.*, vol. 3, no. 1, pp. 14–21, 1995.

[27] A. Giménez, C. Balaguer, A. M. Sabatini, and V. Genovese, "The MATS robotic system to assist disabled people in their home environments," in *Intelligent Robots and Systems, 2003.(IROS 2003). Proceedings. 2003 IEEE/RSJ International Conference on*, 2003, vol. 3, pp. 2612–2617.

[28] S.-J. Blakemore and J. Decety, “From the perception of action to the understanding of intention,” *Nat. Rev. Neurosci.*, vol. 2, no. 8, pp. 561–567, 2001.

[29] Y. Xiao, Z. Zhang, A. Beck, J. Yuan, and D. Thalmann, “Human–robot interaction by understanding upper body gestures,” *Presence Teleoperators Virtual Environ.*, vol. 23, no. 2, pp. 133–154, 2014.

[30] B. Huber, “Foot position as indicator of spatial interest at public displays,” in *CHI’13 Extended Abstracts on Human Factors in Computing Systems*, 2013, pp. 2695–2700.

[31] A. S. Clair, R. Mead, M. J. Matarić, and others, “Monitoring and guiding user attention and intention in human-robot interaction,” in *ICRA-ICAIR Workshop, Anchorage, AK, USA*, 2010, vol. 1025.

[32] A. Tavakkoli, R. Kelley, C. King, M. Nicolescu, M. Nicolescu, and G. Bebis, “A vision-based architecture for intent recognition,” *Adv. Vis. Comput.*, pp. 173–182, 2007.

[33] J. Rios-Martinez, A. Escobedo, A. Spalanzani, and C. Laugier, “Intention driven human aware navigation for assisted mobility,” in *Workshop on Assistance and Service robotics in a human environment at IROS*, 2012.

[34] J. Perry, J. R. Davids, and others, “Gait analysis: normal and pathological function.,” *J. Pediatr. Orthop.*, vol. 12, no. 6, p. 815, 1992.

[35] T. Öberg, A. Karsznia, and K. Öberg, “Basic gait parameters: reference data for normal subjects, 10-79 years of age,” *J. Rehabil. Res. Dev.*, vol. 30, pp. 210–210, 1993.

[36] T. Oberg, A. Karsznia, and K. Oberg, “Joint angle parameters in gait: reference data for normal subjects, 10-79 years of age.,” *J. Rehabil. Res. Dev.*, vol. 31, no. 3, pp. 199–213, 1994.

[37] E. H. Melis, R. Torres-Moreno, H. Barbeau, and E. D. Lemaire, “Analysis of assisted-gait characteristics in persons with incomplete spinal cord injury,” *Spinal Cord*, vol. 37, no. 6, pp. 430–439, 1999.

[38] A. Fattouh, M. Sahnoun, and G. Bourhis, “Force feedback joystick control of a powered wheelchair: preliminary study,” in *Systems, Man and Cybernetics, 2004 IEEE International Conference on*, 2004, vol. 3, pp. 2640–2645.

[39] T. Lu, “A motion control method of intelligent wheelchair based on hand gesture recognition,” in *Industrial Electronics and Applications (ICIEA), 2013 8th IEEE Conference on*, 2013, pp. 957–962.

[40] B. Rebsamen *et al.*, “A brain controlled wheelchair to navigate in familiar environments,” *Neural Syst. Rehabil. Eng. IEEE Trans. On*, vol. 18, no. 6, pp. 590–598, 2010.

[41] S. Dubowsky *et al.*, “PAMM-a robotic aid to the elderly for mobility assistance and monitoring: a ‘helping-hand’ for the elderly,” in *Robotics and Automation, 2000. Proceedings. ICRA’00. IEEE International Conference on*, 2000, vol. 1, pp. 570–576.

[42] G. Lacey, S. Mac Namara, and K. M. Dawson-Howe, “Personal adaptive mobility aid for the infirm and elderly blind,” in *Assistive Technology and Artificial Intelligence*, Springer, 1998, pp. 211–220.

[43] M. Alwan, A. Ledoux, G. Wasson, P. Sheth, and C. Huang, “Basic walker-assisted gait characteristics derived from forces and moments exerted on the walker’s handles: results on normal subjects,” *Med. Eng. Phys.*, vol. 29, no. 3, pp. 380–389, 2007.

[44] O. Chuy, Y. Hirata, Z. Wang, and K. Kosuge, “Motion control algorithms for a new intelligent robotic walker in emulating ambulatory device function,” in *Mechatronics and Automation, 2005 IEEE International Conference*, 2005, vol. 3, pp. 1509–1514.

[45] Y.-H. Hsieh, Y.-C. Huang, K.-Y. Young, C.-H. Ko, and S. K. Agrawal, “Motion Guidance for a Passive Robot Walking Helper via User’s Applied Hand Forces,” *IEEE Trans. Hum.-Mach. Syst.*, vol. 46, no. 6, pp. 869–881, 2016.

[46] A. Frizera, R. Ceres, J. L. Pons, A. Abellanas, and R. Raya, “The smart walkers as geriatric assistive device. the simbiosis purpose,” *Gerontechnology*, vol. 7, no. 2, p. 108, 2008.

[47] A. Frizera Neto, R. Ceres, E. Rocón de Lima, and J. L. Pons, “Empowering and assisting natural human mobility: the simbiosis walker,” *Int. J. Adv. Robot. Syst.*, vol. 8, no. 3, pp. 34–50, 2011.

[48] A. Morris *et al.*, “A robotic walker that provides guidance,” in *Robotics and*

Automation, 2003. Proceedings. ICRA'03. IEEE International Conference on, 2003, vol. 1, pp. 25–30.

[49] M. Patel, J. V. Miro, and G. Dissanayake, "A Hierarchical Hidden Markov Model to support activities of daily living with an assistive robotic walker," in *2012 4th IEEE RAS EMBS International Conference on Biomedical Robotics and Biomechatronics (BioRob)*, 2012, pp. 1071–1076.

[50] M.-F. Chang, W.-H. Mou, C.-K. Liao, and L.-C. Fu, "Design and implementation of an active robotic walker for Parkinson's patients," in *SICE Annual Conference (SICE), 2012 Proceedings of*, 2012, pp. 2068–2073.

[51] M. Martins, "Real Time Control of the ASBGo walker through a physical human-robot interface.," *Measurement*, vol. 48, pp. 77–86, 2013.

[52] A. J. Rentschler, R. Simpson, R. A. Cooper, and M. L. Boninger, "Clinical evaluation of Guido robotic walker.," *J. Rehabil. Res. Dev.*, vol. 45, no. 9, 2008.

[53] G. Lee, T. Ohnuma, N. Y. Chong, and S.-G. Lee, "Walking Intent-Based Movement Control for JAIST Active Robotic Walker," *IEEE Trans. Syst. Man Cybern. Syst.*, vol. 44, no. 5, pp. 665–672, May 2014.

[54] T. Ohnuma, G. Lee, and N. Y. Chong, "Development of JARoW-II active robotic walker reflecting pelvic movements while walking," *Intell. Serv. Robot.*, vol. 10, no. 2, pp. 95–107, 2017.

[55] C. A. Cifuentes, C. Rodriguez, A. Frizera-Neto, T. F. Bastos-Filho, and R. Carelli, "Multimodal Human-Robot Interaction for Walker-Assisted Gait," *IEEE Syst. J.*, vol. PP, no. 99, pp. 1–11, 2014.

[56] S. Fahn, "The freezing phenomenon in parkinsonism.," *Adv. Neurol.*, vol. 67, p. 53, 1995.

[57] M. M. Martins, C. P. Santos, A. Frizera-Neto, and R. Ceres, "Assistive mobility devices focusing on Smart Walkers: Classification and review," *Robot. Auton. Syst.*, vol. 60, no. 4, pp. 548–562, 2012.

[58] M. Martins, C. Santos, A. Frizera, and R. Ceres, "A review of the functionalities of smart walkers," *Med. Eng. Phys.*, vol. 37, no. 10, pp. 917–928, Oct. 2015.

[59] R. B. Davis III, S. Ounpuu, D. Tyburski, and J. R. Gage, "A gait analysis data

collection and reduction technique," *Hum. Mov. Sci.*, vol. 10, no. 5, pp. 575–587, 1991.

[60] K. Wan and H. Sawada, "3D Motion prediction of human upper body by tracking reflective markers on a moving body," *Chest*, vol. 3, p. T4, 2007.

[61] L. Sigal, A. O. Balan, and M. J. Black, "Humaneva: Synchronized video and motion capture dataset and baseline algorithm for evaluation of articulated human motion," *Int. J. Comput. Vis.*, vol. 87, no. 1, pp. 4–27, 2010.

[62] A. Cappozzo, U. Della Croce, A. Leardini, and L. Chiari, "Human movement analysis using stereophotogrammetry: Part 1: theoretical background," *Gait Posture*, vol. 21, no. 2, pp. 186–196, 2005.

[63] A. Muro-de-la-Herran, B. Garcia-Zapirain, and A. Mendez-Zorrilla, "Gait analysis methods: An overview of wearable and non-wearable systems, highlighting clinical applications," *Sensors*, vol. 14, no. 2, pp. 3362–3394, 2014.

[64] M. O. Derawi, H. Ali, and F. A. Cheikh, "Gait Recognition using Time-of-Flight Sensor.," in *BIOSIG*, 2011, pp. 187–194.

[65] H. Liu, Y. Cao, and Z. Wang, "Automatic gait recognition from a distance," in *Control and Decision Conference (CCDC), 2010 Chinese*, 2010, pp. 2777–2782.

[66] M. Gabel, R. Gilad-Bachrach, E. Renshaw, and A. Schuster, "Full body gait analysis with Kinect," in *Engineering in Medicine and Biology Society (EMBC), 2012 Annual International Conference of the IEEE*, 2012, pp. 1964–1967.

[67] A. Fern'ndez-Baena, A. Susín, and X. Lligadas, "Biomechanical validation of upper-body and lower-body joint movements of kinect motion capture data for rehabilitation treatments," in *Intelligent Networking and Collaborative Systems (INCoS), 2012 4th International Conference on*, 2012, pp. 656–661.

[68] A. M. Sabatini, C. Martelloni, S. Scapellato, and F. Cavallo, "Assessment of walking features from foot inertial sensing," *Biomed. Eng. IEEE Trans. On*, vol. 52, no. 3, pp. 486–494, 2005.

[69] T. Wang *et al.*, "Walking analysis of young and elderly people by using an intelligent walker ANG," *Robot. Auton. Syst.*, vol. 75, pp. 96–106, 2016.

[70] C. D. Lim, C.-M. Wang, C.-Y. Cheng, Y. Chao, S.-H. Tseng, and L.-C. Fu,

"Sensory Cues Guided Rehabilitation Robotic Walker Realized by Depth Image-Based Gait Analysis."

[71] C. Joly, C. Dune, P. Gorce, and P. Rives, "Feet and legs tracking using a smart rollator equipped with a Kinect," in *Workshop on" Assistance and Service Robotics in a Human Environment" in conjonction with IEEE/RSJ Int. Conf. on Int. Rob. and Sys.(IROS)*, 2013.

[72] R. Z.-L. Hu, A. Hartfiel, J. Tung, A. Fakih, J. Hoey, and P. Poupart, "3D Pose tracking of walker users' lower limb with a structured-light camera on a moving platform," in *Computer Vision and Pattern Recognition Workshops (CVPRW), 2011 IEEE Computer Society Conference on*, 2011, pp. 29–36.

[73] S. Page, M. M. Martins, L. Saint-Bauzel, C. P. Santos, and V. Pasqui, "Fast embedded feet pose estimation based on a depth camera for smart walker," in *Robotics and Automation (ICRA), 2015 IEEE International Conference on*, 2015, pp. 4224–4229.

[74] C. V. Granger, G. L. Albrecht, and B. B. Hamilton, "Outcome of comprehensive medical rehabilitation: measurement by PULSES profile and the Barthel Index.," *Arch. Phys. Med. Rehabil.*, vol. 60, no. 4, pp. 145–154, 1979.

[75] R. Baker, "Gait analysis methods in rehabilitation," *J. NeuroEngineering Rehabil.*, vol. 3, no. 1, p. 1, 2006.

[76] N. Mezghani *et al.*, "Automatic classification of asymptomatic and osteoarthritis knee gait patterns using kinematic data features and the nearest neighbor classifier," *Biomed. Eng. IEEE Trans. On*, vol. 55, no. 3, pp. 1230–1232, 2008.

[77] M. D. Djuric-Jovicic, N. S. Jovicic, S. M. Radovanovic, I. D. Stankovic, M. B. Popovic, and V. S. Kostic, "Automatic identification and classification of freezing of gait episodes in Parkinson's disease patients," *Neural Syst. Rehabil. Eng. IEEE Trans. On*, vol. 22, no. 3, pp. 685–694, 2014.

[78] G. Cola, M. Avvenuti, A. Vecchio, G.-Z. Yang, and B. Lo, "An On-Node Processing Approach for Anomaly Detection in Gait," *Sens. J. IEEE*, vol. 15, no. 11, pp. 6640–6649, 2015.

[79] A. B. Gardner, A. M. Krieger, G. Vachtsevanos, and B. Litt, "One-class novelty detection for seizure analysis from intracranial EEG," *J. Mach. Learn. Res.*, vol. 7,

no. Jun, pp. 1025–1044, 2006.

[80] L. Clifton, D. A. Clifton, P. J. Watkinson, and L. Tarassenko, “Identification of patient deterioration in vital-sign data using one-class support vector machines,” in *Computer Science and Information Systems (FedCSIS), 2011 Federated Conference on*, 2011, pp. 125–131.

[81] M. A. Pimentel, D. A. Clifton, and L. Tarassenko, “Gaussian process clustering for the functional characterisation of vital-sign trajectories,” in *2013 IEEE International Workshop on Machine Learning for Signal Processing (MLSP)*, 2013, pp. 1–6.

[82] R. J. Kosinski, “A literature review on reaction time,” *Clemson Univ.*, vol. 10, 2008.

[83] Y. Balash, M. Hadar-Frumer, T. Herman, C. Peretz, N. Giladi, and J. M. Hausdorff, “The effects of reducing fear of falling on locomotion in older adults with a higher level gait disorder,” *J. Neural Transm. Vienna Austria 1996*, vol. 114, no. 10, pp. 1309–1314, 2007.

[84] H. Bateni and B. E. Maki, “Assistive devices for balance and mobility: benefits, demands, and adverse consequences,” *Arch. Phys. Med. Rehabil.*, vol. 86, no. 1, pp. 134–145, 2005.

[85] V. Vapnik, “Pattern recognition using generalized portrait method,” *Autom. Remote Control*, vol. 24, pp. 774–780, 1963.

[86] L. A. Zadeh, “Fuzzy sets,” *Inf. Control*, vol. 8, no. 3, pp. 338–353, 1965.

[87] Luis Garrote and Urbano Nunes, “User-Intent Reinforced Robot-Assisted Navigation for a Robotic Walker Framework,” Technical Report, 2016.

[88] A. Morris *et al.*, “A robotic walker that provides guidance,” in *Robotics and Automation, 2003. Proceedings. ICRA’03. IEEE International Conference on*, 2003, vol. 1, pp. 25–30.

[89] W.-H. Mou, M.-F. Chang, C.-K. Liao, Y.-H. Hsu, S.-H. Tseng, and L.-C. Fu, “Context-aware assisted interactive robotic walker for Parkinson’s disease patients,” in *Intelligent Robots and Systems (IROS), 2012 IEEE/RSJ International Conference on*, 2012, pp. 329–334.

[90] G. Lee, E.-J. Jung, T. Ohnuma, N. Y. Chong, and B.-J. Yi, “JAIST robotic walker

control based on a two-layered kalman filter," in *Robotics and Automation (ICRA), 2011 IEEE International Conference on*, 2011, pp. 3682–3687.

[91] K.-T. Yu, C.-P. Lam, M.-F. Chang, W.-H. Mou, S.-H. Tseng, and L.-C. Fu, "An interactive robotic walker for assisting elderly mobility in senior care unit," in *Advanced Robotics and its Social Impacts (ARSO), 2010 IEEE Workshop on*, 2010, pp. 24–29.

[92] J.-Y. Bouguet, "Camera calibration toolbox for matlab," 2004.

[93] D. Scharstein and R. Szeliski, "A taxonomy and evaluation of dense two-frame stereo correspondence algorithms," *Int. J. Comput. Vis.*, vol. 47, no. 1–3, pp. 7–42, 2002.

[94] S. P. Lloyd, "Least squares quantization in PCM," *Inf. Theory IEEE Trans. On*, vol. 28, no. 2, pp. 129–137, 1982.

[95] G. Wasson, P. Sheth, M. Alwan, K. Granata, A. Ledoux, and C. Huang, "User intent in a shared control framework for pedestrian mobility aids," in *Intelligent Robots and Systems, 2003.(IROS 2003). Proceedings. 2003 IEEE/RSJ International Conference on*, 2003, vol. 3, pp. 2962–2967.

[96] F. Shi, Q. Cao, C. Leng, and H. Tan, "Based on force sensing-controlled human-machine interaction system for walking assistant robot," in *Intelligent Control and Automation (WCICA), 2010 8th World Congress on*, 2010, pp. 6528–6533.

[97] D. Chugo *et al.*, "Standing assistance control using a physical strength of a patient with load estimation," in *2012 IEEE RO-MAN*, 2012, pp. 234–239.

[98] D. Chugo, H. Ozaki, Y. Sakaida, S. Yokota, and K. Takase, "Seating motion analysis and its assistance on a robotic walker," in *2010 IEEE RO-MAN*, 2010, pp. 494–499.

[99] B. E. Boser, I. M. Guyon, and V. N. Vapnik, "A training algorithm for optimal margin classifiers," in *Proceedings of the fifth annual workshop on Computational learning theory*, 1992, pp. 144–152.

[100] J. Platt and others, "Probabilistic outputs for support vector machines and comparisons to regularized likelihood methods," *Adv. Large Margin Classif.*, vol. 10, no. 3, pp. 61–74, 1999.

[101] N. B. Alexander, “Gait disorders in older adults,” *J. Am. Geriatr. Soc.*, vol. 44, no. 4, pp. 434–451, 1996.

[102] C.-C. Chang and C.-J. Lin, “LIBSVM: A library for support vector machines,” *ACM Trans. Intell. Syst. Technol. TIST*, vol. 2, no. 3, p. 27, 2011.

[103] V. Valdimir and N. Vapnik, *The nature of statistical learning theory. 1995*. Springer.

[104] C. J. Burges, “A tutorial on support vector machines for pattern recognition,” *Data Min. Knowl. Discov.*, vol. 2, no. 2, pp. 121–167, 1998.

[105] M. A. Pimentel, D. A. Clifton, L. Clifton, and L. Tarassenko, “A review of novelty detection,” *Signal Process.*, vol. 99, pp. 215–249, 2014.

[106] H. E. Solberg and A. Lahti, “Detection of outliers in reference distributions: performance of Horn’s algorithm,” *Clin. Chem.*, vol. 51, no. 12, pp. 2326–2332, 2005.

[107] F. Angiulli and C. Pizzuti, “Fast outlier detection in high dimensional spaces,” in *European Conference on Principles of Data Mining and Knowledge Discovery*, 2002, pp. 15–27.

[108] I. Diaz and J. Hollmén, “Residual generation and visualization for understanding novel process conditions,” in *Neural Networks, 2002. IJCNN’02. Proceedings of the 2002 International Joint Conference on*, 2002, vol. 3, pp. 2070–2075.

[109] D. M. Tax and R. P. Duin, “Support vector domain description,” *Pattern Recognit. Lett.*, vol. 20, no. 11, pp. 1191–1199, 1999.

[110] B. Schölkopf, J. C. Platt, J. Shawe-Taylor, A. J. Smola, and R. C. Williamson, “Estimating the support of a high-dimensional distribution,” *Neural Comput.*, vol. 13, no. 7, pp. 1443–1471, 2001.

[111] M. Iosa, A. Cereatti, A. Merlo, I. Campanini, S. Paolucci, and A. Cappozzo, “Assessment of waveform similarity in clinical gait data: the linear fit method,” *BioMed Res. Int.*, vol. 2014, 2014.

[112] G. E. Hinton, “Connectionist learning procedures,” *Artif. Intell.*, vol. 40, no. 1, pp. 185–234, 1989.

[113] M. Müller, “Dynamic time warping,” *Inf. Retr. Music Motion*, pp. 69–84, 2007.

[114] L. Wu, S. L. Oviatt, and P. R. Cohen, “Multimodal integration-a statistical view,” *Multimed. IEEE Trans. On*, vol. 1, no. 4, pp. 334–341, 1999.

[115] B. Schölkopf, J. C. Platt, J. Shawe-Taylor, A. J. Smola, and R. C. Williamson, “Estimating the support of a high-dimensional distribution,” *Neural Comput.*, vol. 13, no. 7, pp. 1443–1471, 2001.

[116] Y. Meirovitch, D. Bennequin, and T. Flash, “Geometrical Invariance and Smoothness Maximization for Task-Space Movement Generation,” *IEEE Trans. Robot.*, vol. 32, no. 4, pp. 837–853, Aug. 2016.

[117] S. H. Park, J. M. Goo, and C.-H. Jo, “Receiver operating characteristic (ROC) curve: practical review for radiologists,” *Korean J. Radiol.*, vol. 5, no. 1, pp. 11–18, 2004.

[118] F. J. Provost, T. Fawcett, and R. Kohavi, “The case against accuracy estimation for comparing induction algorithms.,” in *ICML*, 1998, vol. 98, pp. 445–453.

[119] J. Davis and M. Goadrich, “The relationship between Precision-Recall and ROC curves,” in *Proceedings of the 23rd international conference on Machine learning*, 2006, pp. 233–240.

[120] L. Garrote, C. Premebida, M. Silva, and U. Nunes, “An RRT-based navigation approach for mobile robots and automated vehicles,” in *Industrial Informatics (INDIN), 2014 12th IEEE International Conference on*, 2014, pp. 326–331.

[121] K. Harato, T. Nagura, H. Matsumoto, T. Otani, Y. Toyama, and Y. Suda, “A gait analysis of simulated knee flexion contracture to elucidate knee-spine syndrome,” *Gait Posture*, vol. 28, no. 4, pp. 687–692, Nov. 2008.

[122] D. A. Neumann, *Kinesiology of the Musculoskeletal System: Foundations for Rehabilitation*. Elsevier Health Sciences, 2013.

[123] J. K. Moore, S. K. Hnat, and A. J. van den Bogert, “An elaborate data set on human gait and the effect of mechanical perturbations,” *PeerJ*, vol. 3, p. e918, 2015.